AN ABSTRACT OF THE THESIS OF

François Baratange for the degree of Master of Science in Mechanical Engineering presented on July 16, 1999. Title: Enhanced Sensor for Vehicle Dynamics Evaluation.

Abstract approved: Redacted for Privacy

Swavik A. Spiewak

Vehicle dynamics evaluation is divided in two domains: ride quality and handling. The evaluation of characteristics related to both of these domains requires the knowledge of the vibrations developed by the vehicle. Vibrations can be described by acceleration, velocity or displacement (linear or angular). The inertial properties of large vehicles imply low frequency vibration characteristics.

Estimation of the ride quality involves primarily acceleration. Currently, sensors allow the measurement of near zero frequency acceleration with high precision. Therefore, they are suitable and satisfactory for ride quality evaluation. Standards for passenger acceleration exposure tolerance have been established. However, in the vehicle handling domain, the measurement of displacement is very important, since it defines the motion of the vehicle body and its response to the driver's actions. Obtaining the displacement by double integration of the acceleration is, by its simplicity, attractive. However, commercial accelerometers always exhibit considerable zero drift, mostly caused by low frequency thermal phenomena. This drift is amplified by double integration, which results in strong distortion of the obtained displacements. Therefore, for vehicle motion measurement, the signal obtained from acceleration requires further processing.

The purpose of this research is to evaluate vehicle dynamics using commercial DC accelerometers. A method for the recovery of vehicle displacements from an

acceleration record is proposed. It combines a double integration and a model-based estimation method.

The output signal of the accelerometer is decomposed in three parts: (1) the actual acceleration, (2) the sensor drift, and (3) the remainder of error and random noise. The output signal of the accelerometer is numerically integrated and converted to displacement units. The estimation procedure requires a model structure describing the general form of displacement (obtained by the double integration of the sensor output) in response to the excitation of the vehicle.

Therefore, the estimation procedure employs a parameterized model of the; (1) anticipated displacement, and (2) displacement signal drift. The vehicle displacement model is derived by taking into account first principles that govern the vehicle dynamics. Parameters to be estimated have a physical interpretation (for example the natural frequency and the damping ratio of the vehicle considered as a single degree of freedom system). The structure of drift model is of empirical nature. The corresponding parameters to be estimated can not, a priori, be translated into obvious physical characteristics of the sensor. Based on this model structure, (1)+(2), and the double integration of the accelerometer output, the parameters of the model are estimated using the Levenberg-Marquardt method.

ENHANCED SENSORS FOR VEHICLE DYNAMICS EVALUATION

by

François Baratange

A THESIS

submitted to

Oregon State University

in partial fulfillment of
the requirements for the
degree of

Masters of Science

Presented July 16, 1999
Commencement June 2000

Master of Science thesis of François Baratange presented on July 16, 1999

APPROVED:

Redacted for Privacy

Major Professor, representing Mechanical Engineering

Redacted for Privacy

Head of Department of Mechanical Engineering

Redacted for Privacy

Dean of Graduate School

I understand that my thesis will become part of the permanent collection of Oregon State University libraries. My signature below authorizes release of my thesis to any reader upon request

Redacted for Privacy

François Baratange, Author

ACKNOWLEDGMENT

I would like to express my appreciation to my advisor, Dr. Swavik A. Spiewak. Without his guidance and support, this thesis would not have been accomplished. I would also like to thanks Dr. Sollitt and Dr. Yim for their help and their interest in my research.

I would like to sincerely thank my parents for their love, encouragement and support through all my years in college.

TABLE OF CONTENTS

TABLE OF CONTENTS (Continued)

TABLE OF CONTENTS (Continued)

LIST OF FIGURES

LIST OF FIGURES (Continued)

LIST OF FIGURES (Continued)

LIST OF TABLES

LIST OF APPENDICES

LIST OF APPENDIX FIGURES

LIST OF APPENDIX TABLES

LIST OF ABBREVIATIONS

AC = Alternate Current

ADC = Analog to Digital Converter

DC = Direct Current

DAQ = Data Acquisition System

G = Graphical Programming Language

IC = Integrated Circuit

ISO = International Standards Organization

MEMS= Micro Electro Mechanical Systems

MM = Micro-Machined

MSE = Mean Square Error

SAE = Society of Automotive Engineer

VI = Virtual Instrument

NOMENCLATURE

$a(t)$ = linear acceleration over time

$y(t)$ = displacement over time

$G(s)$ = double integrator transfer function in the s-domain

$A(s)$ = acceleration input is the s-domain

$Y(s)$ = displacement output in the s-domain.

$(XYZ)_G$ = local coordinate system at vehicle center of mass comprises of X_G, Y_G and Z_G axes

G = center of gravity of the vehicle

(XYZ) = global coordinate system comprises of X, Y and Z axes.

X = translation of point G relatively to point 0, along the X-axis

Y = translation of point G relatively to point 0, along the Y-axis

Z = translation of point G relatively to point 0, along the Z-axis

θ = rotation of the body about the X-axis, the angle $<X,X_G>$ (roll angle)

ϕ = rotation of the body about the Y-axis, the angle $<Y,Y_G>$ (pitch angle)

φ = rotation of the body about the Z-axis, the angle $<Z,Z_G>$ (yaw angle)

P1, P2 = pendulous servo accelerometer position sensors

RL = pendulous servo accelerometer stable resistor

Eo = pendulous servo accelerometer output voltage

g = gravity constant

T_{ext} = sensor external temperature

T_{int} = sensor internal temperature

$f_{out}(t)$ = sensor output signal

$f_{act}(t)$ = actual input acceleration or angular velocity

$f_d(t)$ = sensor drift related to low frequency thermal phenomena

$f_{rem}(t)$= remaining random noise and error

$Y_d(A_p, t)$ = model of the error caused by drift

$Y_{act}(B_q, t)$ = model of the actual displacements

$Y_{out}(A_p, B_q, t)$ = model of the signal-based estimate of the displacement

$Y_{SBE}(t)$ =signal-based estimate of the displacement

$\varepsilon(t)$ = error due to non-modeled phenomena

$\hat{\varepsilon}(t)$ = estimate of error due to non-modeled phenomena

$\hat{A}_p, \hat{B}_q$ = estimated final parameters

δ = small number

$\{t_1,...,t_n\}$ = time sequence

Y_{SBE} = discrete signal-based estimate signal

• = discrete model-based estimate signal

$\varepsilon(t)$ = error due to non-modeled phenomena

ξ = damping ratio

y_o = maximum amplitude

ω_d = damped natural angular frequency of the response

ω_n = natural angular frequency

ϕ = phase shift

$f_w(t)$ = Weibull function

A = set of parameters formed by a_0, a_1, a_2, a_3, a_4 and a_5

B = set of parameters formed by b_0, b_1, b_2, and b_3

U = sensor output voltage signal

S_v = accelerometer sensitivity

y_I = i^{th} element of the sequence $Y[i]$

x_j = j^{th} element of the sequence $X[i]$

Δt = sampling period (inverse of the sampling frequency)

x_{-1} = initial condition of numerical integration

x_n = final condition of numerical integration

χ^2 = the chi square value function

σ_I = the standard deviation of the data point (x_i, y_i)

Err = percentage error

p_{actual} = actual value of the parameter

$p_{estimated}$ =estimated value of the parameter

fn = sprung mass natural frequency

ENHANCED SENSORS FOR VEHICLE DYNAMICS EVALUATION

CHAPTER 1

INTRODUCTION

1.1 Vehicle Dynamics Testing

Each time one uses a car, both the driver and the car are subject to a set of stimuli coming from the surrounding environment. For the vehicle, these stimuli come essentially from road conditions variations, aerodynamic forces and internally generated forces. For the driver, the stimuli can be transmitted through the vehicle, major examples being chassis vibrations transmitted through the seat, noise, etc...). Stimuli of less importance can be inherent of the vehicle (usually of less importance: interior space design, ventilation...). Investigating the vehicle behavior and stimuli experienced by the driver during a ride constitutes a part of the vehicle dynamic research. Specifically, it constitutes the vehicle dynamics evaluation. It can be decomposed into two principal domains (A. Zeid, 1996):

- Study of ride, which evaluates the passenger's response to road/terrain irregularities with the objective of improving comfort and road isolation while maintaining wheel/ground contact. Suspension system design is mostly based on ride analysis.
- Handling and drivability, which evaluates respectively the dynamics of the car in response to driver's steering input and surrounding environment inputs (road surface irregularities, wind gust...). It includes cornering, directional stability, rollover, and load transfer.

For the driver and the passengers, the sensation of ease or discomfort is, as explained previously, the result of many different factors that are still not clearly

defined, even though significant progress has been made through the last decades. Handling and ride quality in their broadest sense are probably the most widely discussed aspects of vehicle performance and yet, because they rely so heavily on subjective judgments, they are equally one of the least understood aspects. It remains a subject of vigorous debate - one only has to open any technical or popular motoring magazine for examples - probably because it has proved impossible to quantify with any scientific rigor what constitutes "good" handling or ride properties (MIRA, 1998).

There are two approaches to test vehicle dynamics: subjective testing and objective testing. Subjective testing constitutes the traditional technique for comparing vehicles and relies on the personal judgement of a "ride jury". Its requires as much expertise in surveying as in dynamics. These techniques, even if of proven help and efficiency, turn out to be limited and controversial. Objective vehicle dynamics testing relies on the measurement of physical parameters during a given test. Only the phenomena originating from vibrations of the vehicle structure and inertia effects are taken into consideration. It turns out that these factors are the ones most significantly sensed by the driver. Moreover, they can be measured objectively. This work focuses only on objective criteria measurement.

For this purpose, different vehicle dynamics tests protocols are available today. They have been clearly defined and standardized by the International Standards Organization and by the Society of Automotive Engineers. The realization of these tests leads to the knowledge of some characteristics of the vehicle, subject to the standards used, in the ride quality domain as well as in the handling domain. However the parameters and criteria evaluated by the tests, are often abstract and require advanced knowledge of the vehicle dynamics. Most of these tests have a common feature; they are based on the actual record of a signal, such as acceleration, angular velocity or force. Thus the use of a sensor, like an accelerometer or a gyroscope, is necessary. Whatever the sensor is, the recorded signal can be contaminated by noise or corrupted by error due to the sensor operation itself. This error may mislead analyses

and conclusions. This is especially true when displacements are derived from an acceleration record, as will be discussed further in the text. The error corrupting the actual acceleration is mostly due to the drift of the zero offset output level caused by internal and external heat affecting the sensor. The cause and effect of this drift is discussed in more detail in the following section.

1.2 Signal Drift

While random noise plays a major contribution in reducing the sensor accuracy, drift is another important characteristic to take into consideration. The phenomenon of drift manifests itself as a gradual change of the output voltage of the sensor. It results in changing the zero level of the output offset leading to reduce the sensor accuracy.

Drift beyond a certain limit will introduce unacceptable errors. Moreover, it constitutes a major difficulty since it is not well understood and therefore difficult to recognize and isolate the error contained in the signal. This section discusses firstly the key characteristics of the drift and secondly, the problems triggered by an excessive amount of signal drift.

1.2.1 Principal Characteristics of the Drift

Drift, a component of the noise, can be defined as an undesirable change in output signal, over time, which is not a function of the measured quantity (Kislter Corporation, 1998). Drift results in reducing the stability of the zero level of the sensor output. This change is an unknown function of time since drift may result from changes of temperature, line voltage or amplifier characteristics, which are commonly used in the sensor circuitry (Jitpraphai, 1997). However, in the case under consideration it is reasonable to assume that drift does not depend on the external

temperature. Changes during the short duration tests performed (maximum 16 seconds) are insignificant.

The most relevant characteristic of the drift in this research is its low frequency. This is due to the thermal origin of the drift phenomenon. To illustrate this, Fig. 1.1 shows the double integrated output of a Kistler accelerometer (K-Beam® 8390A2) not subjected to any external excitation. Therefore the corresponding displacement should be a perfect zero line. Thus the signal plotted on Fig1.1 is totally due to a drift. Its approximate period is 16 seconds and its peak-to-peak amplitude is 18 mm.

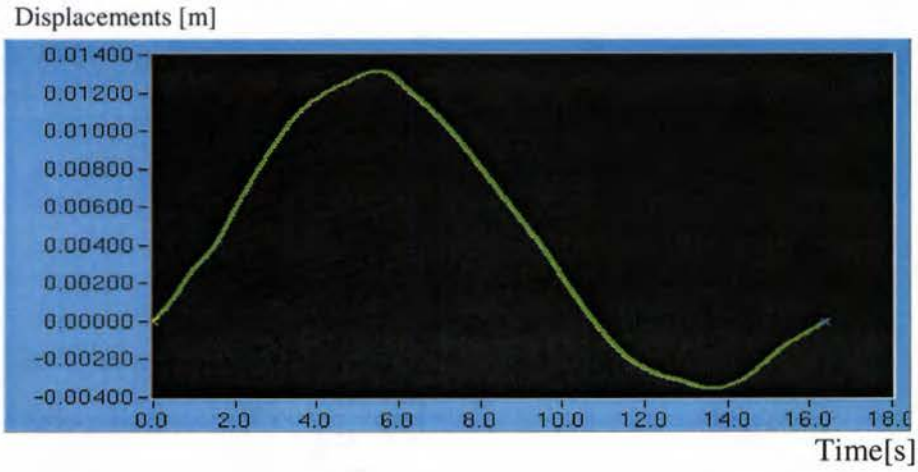

Figure 1.1 The effect of drift on the estimated sensor displacement.

1.2.2 Problems Caused by the Drift

The signals measured in this research are of low frequency. If drift is too significant, it will directly interfere with the actual quantity measured. Even if the best sensor available is used, an error due to thermal drift will be present and, if not suppressed, will obscure the actual measured displacement.

This corruption is dramatically amplified if the signal is integrated, as in the case of a displacement calculation based on acceleration data. Displacements are derived from acceleration by a simple double integration as in Eq. 1.1.

$$a(t) = \frac{d^2 y(t)}{dt^2} \Rightarrow y(t) = \iint a(t)\,dt \tag{1.1}$$

where

$a(t)$ -linear acceleration over time [m/s^2],

$y(t)$ -corresponding displacement over time [m].

Considering the double integration process as an input-output system, the transfer function of such a system can be written as:

$$G(s) = \frac{Y(s)}{A(s)} = \frac{1}{s^2} \tag{1.2}$$

where

$G(s)$ -transfer function in the s-domain,

$A(s)$ -acceleration input is the s-domain,

$Y(s)$ -displacement output in the s-domain.

The corresponding Bode plots are shown on Fig 1.2. On the amplitude plot the slope is - 40 db/dec.

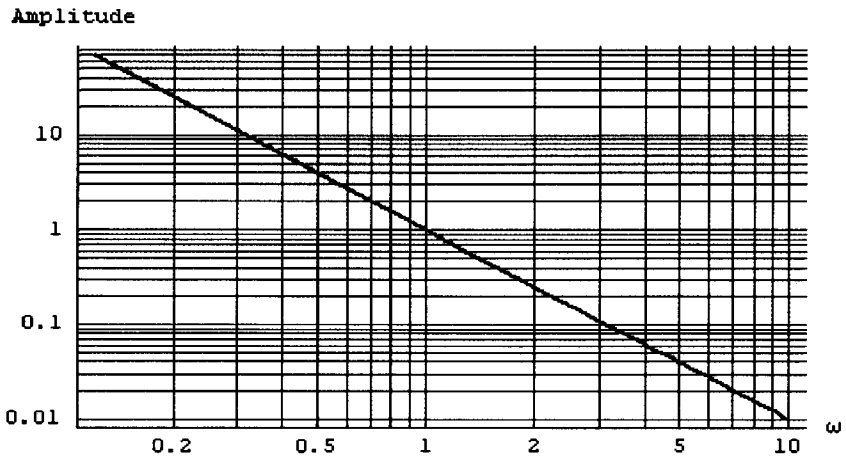

(a)

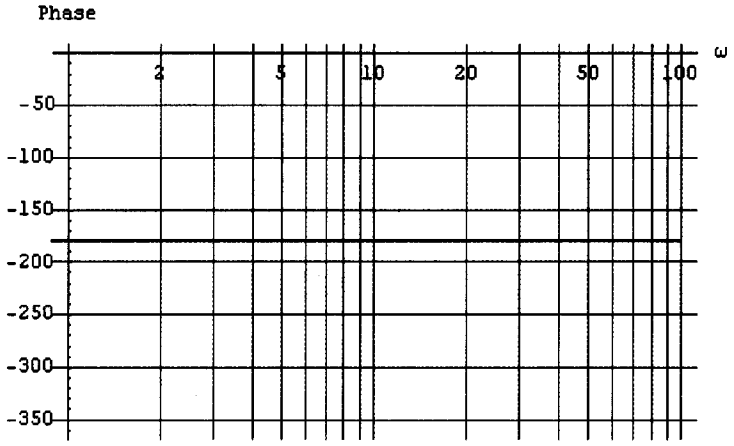

(b)

Figure 1.2 Bode plots for integrator system amplitude (a) and phase (b)

The process of integration increases the amplitude of any low frequency components of a signal. Fig. 1.3 shows the direct double integration of a vertical acceleration record taken from a car chassis driven on a rough road. The result obtained could mislead one to assume that the car chassis elevates 25 cm off the road, which is not possible.

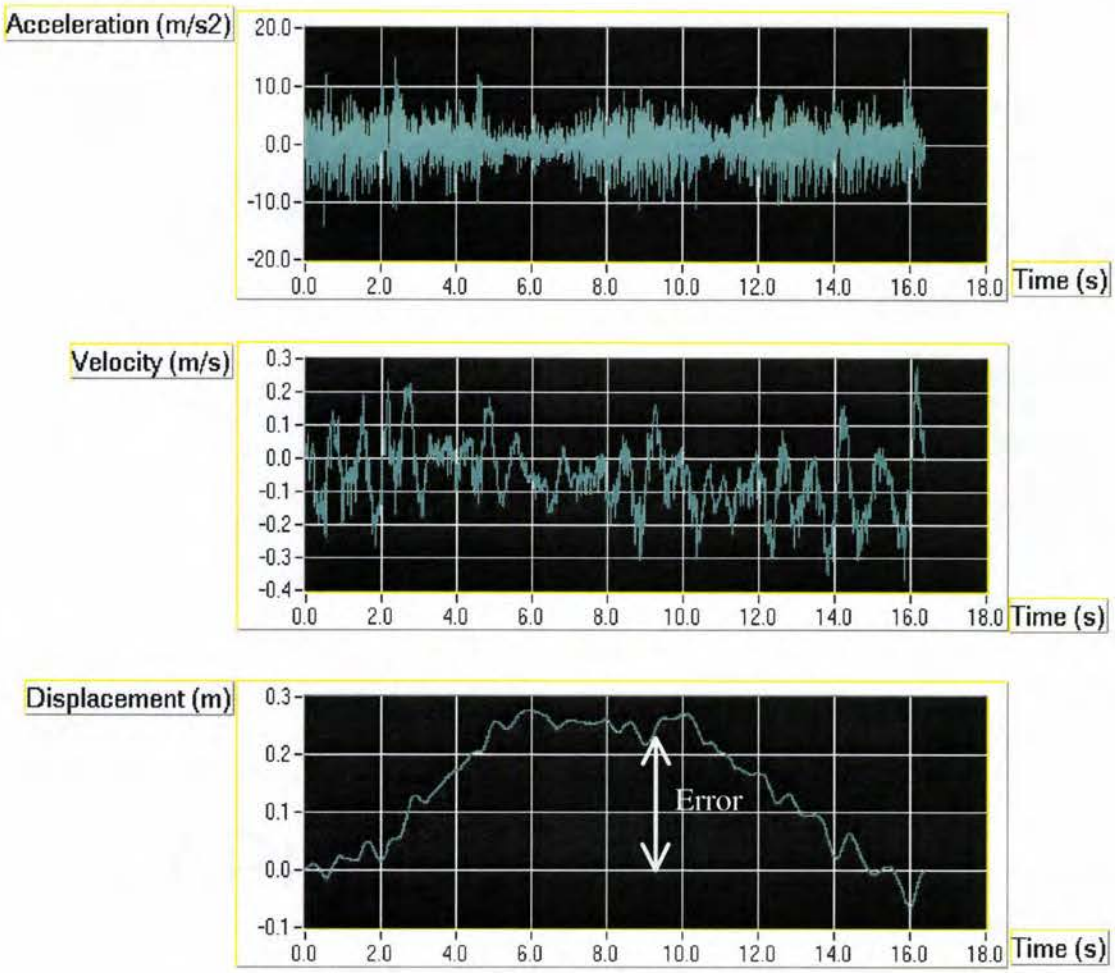

Figure 1.3 Error due to drift after double integration.

1.3 Scope of Work

The purpose of this research is to introduce a method allowing the computation of realistic displacements from acceleration data using sensors currently available. The displacements have been chosen because they provide good intuitive insight and interpretation of vehicle dynamics, contrary to other parameters evaluated by the standards tests currently in use as mentioned in Section 1.1. Moreover,

accelerometers, unlike proximity sensors, do not require any reference fixture. This allows their utilization in a moving environment like a vehicle.

This research focuses on an application of high quality accelerometer and high quality gyroscope to vehicle testing. The method developed is based on the attenuation of errors in the recorded signal from these sensors, so that visualization and rigorous analysis is possible. A mathematical model representing the acquired signal (real acceleration or angular velocity plus the error component) is used. It facilitates the estimation of the actual displacement and the error component in the raw signal and allows their separation. Application of the estimated displacement signal in vehicle dynamics tests will allow the evaluation of certain characteristics, which can not be obtained by using currently available sensors and procedures.

1.4 Chapter Overview

Evaluation of vehicle dynamics is introduced in Chapter 2. Traditional techniques of evaluation are reviewed. Basics of DC accelerometers and gyroscopes utilized within this research are reviewed with respect to their advantages and drawbacks for applications related to vehicle vibration measurements.

In Chapter 3, concepts underlying a proposed method for the recovery of vehicle displacements from an acceleration record are introduced. The model-based estimation of the displacements and the models it relies on are discussed. Parameter estimation algorithms are reviewed.

In Chapter 4, the underlying processing and algorithms employed for the implementation of the method to measure the vertical displacements of the vehicle (driving over an obstacle) are presented. Discussion and results of the "bump test" and experiments conducted for verification of the displacement estimation program are

presented in Chapter 5. Finally, conclusions and recommendations for future directions of this research are explored in Chapter 6.

CHAPTER 2

LITERATURE REVIEW

Vehicle dynamics testing implicate the use of various analytical and experimental means, such as mathematical model, dynamic and control theory, computer simulation, data processing as well as data acquisition system (computer-interfaced system, gyroscope or accelerometer). This chapter begins with definitions and illustrations of the six variables commonly used to describe the spatial motion of a vehicle body. Next, generic concepts in vehicle dynamics are introduced including the models used and current tests for evaluation of dynamic characteristics related to handling and ride quality. Finally, the sensors suitable for measuring vibration of a vehicle body are described.

2.1 Spatial Motion of a Vehicle Body

To visualize the complete motion of a rigid body in space, six coordinates are required: three translations and three rotations. These six parameters allow the determination of a position of the coordinate system attached to the body with respect to the reference coordinate system.

On Fig. 2.1, the coordinate system $(XYZ)_G$, the origin G being the center of gravity of the body considered, is the local coordinate system. Its position is determined with respect to the (XYZ) coordinate system, which constitutes the global reference coordinate system.

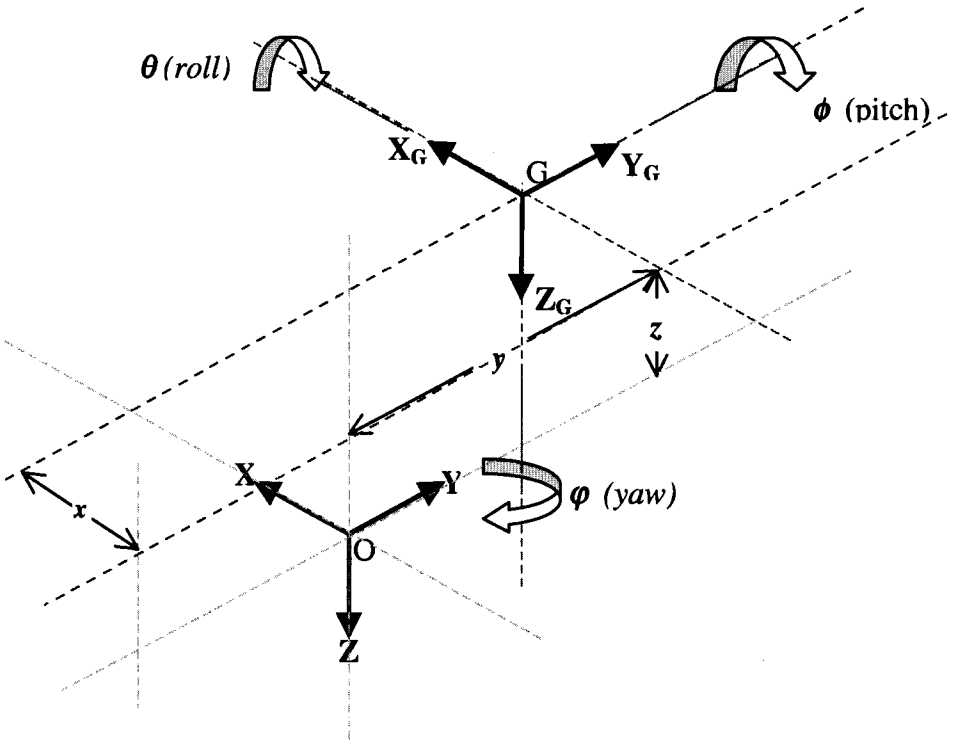

Figure 2.1 Six coordinates describing motions of a rigid body.

The variables required to describe the motion of $(XYZ)_G$ relatively to (XYZ) are:

X - the translation of point G relatively to point 0, along the X-axis,

Y - the translation of point G relatively to point 0, along the Y-axis,

Z - the translation of point G relatively to point 0, along the Z-axis,

θ - The rotation of the body about the X-axis, the angle $<X,X_G>$ (roll angle),

ϕ - The rotation of the body about the Y-axis, the angle $<Y,Y_G>$ (pitch angle),

φ - The rotation of the body about the Z-axis, the angle $<Z,Z_G>$ (yaw angle),

Illustration of these coordinates, applied to a car chassis in shown in the following figure.

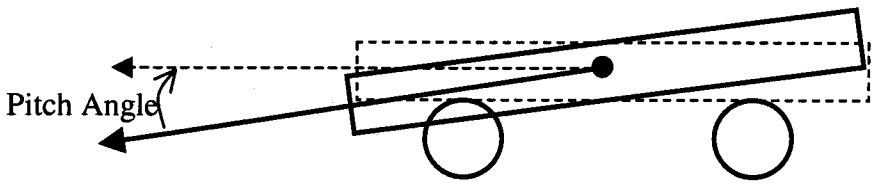

(a)

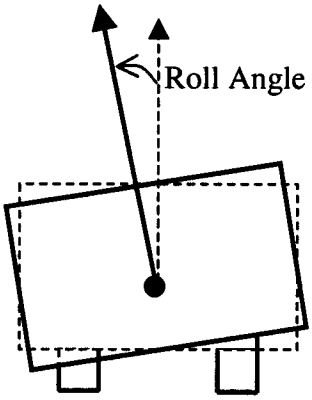

(b)

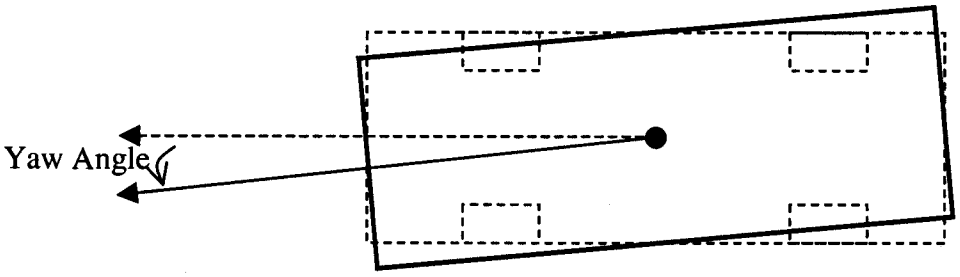

(c)

Figure 2.2 Pitch (a), roll (b) and yaw (c) on a vehicle body

"Pitching" motion typically occurs during breaking or while running over an obstacle. "Rolling" motion and "yawing" motion occur mostly during a curve. The vertical displacement (z along the Z-axis) is commonly called bounce.

2.2 Investigating Vehicle Dynamics

A goal of studying dynamic systems is to predict the response to different stimuli. A behavior of the car constitutes the dynamic response, that is, its dominant motion in terms of displacements, velocities or accelerations related to the 6 degrees of freedom described in the previous section. The stimuli can be anything that triggers a change in any subset of these 6 parameters. For example it could be road irregularities, a bump, a sharp curve, braking or simply changing lane. Moreover, most of the standards vehicle dynamics tests have recourse, at some point, to the use of a model. Different mathematical models have been developed to understand the behavior of the vehicles, run simulation and optimize design.

2.2.1 Models Used in Vehicle Dynamics

Achieving a prediction of the behavior of a vehicle implies the use of a model. According to the model, equations of motion based on Newton's laws for each mass constituting the system are formulated. Knowing the excitation of the system, the response can, in principle, be determined by solving the equations of motion. As the degrees of freedom of the system increase, the analysis becomes increasingly complex, which means a need of more powerful computer and more time (J. Y. Wong, 1993).

Types of model range from large-scale highly detailed computer model with a high number of degree-of-freedom to small-scale simplified model with a low number of degree-of-freedom.

2.2.1.1 Large-scale Model

Large-scale models are usually nonlinear, complex and consist of coupled differential equations that are solved using numerical methods on a computer. These models require powerful computers and a long development time, but are capable of producing spectacular animation model. This type of model was used, for example, in the elaboration of simulation software like CarSiM™. This program was originally developed at "The University of Michigan Transportation Research Institute" (UMTRI). This software allows the prediction of the handling and braking behavior of a vehicle. The program is based on a nonlinear 18 degree-of-freedom 3D mathematical model. It is based on over 20 years of research at The University of Michigan Transportation Research. It includes independent front and rear suspensions (based on models with nonlinear springs, nonlinear dampers, nonlinear kinematics), nonlinear tire model, major suspension effects, steering system gain, nonlinear aerodynamics effects. It is then possible to monitor the results through a wire-frame animator.

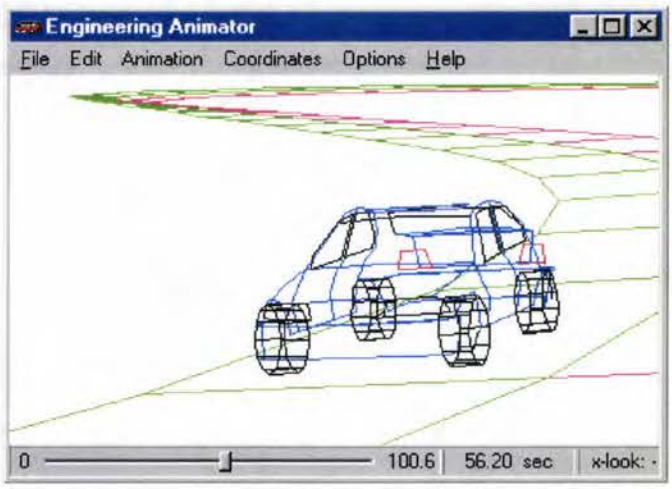

Figure 2.3 CarSim wire-frame animator (UMTRI, 1998).

For a passenger car with independent front suspensions, a seven-degree-of-freedom model, as shown on Fig. 2.4, can be used. The mass of the vehicle body is generally called "sprung mass", whereas the mass of the running gear together with the associated components is called the "unsprung mass".

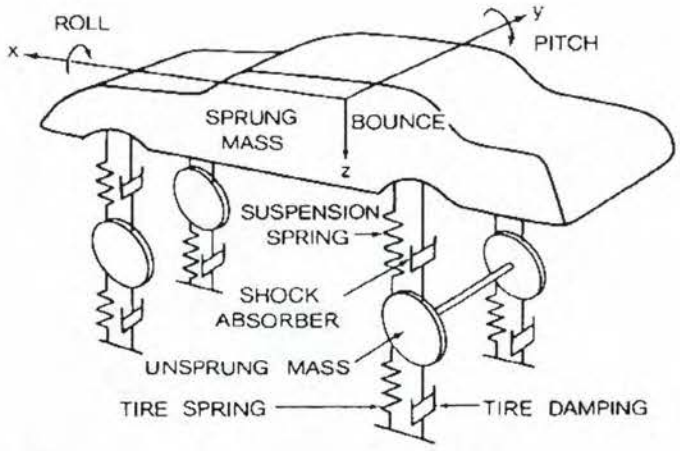

Figure 2.4 A seven-degree-of-freedom ride model for a passenger car (J. Y. Wong,1993).

In this model, the degrees of freedom taken into consideration are:

- Pitch, bounce and roll of the vehicle body.
- Bounce of the two different front wheels.
- Bounce and roll of the solid rear axle.

2.2.1.2 Small-scale Model

Small-scale models are often linear but can be nonlinear as well. They consist mostly of a simple differential equations system related to a small number of degrees of freedom. These models are characterized by a fast computational time and small development time. They can be rerun hundreds of time for parametric studies. They often represent a simplification of the system by taking into consideration only some of the major motions of the vehicle. For example, for suspension concerns a linear model with two degrees of freedom can be used, as shown on Fig. 2.7. This model is called a "quarter-car model", simply because it models one corner (quarter) of a car. As one can see in the Fig. 2.5, it includes one tire, represented by a vertical spring, the mass of the axle supported by the tire, a suspension spring and a damper, and the mass of the body supported by the suspension for that tire.

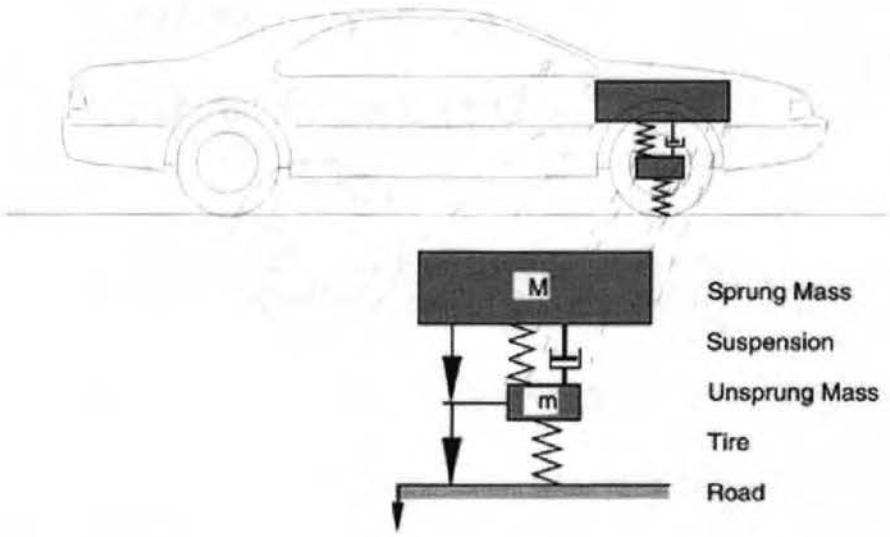

Figure 2.5 A quarter-car model (T.D. Gillespie, 1992).

The problem with the quarter-vehicle model is that one is able to study dynamic behavior in the vertical direction only. Studying dynamic behavior in the vertical direction can be very valuable and can be used to study vibrations which are produced on the sprung mass and caused by inputs from road roughness and radial forces arising from tire/wheel non-uniformities (SAE, 1992). Understanding the dynamic behavior of this system is necessary to isolate the vehicle from the roughness of the road.

If the interest of the study lies in bounce and pitch vibration of the vehicle body (sprung mass), a two-degree-of-freedom model, as shown in Fig 2.6, might be implemented. In this model damping is neglected.

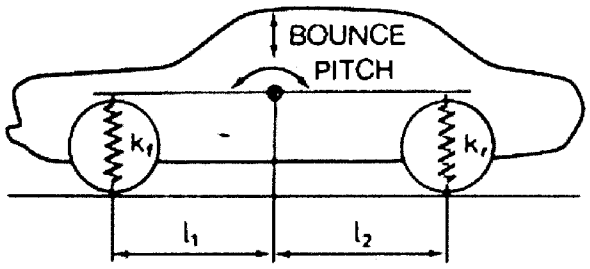

Figure 2.6 A two-degree-of-freedom ride model for bounce and pitch of the sprung mass (J. Y. Wong, 1993).

It is important to notice that generally, bounce and pitch are usually studied in problem dealing with "ride" concerns. Indeed Pitch motions are important because they are the primary source of fore-aft vibrations at locations above the center of gravity, where the driver is normally seated (SAE, 1992). Lateral motion, yaw and roll are most crucial in problem dealing with "handling" concerns (A. Zeid, 1996).

2.2.2 Testing Handling

Objective analysis to back up subjective evaluation of vehicle handling is now recognized as being a fundamental part of any chassis development program. Moreover, in addition to isolated vehicle analysis, benchmark or group testing can be employed in order to rank a vehicle, identify deficiencies in handling behavior and obtain a greater understanding of the handling characteristics of each individual vehicle (IDIADA Vehicle Dynamics, 1998). In order to quantify a vehicle's handling capabilities, numerous test protocols has been issued by the International Standard Organization and the Society of Automotive Engineers. Some car manufacturers, like Toyota, have developed their own specific test. The following table gives examples of these established handling tests.

Steady state constant radius	ISO 4138
Straight-line braking	ISO 6597
Braking in a turn	ISO 7975
Severe lane change	ISO/TR 3888
Steer step input	ISO 7401
Toyota Fish-hook	TSA 1544

Table 2.1 Examples of standard vehicle handling and their respective reference.

Performing handling tests on a given vehicle leads to information concerning its dynamics performances. For example, the position of the center of gravity height and roll/pitch/yaw moment of inertia can be evaluated. Their evaluation requires specific devices (frame/elevator assembly providing input excitation to the chassis, steering input measurement system) not commercially available (Heitz Chassis Lab, INC., 1995). The most widely used sensors in handling testing are gyroscopes and accelerometers.

2.2.3 Testing Ride Quality

Contrary to handling studies, ride quality studies require that the human body response, along with the vehicle response, be taken into consideration. The objective of the study of ride is to provide guiding principles for the control of the vibration of the vehicle so that the passenger's sensation of discomfort does not exceed a certain level (Wong, 1993). Issues which must be addressed in determining ride quality have been already summarized in the project report (Bjorn, Knudsen and Sprunger OSU, 1999) located in Appendix A. As explained in this report, currently, ride quality assessments mostly rely on the ISO 2631 "Evaluation of human exposure to whole-

body vibration" issued by the International Organization for Standardization. It establishes tolerance curves for the human body subjected to vibration (Fig. A.2 in Appendix A). If the vibrations of a vehicle are recorded by an accelerometer, spectral analysis combined with these tolerance curves yields information on the ride quality performances of the vehicle.

2.3 Measuring Vibrations on a Vehicle Body

Perform a vibration measurement involve several stages, as shown on Fig.2.7, this can be called the measurement chain (J. D. Smith, 1989). Usually, the mechanical change under consideration (displacement, velocity or acceleration in this case) cannot be measured directly, thus the first task for the transducer is to convert this mechanical change into an "electrical" change, such as resistance, charge, voltage or capacitance. The second stage is to convert the electrical change into an electrical voltage (current).

An intermediate third stage may be required. It consists of conditioning the signal, for example; buffer, amplify, or filter....

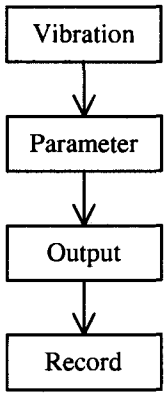

Figure 2.7 Sequence of stages in measuring vibration (J. D. Smith, 1989).

The next stage is to record the signal for analysis. It is important that the information not be distorted or destroyed in any stage of the measurement. Usually the most sensible stage is the initial transducer, which is the actual capture of the vibrating signal. For vehicle vibration, especially for ride quality (according to the ISO 2631 paper), the primary quantity of vibration magnitude shall be acceleration. Consequently, accelerometers are certainly the most commonly used sensors in vehicle testing. However, since this work considers the angular velocity/displacement as a point of interest as well, a gyroscope is considered. Assuming no vibrations perturbations from this environment, the most common distortion is a drift of the output signal as described in Chapter 1.

For both sensors, a wide range of products, based on different technologies, is available from the industry. In the following sections, examples of the technologies used are presented for both accelerometers and gyroscopes.

2.3.1 Accelerometers

At present, a variety of new devices and technologies are on the market. Prices have dramatically decreased, while the cost/performance ratio has improved (Analog Devices, 1998). However, the operation of every accelerometer is based on the same fundamental property. Newton's 1st Law of Motion controls the proof mass, which constitutes the key element of an accelerometer. It attempts to "remain in state," moving or stationary.

The piezoelectric accelerometer is the most widely used. It is less expensive and can fit on one's hand but cannot measure either static accelerations or low frequency vibrations commonly found in vehicle motion. Thus, in the vehicle testing domain, accelerometers have to measure static and/or low frequency acceleration. To achieve this, the sensor used must be able to provide a DC response. This type of

accelerometer is called a DC accelerometer. Several technologies are available today for static or near zero frequency acceleration measurement. The most widely used ones are (J. Doscher, Analog devices, 1998):

- Electromechanical servo.
- Micromachined piezo resistive.
- Micromachined capacitive.

Each one these four technologies is presented and discussed in the following sections.

2.3.1.1 Electromechanical Servo Accelerometer

A generic closed-loop pendulous servo accelerometer is used as an example (Fig. 2.8). The principle of operation can be summarized as follow. The sensing element is a torquer. Whenever the accelerometer case is accelerated, the pendulous mass will tend to remain at a fixed position due to its own inertia.

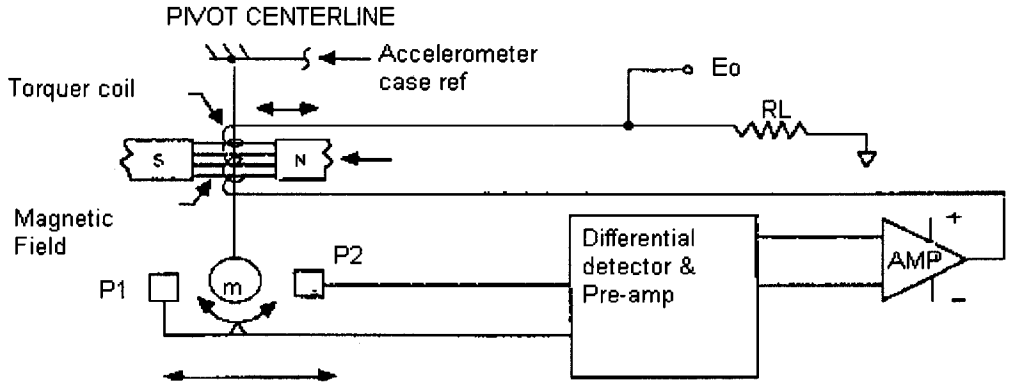

Figure 2.8 Schematic of a servo-accelerometer mechanism (Terra Technology, 1996).

The motion of the mass is detected by a position sensor, which is constituted, in this example, by two proximity sensors, *P1* and *P2*, and a differential detector, as

shown on Fig. 2.8. The output signal is then applied to an electronic amplifier, or servo amplifier. The output current from the servo amplifier is applied to a torquer coil, which then develops a torque equal but directly opposed to the initial torque of the pendulous mass. This compensation torque is called "force-balance". By measuring the current through a stable resistor (*RL*), an output voltage (*Eo*) is created. It is the direct analog representation of the acceleration. That is, the voltage through the resistor is directly proportional to input acceleration.

Figure 2.9 A pendulous servo-accelerometer (Durham Instruments, 1998).

This type of sensor is very accurate for static and low frequency measurement. They are indeed the most accurate kind of accelerometer available today. On the other hand, they are suitable only for low frequency vibrating systems. Moreover, they tend to be relatively fragile and their major drawback is that they are expensive.

2.3.1.2 Micromachined Piezoresistive Accelerometer

This generation of sensors is fabricated using a modern technique called bulk micromachining. It consists of producing a continuous piece of single-crystal silicon. They are categorized as micro-electro-mechanical systems (MEMS). The sensor element is chemically etched into the interior of the wafer. Thereby it eliminates adhesive joints and improves the accelerometer stability.

The piezoresistive strain-gauge-sensing element is a solid-state, silicon resistor, which changes electrical resistance in proportion to applied mechanical stress. Its change of resistance is large relative to its change in length. In other words, its gage factor is large. Since it is a single crystal, it is not only strong, but also virtually free of mechanical hysteresis with inherently good linearity (Dycor Industrial Research Ltd., 1997).

Figure 2.10 A silicon bulk piezoresistive accelerometer (Sintef Corporation, 1998)

Unlike piezoelectric accelerometers, piezoresistive accelerometers act as both AC and DC response sensors. Hence, they are useful for measuring the steady-state acceleration (zero frequency) and low frequency acceleration, present in vehicle vibrations and motion. On the other hand, piezoresistive materials are temperature-sensitive (they're used in thermistors), which will adversely affect the accelerometer repeatability, leading to poor temperature performance. Moreover the piezoresistive strain gauge is fragile, which makes this kind of transducer fairly delicate to manipulate. Also, micromachined (MM) piezoresistive accelerometers are relatively expensive.

2.3.1.3 Micromachined Capacitive Accelerometer

Contemporary MEMS capacitive accelerometers are built following a technique comparable to bulk micromachining. This technique is called surface micromachining. As its name indicates, surface micromachining differs from bulk micromachining in that the sensor element is built onto the surface of a silicon wafer, rather than etched into the interior of the wafer (Lemaire, C. and Sulouff, B., 1995).

The principle upon which the acceleration measurement is based is that of the electrical property of capacitance. A simple capacitor is formed by placing two metal plates in parallel. The fundamental property of such a device is that the capacitance is proportional to the distance between the two plates. Thus, at the heart of a capacitive accelerometer is a small mass which is held in position between two small walls, acting as electrodes, with a spring on either side of the mass. The walls are solidly attached to a circuit board, which is attached to the accelerometer housing. A dual capacitor system is thus formed. The first capacitance corresponds to the system formed by left wall and the mass, the second one the mass and the right wall.

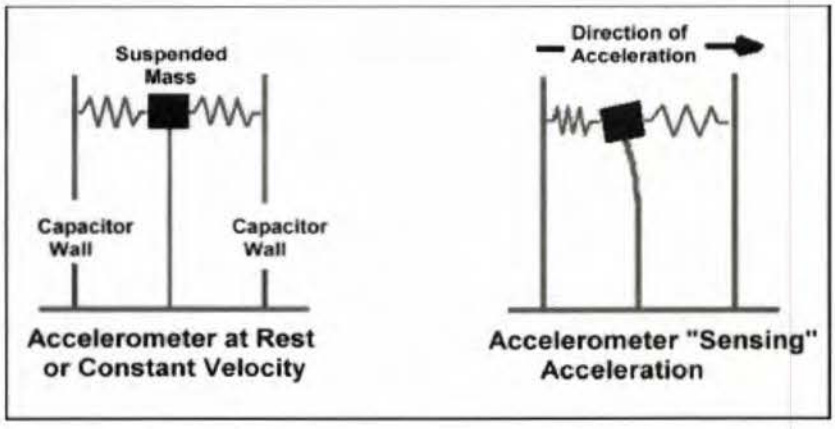

Figure 2.11 The "idea behind a capacitive accelerometer" (Ed Livesay, 1998).

As shown on the Fig. 2.11, while motionless, or while traveling at a constant velocity, the mass is evenly spaced between the two-capacitor walls, resulting in an equal capacitance on both sides. When motion occurs, the mass attempts to "remain in state", the distance between the mass and the walls are changed. Hence, the capacitance of the system formed by left wall and the mass, and the capacitance of the system formed by the mass and the right wall are not equal anymore. The change of capacitance is being sensed and measured, which id proportional to the displacement of the mass and then related to the acceleration encountered.

Capacitive accelerometer can be both AC and DC response capable. Being built following the standard IC forms factor, they are easy to handle and integrate with other IC devices. This type of accelerometer has the highest ratio of performance/cost among all the types present on the market. Moreover, their small size and low cost make then even more attractive. As presented in Fig. 2.12, single units capable of measuring acceleration in three perpendicular directions are presently available from the manufacturers.

Figure 2.12 An tri-axial capacitive accelerometer (Kistler Corporation, 1997).

2.3.2 Gyroscopes

The first known gyroscopic device was built by G.C. Bohnenberger, in 1810. The French scientist Foucault, to study the earth rotation, designed a 67 meter long pendulum in iron. Unsatisfied with the results obtained, in 1852, he built a gimbaled wheel, based on Bohnenberger research. This device turns out to be more accurate and compact than his first device. Over the 189 years separating, the first gyroscope and today, tremendous progress have been made. Contemporary manufacturers offer micromachined gyroscope less than one inch long.

There are two branches of gyroscope design: mechanical gyros that operate using the inertial properties of matter, and optical gyros that operate using the inertial properties of light. Each technology is presented and discussed in the following sections.

2.3.2.1 Mechanical Gyroscope

Original gyro designs, called gimbaled systems, like Foucault's one, were based on the preservation of rotational momentum and consisted of a spinning disk or rotor connected to the moving body of interest by low-friction gimbals. When the body underwent rotation, the spinning rotor maintained its original orientation (preserving its angular momentum). Usually, mechanical gyroscopes provide a signal proportional to the rate of the rotation (angular velocity). That is why they are also called rate gyros. As shown on Fig. 2.13, they exist in one and two axis configuration.

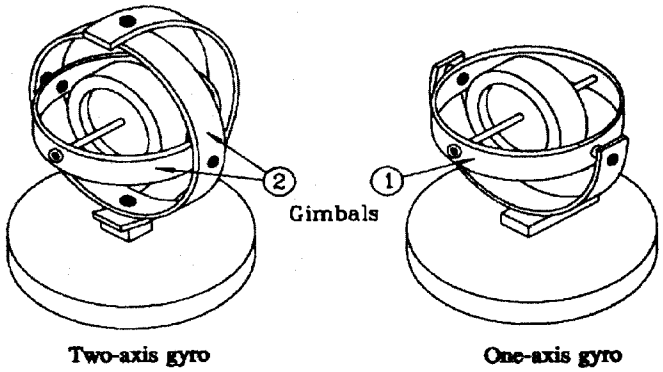

Figure 2.13 One- and two-axis mechanical gyroscope configuration (Lawrence, 1992).

Fig. 2.13 does not represent contemporary gyroscope designs but it illustrates the concept of operation. Today, modern technologies, like MEMS, and materials are used. Whatever technology is used, mechanical gyroscopes have several key elements in common; spinning motor, rotating mass, suspension system, pickoff. The materials used to fabricate these elements might be different from one design to another. Substitutes for the rotating mass in the form of spinning fluids, nuclear and atomic inertial effects are being used or tested. Many attempts to refine the suspension system for the rotating mass as been made. These attempts have lead to the employment of gas bearings and electrostatic and electromagnetic suspensions, as well as fluid suspension technique (Litton System, 1997).

It is important to note that, friction in the support bearings, external influences, and small imbalances inherent in the construction of the rotor cause even the best mechanical gyros to drift with time. Typical high quality systems employed in inertial navigation packages by commercial airlines industry may drift about 0.1^0 during a 6-hour flight (Martin, 1986).

An example dynamically tuned mechanical gyroscope is briefly described. It uses dynamic reaction torques produced in an inside-out two-degree-of-freedom

system with an elastically supported tuned-gimbal suspension. A schematic of the basic tuned gyro is shown in figure 2.14.

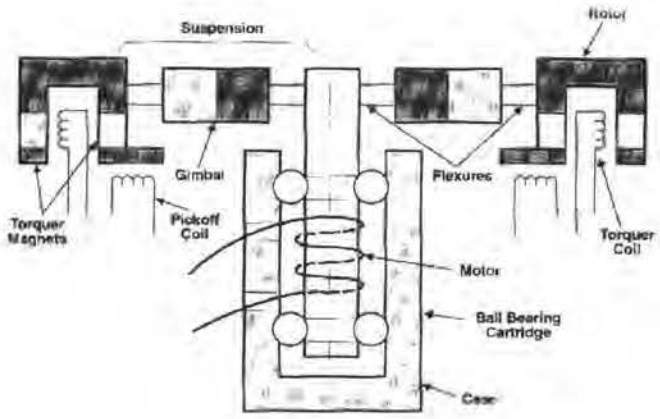

Figure 2.14 Basic tuned gyroscope (G2000 from Litton System, 1997).

In Fig. 2.14, the motor is a synchronous type as normally used in precision gyroscopes. The ball bearing set (cartridge) connects the lower end of the shaft to the case. The tuned suspension system torsionnally decouples the rotor from the case-fixed shaft at spin speed thus enabling the rotor to operate as a near free body about any axis perpendicular to the shaft axis (Litton System, 1997).

Another mechanical gyroscope design commonly used is the vibrating type. Instead of using angular momentum to sense rotation, vibrating gyroscopes use Coriolis acceleration effects to sense when they rotate. This is accomplished by establishing an oscillatory motion orthogonal to the input axis in a sensing element within the gyro. When the sensor is rotated about its input axis, the vibrating element experiences Coriolis forces in a direction tangential to the rotation, orthogonal to the vibratoring and rotating axes (Verplaetse, 1996).

Mechanical gyros, at present, are more commonly available for the types of applications discussed in this research. Moreover they are usually less expensive that the other main kind of gyroscopic device, that is the optical gyroscope, which is presented in the following section.

2.3.2.2 Optical Gyroscope

Optical gyroscopes are based on a fundamental effect of light called the Sagnac effect. Without going in too much detail, this complex theory can be understood as follows. Interferometer fringe shift (path length) can be related to rotation rate (Lawrence, 1992). These sensors use two light waves, traveling in opposite directions around a fixed path. When the device is rotated, the light wave traveling against the direction of rotation will complete a revolution faster than the light wave traveling with the rotation. This effect is detected by means of the phase difference in the two light waves.

The first operational ring-laser gyro was developed by Warren Macek of Sperry Corporation in 1962. Today, the ring laser gyro (RLG), zero lock-ring laser gyro (ZLG), and the interferometric fiber optical gyro (IFOG) are the main types of optical gyros currently being developed (Verplaetse, 1996).

Optical gyros are typically more expensive than mechanical gyros and are currently used primarily in navigational applications. Moreover, they are generally fairly large. On the other hands, they exhibit better drift performance than the most of the mechanical gyroscopes.

2.3.3 Example of two Suitable Sensors

For each sensor, the main criterion of selection is the performance /cost ratio. Performances are judged in terms of accuracy, which is the result of the drift performance, suitable range (± 2 or 3 g), sensitivity. The other aspects taken into consideration are the size and the facility to integrate the sensor into a data acquisition system (DAQ). In fact the whole DAQ system has to be portable and easily set up in the vehicle.

2.3.3.1 Accelerometer Chosen: Kislter K-Beam® 8390A2

Moving vehicles exhibit vibrations in every direction. Therefore an tri-axial accelerometer seems to be most appropriate. As one can see on Fig. 2.15, the surface micromachined capacitive accelerometers provide the highest performance/cost ratio among DC accelerometers.

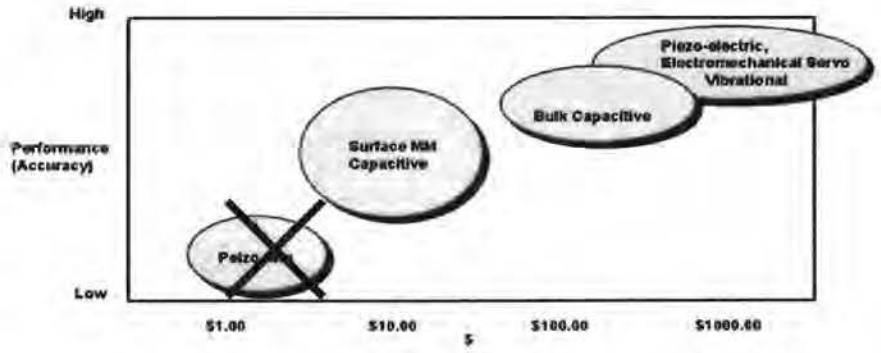

Figure 2.15 Performance/cost ratio for different accelerometers (Doscher, 1998).

Moreover, as one can see on Fig 2.16. capacitive accelerometers have better linearity, as well as a wider temperature and a wider bandwidth range than piezoresistive accelerometers.

Parameter	Piezoresistive		Capacitive
	Silicon	Thick film	
DC response	Yes	Yes	Yes
Bandwidth	Moderate	Low	Wide
Self-generating	No	No	No
Impedance	Low	Low	Very high
Signal level	Low	Low	Moderate
Temperature range (°C)	−55–150	−50–120	−200–200
Linearity	Moderate	Moderate	Excellent
Static calibration (turnover)	Yes	Yes	Yes
Cost	Low	Low	High
Ruggedness	Moderate	Moderate	Good
Suitable for shock	No	No	No

*Unless special designs are used.

Figure 2.16 Comparison of different accelerometer types (Westbrook & Turner, 1994).

Thus, a MM capacitive accelerometer is selected as an optimum device. Kistler Corporation offers a tri-axial sensor that fits all the requirements. A photograph of this accelerometer (Kislter K-Beam® 8390A2) is shown on Fig 2.12. It comes in a very convenient package. The standard unit provides both DC and AC coupled output signals on the standard 9 pin connector. It offers excellent thermal performance (thermal drift of ±5mg/$C^{o)}$ and operates for frequencies ranging from 0 to 150 Hz.

2.3.3.2 Gyroscope Chosen: Litton Two-Axis G-2000

The budget limitation and the size requirement eliminate the optical gyroscopes. Among the mechanical gyros, the MEMS gyroscopes seem to be the most suitable. They offer small-scale devices for a relatively low price. The Litton Two-Axis G-2000 is well suited for the applications of this research. It is a dry tuned gyroscope, based on the dynamically tuned gyroscope design, as introduced in the section 2.3.2.1.

Figure 2.17 G-2000 dynamically tuned gyroscope (Litton Systems, 1998).

As shown in Fig. 2.17, the size (0.75 inch diameter by 0.97 inch long) is on the order of a penny. It provides good drift performance (0.1 to 10^{o}/hour drift class) and high reliability. It comes with a support electronics module. This module is a convenient 3 inch by 4 inch electronic card module. This allows a relatively easy integration in the data acquisition system.

2.4 Attenuation of the Signal Drift

The utilization of a adequate filter can eliminate the low frequency noise (thus the signal drift) typically superimposed on the acceleration data measured by means of accelerometer. However the filter used must not attenuate frequency components of the vibration phenomenon being measured. This method is therefore only suitable when the characteristic frequencies of the vibrations being measured are not lying in the same range as the frequencies attenuated by the filter. If used for vehicle chassis motion measurement, the high pass filter would attenuate the actual acceleration acting on the chassis. Indeed, the characteristic frequencies of the signal drift and the vehicle vibrations are to near. Thus the signal measured would not contain the information that it was suppose to provide.

Another method to attenuate the drift present in a record, is the 'zero centering' procedure. It consists of removing the average value of the signal. This will remove the DC component of the error, provided that the acceleration of the system tested starts and ends at a zero level while the data are acquired. Indeed, not considering the DC component of the noise (or drift) error leads to major distortions in case of integration of the signal, which is the case for displacement visualization. Therefore, zero centering is necessary. However, it is not sufficient since it remove only the DC component s of the error.

Different methods to attenuate thermal drift due to external temperature changes have been introduced. For example, Analog Devices Inc. has proposed two different techniques to improve the thermal behavior of one of their accelerometers. The first method proposed is to subtract a third order polynomial modeling the 0 g drift over temperature where each polynomial coefficient is given by the manufacturer (Kitchin C., 1997). The second method proposed is to use commercial crystal ovens mounted on the sensor to maintain it at a constant operating temperature (Kitchin C., 1997).

2.5 Closure

For ride quality and vehicle handling related research, test protocols have been stated. Performing these tests leads to the evaluation of certain dynamic characteristics of vehicles. The main drawback of these tests is that they often require a considerable amount of equipment (Fig. 2.18). Moreover, the characteristics evaluated are often abstract and not intuitively understandable.

Figure 2.18 Example of a handling testing device (Suspension Kinematics and Compliance Measurement System) (Lotus Engineering, 1998).

Sensors offered by the industry perform excellently for acceleration and angular velocity measurements. Therefore, when no further processing of the data is needed, (acceleration analysis, frequency domain analysis, spectral density) commercial sensors provide a powerful tool. However, even with the priciest sensors available, the signal drift still yields large errors in displacement computations by direct integration of the sensor output. Therefore, the drift needs to be reduced or removed. Some

techniques for attenuation of the thermal drift have been proposed (see end of Section 2.4). Unfortunately, they can only be applied to specific sensors and when the drift is due to significant external temperature changes. This is not the case in vehicle testing.

CHAPTER 3

MODEL-BASED CORRECTION OF SIGNALS FROM INERTIAL SENSORS

Acceleration or velocity signals contain errors due to the sensor drift. This drift leads to large errors in the displacement calculation by integration. Attenuation of the signal drift is necessary to obtain realistic displacement for estimating the vehicle dynamics. The drift is mostly caused by thermal phenomena.

External temperature changes can often be measured. Accurate models of the signal drift as a function of these external temperature changes can be derived, similarly to the technique introduced in Section 2.4. Therefore knowing the external temperature, T_{ext}, and the drift as a function of T_{ext} and time, t, allow the identification of drift in the output signal of the sensor and thus its compensation. Fig 3.1 illustrated this system.

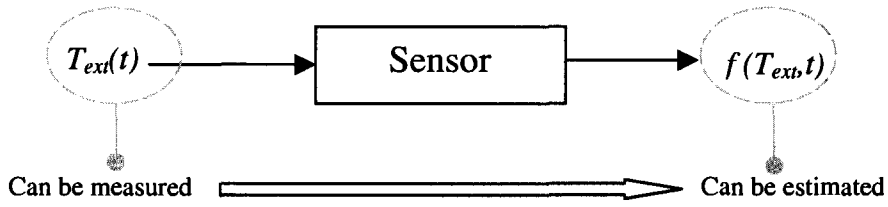

Figure 3.1 Drift due to external temperature variation.

However, even when the external temperature is stable, the output signal drifts. This drift has its origins in low frequency thermal processes in the sensor (internal heat release). Dampers inside of the sensor release a certain amount of heat when excited causing internal temperature variation. Unlike external temperature, the

internal temperature (T_{int}) can not be measured in commercial inertial sensors. This cause of drift can not be isolated (Fig 3.2). Therefore, the signal drift can not be modeled as a function of the internal temperature. An alternative method has to be employed.

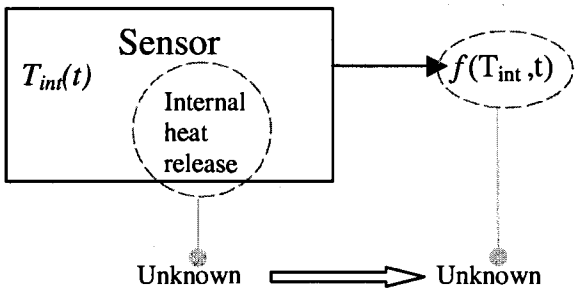

Figure 3.2 Drift due to internal heat release.

This chapter presents a method for estimation of the drift without having the quantitative knowledge of its origin. Specific subjects addressed are: (1) model-based estimation procedure for recovery of displacement from double integrated acceleration, (2) development of a parametric model of the double integrated output signal of an accelerometer and (3) parameter estimation algorithm.

3.1 Model-based Estimation of the Error Due to the Drift

The signal recorded by an inertial sensor can be decomposed in three parts: the actual acceleration or velocity, the sensor drift, and the remaining random noise and error (not correlated with the sensor drift), as described by the following equation, or by Fig 3.3:

$$f_{out}(t) = f_{act}(t) + f_d(t) + f_{rem}(t) \tag{3.1}$$

where

$f_{out}(t)$ - Output signal,

$f_{act}(t)$ - actual input acceleration or velocity,

$f_d(t)$ - sensor drift related to low frequency thermal phenomena,

$f_{rem}(t)$ - remaining random noise and error,

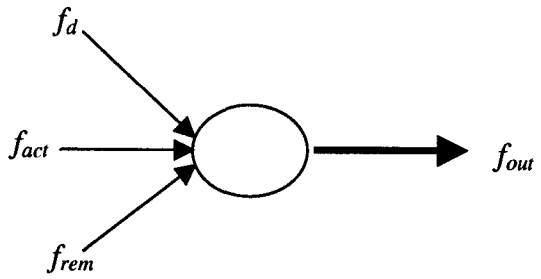

Figure 3.3 Decomposition of the output signal of a sensor.

The signal $f_{act}(t)$ represents the actual acceleration or angular velocity acting on the sensor. The signal $f_{out}(t)$ constitutes the representation of this input as measured by the sensor. This research proposes a method for the recovery of the actual sensor input (in case of displacement computation) by an estimation procedure based upon the decomposition of the sensor output introduced above.

The proposed procedure attempts to find a model (a function of time and suitable parameters associated, directly or indirectly, with physical properties of the system under consideration) that fits the sampled signal with satisfactory accuracy. When using sensors to measure vehicle displacements, different factors affect the composition of the output signal of the sensor, as shown on Fig 3.4. The same notation as in Fig 3.3 is used.

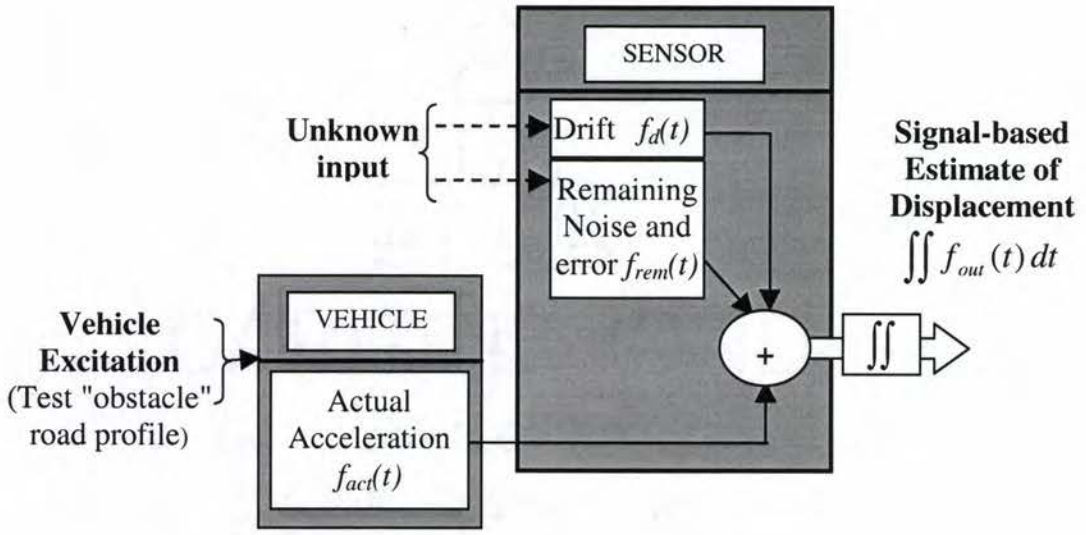

Figure 3.4 Components of the signal-based estimate displacement

The actual acceleration of by the vehicle and the signal drift are independent phenomena. It is assumed that they get superimposed (added) during the signal acquisition. Therefore, superimposing the models of the actual displacement and the error due signal drift yields a resultant model for the whole double integrated signal as shown in Fig 3.5.

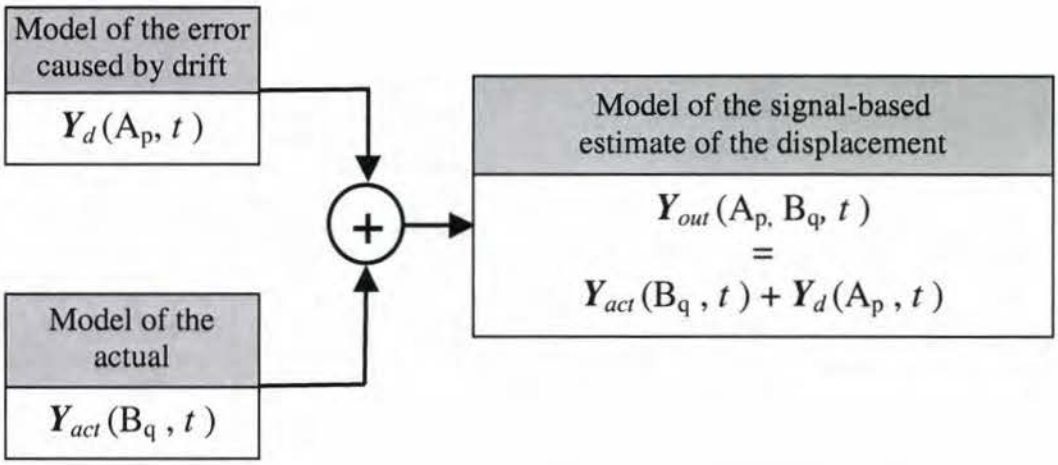

Figure 3.5 Superposition of the drift and actual displacement signal.

A_p and B_q represent finite sets of parameter $\{a_1,a_2,\ldots a_p\}$ and $\{b_1,b_2,\ldots b_q\}$. The model introduced in Fig. 3.5 can not represent exactly the signal-based estimate displacement. This resulting error is represented by the function E (t) and is attributed to the physical phenomena not accounted for by the model structure used. E (t) is defined by Eq 3.2.

$$Y_{SBE}(t) = \iint f_{out}(t)dt = Y_{out}(A_p, B_q, t) + \varepsilon(t) \tag{3.2}$$

where

$Y_{SBE}(t)$ -The signal-based estimate of the displacement,

$\varepsilon(t)$ -The error due to non-modeled phenomena.

Minimization of the function $\varepsilon(t)$ facilitates the parameter estimation in the proposed model $Y_{out}(A_p, B_q, t)$ and gives the most likely values of all parameters $(\hat{A}_p, \hat{B}_q)$. Fig. 3.6 summarizes the procedure in the form of a block diagram.

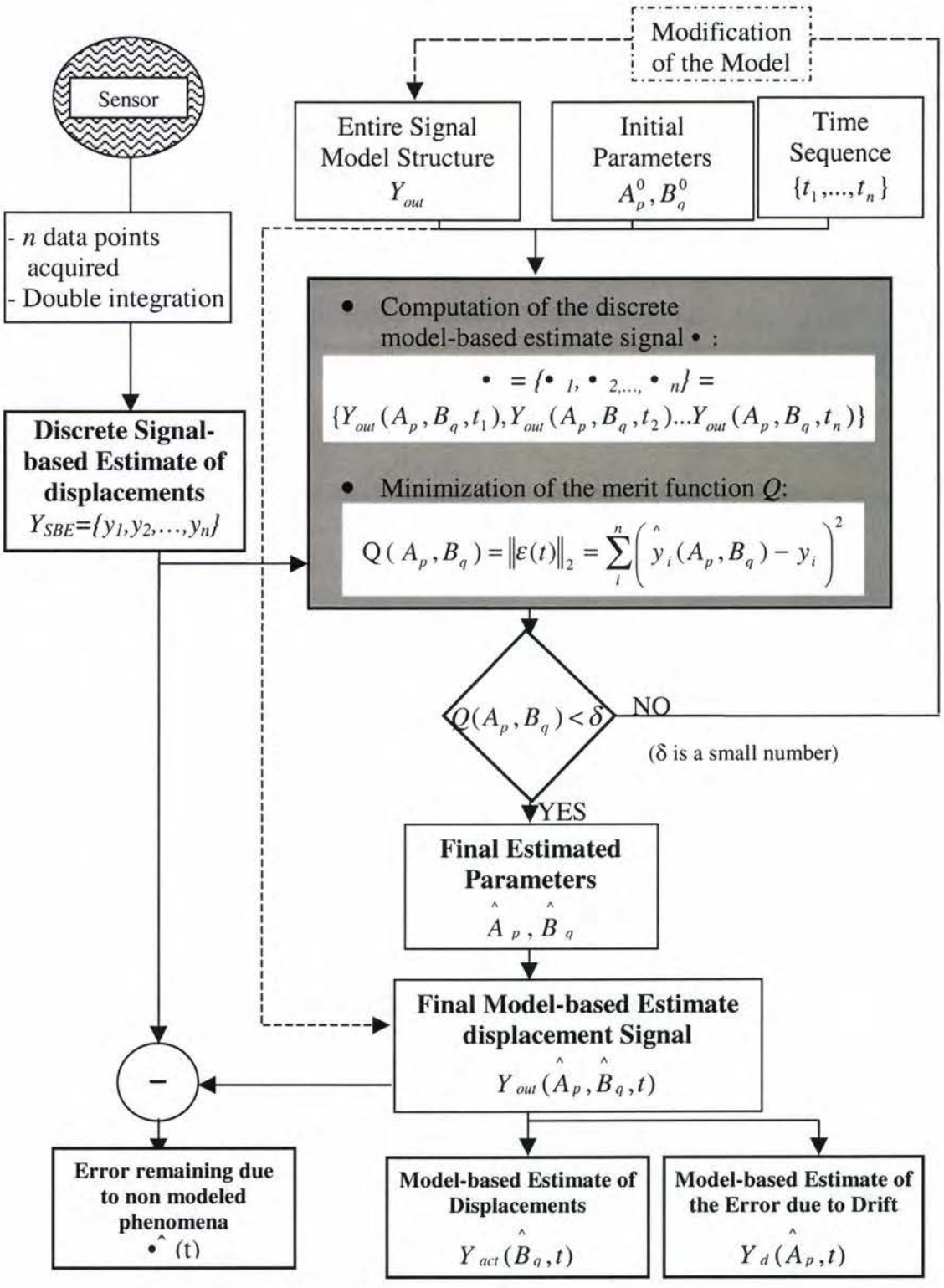

Figure 3.6 Block diagram of the model-based estimation procedure.

The result given by the parameter estimation permits relation of the signal-based estimate of displacement with the model-based estimated signal by the following equation.

$$Y_{out}(\hat{A}_p, \hat{B}_q, t) + \hat{\varepsilon}(t) = \iint f_{out}(t)\,dt = Y_{SBE}(t)$$

(3.3)

The minimized error, $\hat{\varepsilon}(t)$, is small in comparison to the signal $Y_{out}(\hat{A}_p, \hat{B}_q, t)$, therefore:

$$Y_{out}(\hat{A}_p, \hat{B}_q, t) \approx Y_{SBE}(t) \tag{3.4}$$

Section 3.2.3 provides details of the minimized error function $\hat{\varepsilon}(t)$. The actual displacements and the error displacement due to drift are separable. Substituting $\hat{A}_p$ and $\hat{B}_q$ in their respective original structure models yields; the model-based estimate of displacements (Eq. 3.5a) and the error due to the drift (Eq. 3.5b).

$$Y_d(\hat{A}_p, t) \approx \iint f_d(t)\,dt \tag{3.5a}$$

$$Y_{act}(\hat{B}_q, t) \approx \iint f_{act}(t)dt \tag{3.5b}$$

Actual minimization algorithms are discussed in Section 3.1.4. The model for the actual displacements (vehicle response) and a model for the error due to signal drift are described in the following section.

3.2 Modeling the Output Signal of the Sensor

3.2.1 Modeling the Vehicle Response

A model of the vehicle response represents the actual displacements that are to be measured. It describes the expected motion of the vehicle in response to the specific excitation it is subjected to. Therefore the structure of the model accounts for properties of the vehicle and the excitation. This research is concerned with excitations in the form of a strong impulse and only one degree-of-freedom is considered, which substantially simplifies the model development and reduces computational time.

Considering only the vertical displacement response of the vehicle (bounce) to a strong impulse, the motion of the car body (sprung mass supported by suspension springs) will be dominant so the impact of by the tire stiffness and the mass of the wheel axles will be negligible.

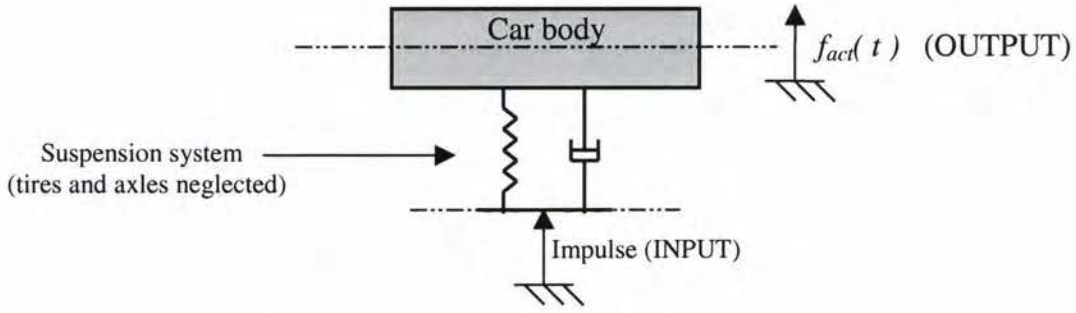

Figure 3.7 Idealized model of a automobile.

It is assumed that rolling over a bump provides a strong impulse input to the system. The impulse response of the vehicle system is modeled as:

$$y(t) = e^{-\xi \omega_n t} y_0 \sin(\omega_d t + \phi) \tag{3.6}$$

Where

ξ - damping ratio,

y_o - maximum amplitude,

ω_d - damped natural angular frequency of the response,

ω_n - natural angular frequency,

ϕ - phase shift.

This impulse response plotted over time is shown on Fig 3.8. Arbitrary coefficients have been chosen.

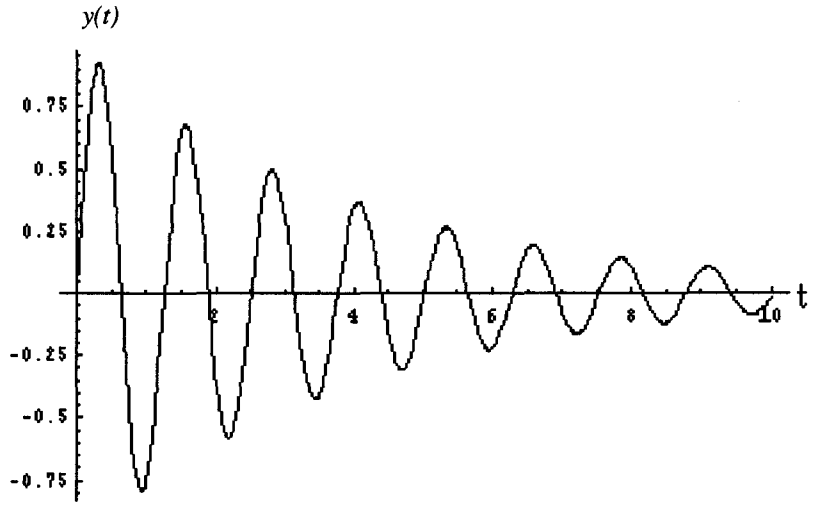

Figure 3.8 Example of an impulse response.

Consequently, the actual displacement model, $Y_{act}(B_q, t)$, is:

$$Y_{act}(\{b_0, b_1, b_2, b_3\}, t) = b_0 e^{b_1 t} \sin(b_2 t + b_3) \tag{3.7}$$

The parameters b_0, b_1, b_2 and b_3 are the following function of the vehicle characteristics:

$$b_0 = y_o \; ; \; b_1 = -\xi\omega_n \; ; \; b_2 = \omega_d \; ; \; b_3 = \phi \tag{3.8a}$$

or

$$\omega_n = \sqrt{b_1^2 + b_2^2} \tag{3.8b}$$

$$\xi = \frac{b_1}{\sqrt{b_1^2 + b_2^2}} \tag{3.8c}$$

It should be remembered that this model is applicable for strong vertical impulse on the car chassis while other movements of the chassis (especially the pitch) are negligible with respect to the vertical displacements. Moreover, It is assumed that the investigated experimental record start synchronously with the impulse.

3.2.2 Modeling the Drift

The sensor drift (Section 1.2) can have several causes. It is therefore difficult to derive a model from rigorous analysis of the sensor as a thermo-electro-mechanical system. In this research a model has been established by directly inspecting the double integrated output of the undisturbed sensor, or after an impulse causing either negligible or rapidly decaying displacements, like for an over-damped system (no actual oscillations). The model derived estimates the displacement error due to signal drift.

A important characteristic of the drift is that it is a low frequency phenomenon (Section 1.2.1). This characteristic provides crucial information for developing a

suitable model. Fig. 3.9 shows the double integrated output signals of a DC accelerometer in case of no net displacement during the displayed time period.

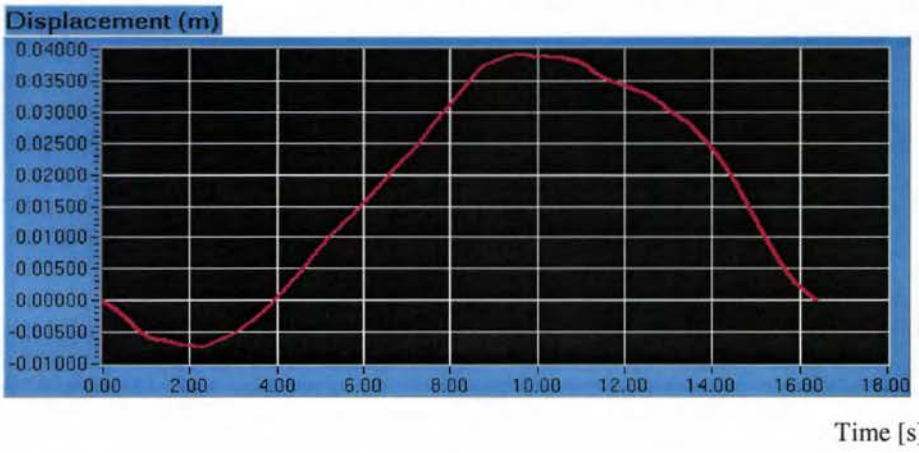

(a)

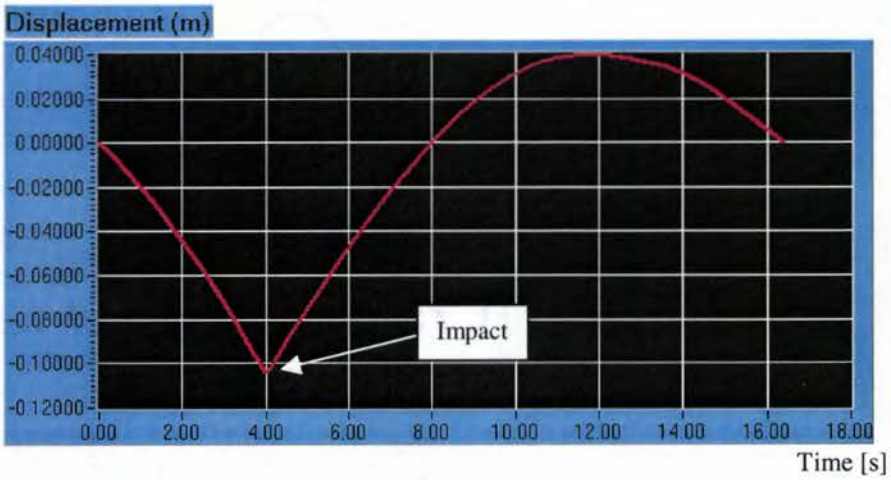

(b)

Figure 3.9 Double integrated signal from an undisturbed DC accelerometer (a) and excited by a short impact but with no net displacement (b).

Signals plotted on Fig. 3.9 exhibit typical shapes of double integrated sensor output for the case of no external excitation or a very short impulse excitation. These graphs represent large displacement errors due to a low frequency drift. In the ideal

situation (no drift) the displacements should be constant except a small perturbation at 4 second for the graph of Fig. 3.9(b). Two simple models investigated in this research to represent the drift error, $Y_d(B_q, t)$, are:

(1) a sum of exponential functions:

$$Y_d(\{a_0, a_1, a_2, a_3\}, t) = a_0 e^{(a_1 t)} + a_2 e^{(a_3 t)}, \tag{3.9}$$

or (2) a fifth order polynomial function:

$$Y_d(\{a_0, a_1, a_2, a_3, a_4, a_5\}, t) = a_0 + a_1 t + a_2 t^2 + a_3 t^3 + a_4 t^4 + a_5 t^5 \tag{3.10}$$

Further tests on undisturbed sensors (Appendix B) proved the polynomial function to be more accurate in representing the observed drift. Considering the double integrated output of a undisturbed sensor, a fifth order polynomial consistently yields a good fit with low mean-square-error (MSE) between the model-based estimate curve and the original signal (Table B.2). Over the thirteen records with the undisturbed accelerometer the average MSE is 2.21E-6 (meter) and the average standard deviation (of the thirteen mean-square-errors) is 1.12E-03 (meter).

To obtain a better representation, the internal heat release in an excited sensor, as introduced earlier, can be investigated in more detail. To investigate this heat, an accelerometer mounted on a "C-shaped" fixture is excited by a short impulse and its response is picked up by the accelerometer. The geometry and the material composing the fixture imply that the displacement impulse response has a high frequency, small amplitude, and decays fast. Variations of the displacement, triggered by the impact are therefore practically negligible with respect to the signal drift. Moreover, a low-pass filter (cutoff at 100 Hz) applied to the output of the sensor removes the high frequency components of the clamp vibrations. Test setup and specifications can be found in Appendix B, Section B.2. The following figure shows the filtered output of the sensor.

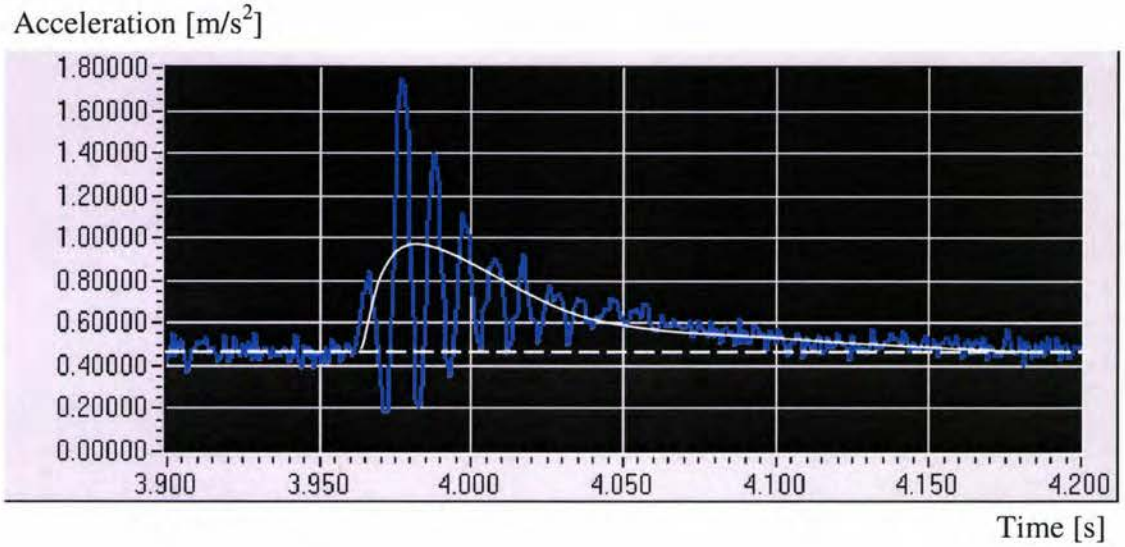

Figure 3.10 Low pass filtered output of an accelerometer excited by an impact causing rapidly decaying oscillations.

Fig. 3.10 shows an acceleration response. The impact occurs shortly after 3.9 sec and the oscillations triggered decay within 0.1 sec. The steady state level offset (white dashed line on Fig. 3.10) exhibited on Fig. 3.10 (0.45 m/s^2) is attributed to the sensor operation. This sensor offset is an inherent characteristic of the sensor used. The value of this offset is indicated by the manufacture and can, therefore, be compensated. The drift appears clearly as short time average of the filtered oscillation (white plain line on Fig. 3.10) departs from the steady state level after the impact. According to the physical properties of the "C-shaped" fixture, the oscillations should be centered about the steady state level. The deviation shows the instability of the zero level of the sensor output during the acquisition time. This instability is attributed to the signal drift caused by an internal heat release.

The drift of the signal illustrated can be fitted by an analytical function. Several functions can be chosen for map the curve. A Weibull function reference with three parameters is chosen in this research because it is defined as (Olkin, 1985):

$$f_w(x) = C\frac{\beta}{\alpha}\left(\frac{x}{\alpha}\right)^{\beta-1}\exp\left[-\left(\frac{x}{\alpha}\right)^{\beta}\right] \tag{3.11}$$

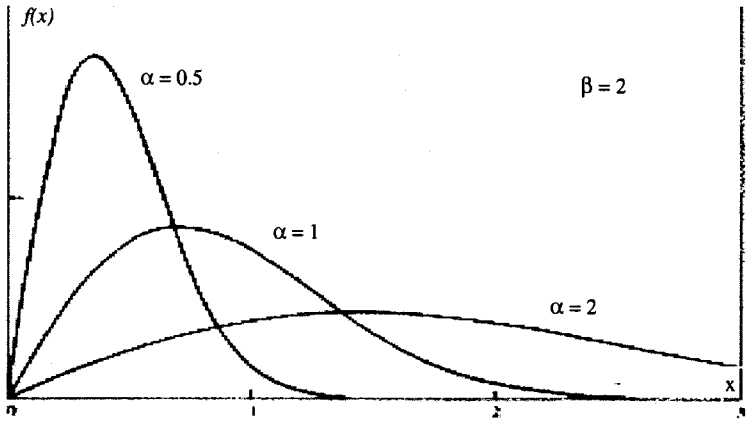

Figure 3.11 Example shapes of the Weibull function (Olkin, 1985).

A fit of the central line by such a function is shown in Fig. 3.12 (see Appendix B for additional test data). The signal has been trimmed to conserve only the actual impulse response part in the record. The acceleration data with the estimated drift removed is shown on Fig. 3.13. Moreover the offset exhibited in the raw signal is removed.

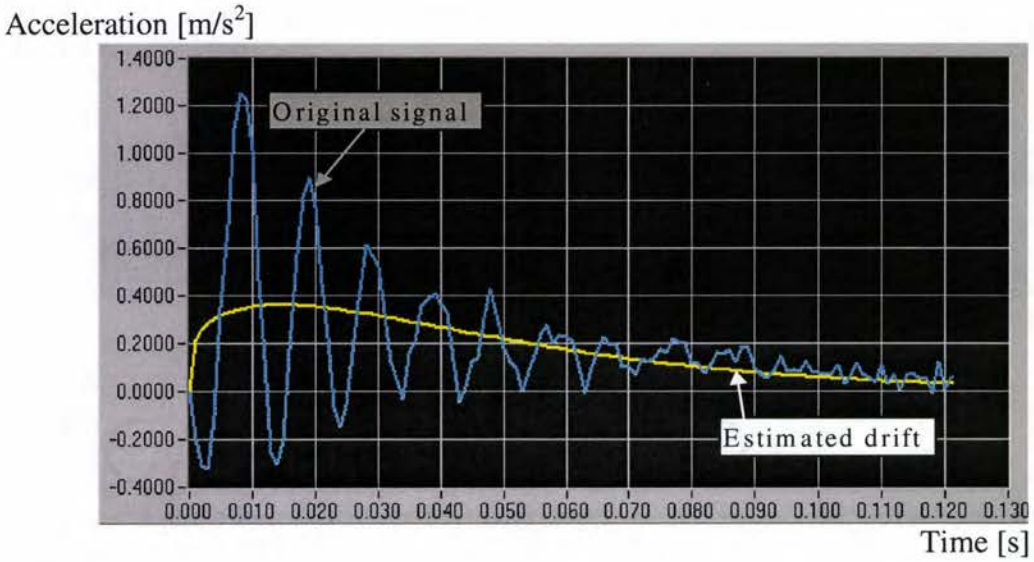

Figure 3.12 Original response signal and estimated drift from an excited accelerometer subjected to no net displacement.

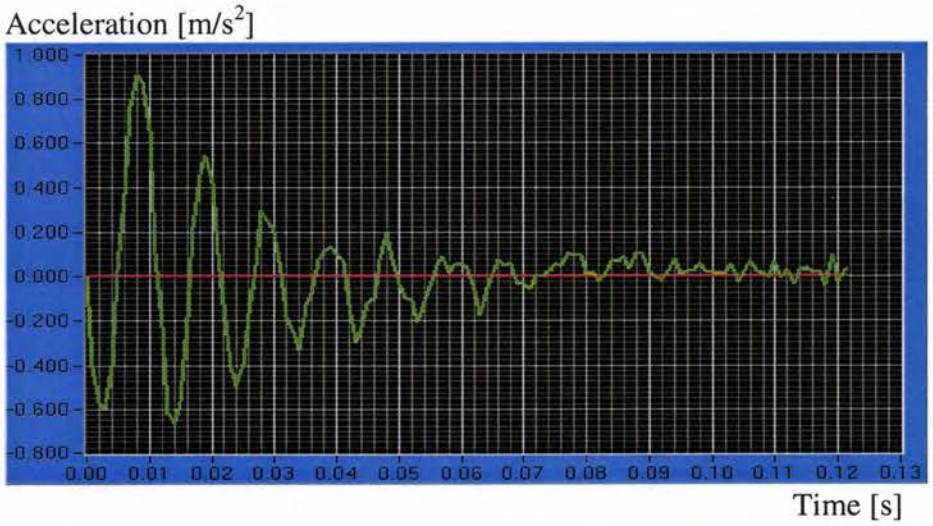

Figure 3.13 Acceleration signal with estimated drift removed.

The maximum amplitude of the deviation of the central line is approximately 0.38 m/s^2, which corresponds to 0.04 g. The results obtained in other experiments show that the amplitude of the drift is proportional to the amplitude of the impact (see Appendix B, Fig. B.3). This observation confirms the hypothesis of the internal heat release in the sensor, which underlies these considerations. The heat release brought into relief in this test can be considered and modeled. A better model of the signal drift could be derived by combining a polynomial and Weibull function. However, for first approach, it is assumed that a polynomial function is sufficient to model the drift correctly.

3.2.3 Non-modeled Phenomena

The model introduced, $Y_{out}(A_p, B_q, t)$, only covers the actual displacement and the signal drift. This model is not comprehensive. Numerous other phenomena occur during the acquisition of the data by the sensor. The noise contained in the signal is not only caused by drift. Noise of a different origin and error due to the sensor operation, $f_{rem}(t)$ in Eq. 3.1, are not modeled. Besides, the model chosen for the actual displacement (Eq. 3.9) is simple one degree of freedom linear model, it does not exhaustively model the actual behavior of the car chassis since numerous factors (tire stiffness, suspension non-linearity) are neglected. After estimation, the non-modeled phenomena constitute the error function $\hat{\varepsilon}(t)$. However the model introduced covers the dominant factors and motions identified in this process.

3.3 Parameters Estimation Algorithms

The parameters estimation method consists of optimizing the parameters of the model $Y_{out}(A_p, B_q, t)$ so that the model signal obtained match, as well as possible, the original signal $Y_{SBE}(t)$. According to the principle of superposition illustrated in Fig.

3.5, the complete model of the double integrated output signal is the sum of the two models respectively developed in Section 3.2.1 and 3.2.2 (Eq 3.12).

$$Y_{out}(A,B,t) = a_0 + a_1 t + a_2 t^2 + a_3 t^3 + a_4 t^4 + a_5 t^5 + b_0 e^{-b_1 t}\sin(b_2 t + b_3) \qquad (3.12)$$

where

A - the set of parameters formed by a_0, a_1, a_2, a_3, a_4 and a_5.

B - the set of parameters formed by b_0, b_1, b_2, and b_3.

The estimation procedure yields the sets of parameters A and B.

This estimation problem is the basis for using non-linear curve fitting methods. They solve the problem not by trying to go directly at the final solution but by trying a series of combinations of values until the "best" possible solution is reached. By definition, this means that non-linear fitting methods are iterative, i.e., they must evolve through several different possible solutions before deciding on the best one (Global technologies, 1998). Several contemporary algorithms are available to perform non-linear fitting.

The Downhill-Simplex algorithm (STScI, 1997), while computationally more intensive than most other methods, is very likely to give an reasonable answer even if the initial values of the parameters were not particularly close to their optimum values. This method usually requires many more iterations than other methods to reach convergence. The user-specified initial step size is used as the initial scale for varying the parameter values, and it is best to set it to about 10 percent of the range between the maximum and minimum permitted values. Note, however, that there is no way to keep the parameter values within the user-specified upper/lower limits with this method.

The Levenberg-Marquardt (Press, 1986), is one of the most widely used non-linear curve-fitting methods. It is very useful for finding solutions to

complex fitting problems. The algorithm begins with a trial solution (i.e., from the parameter initial values) and continuously improves that solution.

Several codes and programs allowing the performance of the Levenberg-Marquardt or Downhill-Simplex non-linear method are presently available. Indeed major mathematical software like Mathematica®, MATLAB® or LabVIEW® feature non-linear curve fitting functions or include them as an external package.

3.4 Closure

A method allowing the model-based estimation of actual displacement from a double integrated acceleration record corrupted by signal drift has been presented. The modeling of the dominant components of the signal-based estimate of the displacements have been presented and discussed. The method is used for an accelerometer but can be applied to gyroscopes.

The next chapter presents the implementation of this method for an accelerometer under the form of a hardware/software package using the concepts and ideas introduced throughout Chapter 3.

CHAPTER 4

MODEL BASED DISPLACEMENT ESTIMATION PACKAGE

The underlying processing and algorithms employed in the computation of displacements are presented in this chapter. The entire procedure is partitioned into four steps: data acquisition procedure, double integration procedure, model parameter estimation, and estimated displacement display. Crucial points of this chain are discussed in detail.

4.1 Comprehensive Displacements Calculation Procedure

The estimation of the displacement from an acceleration data file involves the use of hardware for the data acquisition and software for the displacement computation.

4.1.1 Overview of the Complete Procedure

The entire procedure can be decomposed into four major steps:

1. Data acquisition,
2. Double integration,
3. Model parameter estimation,
4. Displacement correction,

This chain is illustrated in Fig. 4.1.

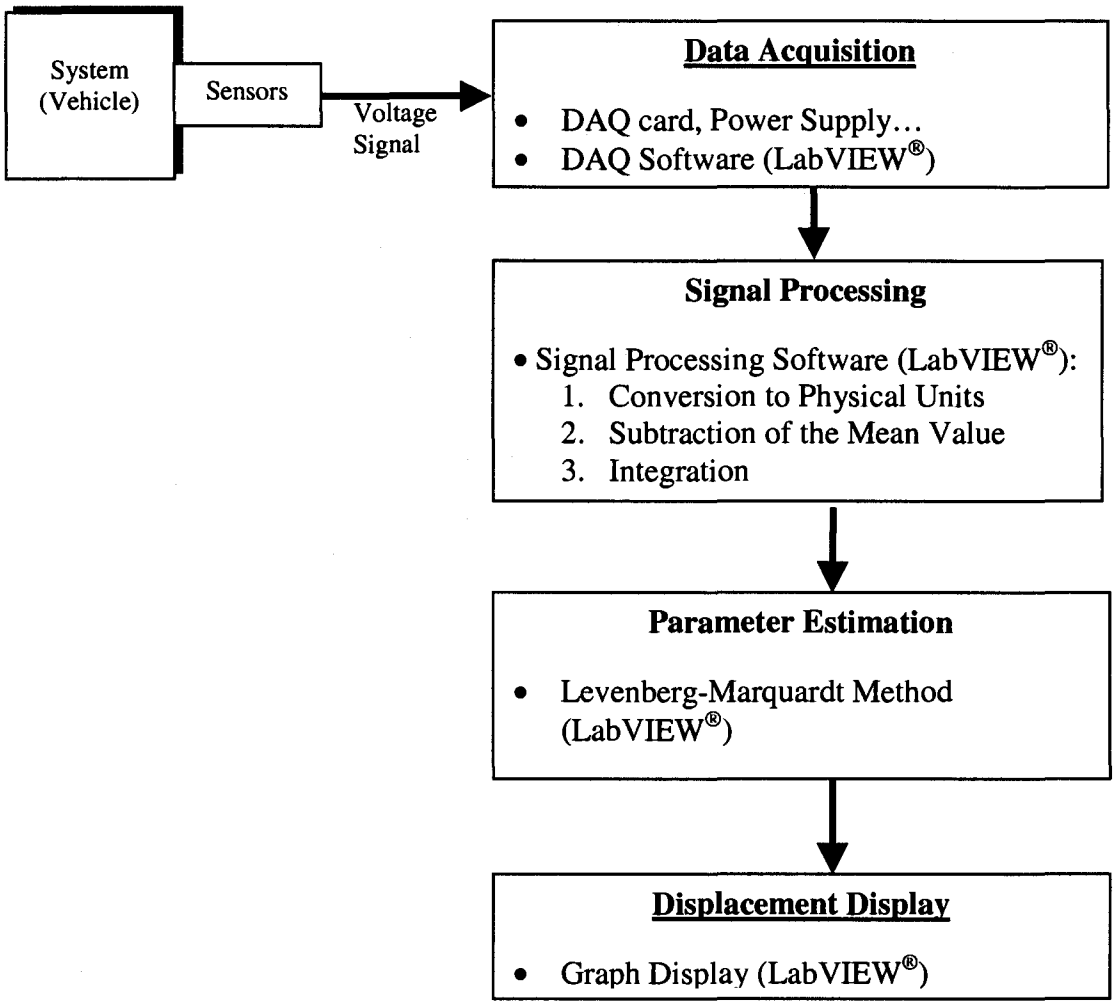

Figure 4.1 A flowchart of the displacement estimation procedure.

The sensor can be a gyroscope or an accelerometer. The voltage signal from the sensor, once picked up, is digitized. Next, all of the tasks are carried out by a LabVIEW®-based program. The voltage signal is converted to acceleration or angular velocity. The average value of the signal is then calculated and subtracted from the signal, removing the possibly present offset. The physical reasons of removing the average are discussed in Section 4.3.1. The adjusted signal is numerically integrated (once for the gyroscope and twice for the accelerometer). Next, according to the procedure introduced in Chapter 3 (see Fig. 3.6), the optimized values of the model

parameters are determined, yielding an estimation of the actual displacement and of the drift.

4.1.2 Introduction to LabVIEW® Programming Environment

LabVIEW® programming environment provides support for every signal processing step after the digitization. LabVIEW® is a development application like C, or Fortran. But unlike those usual languages, LabVIEW® uses graphical programming language, G, to create programs in a flowchart-like form, called a *block diagram.* Thus, it relies on graphic symbols rather than textual statement to describe programming action (National Instrument, 1994).

A LabVIEW® program consists of two parts, a *front panel* and a *block diagram,* displayed in two separate windows. In the *front panel* window, the user interfaces with the program via *Controls* and *Indicators. Controls* allow the control of the inputs of the program while *Indicators* allow the visualization of the outputs. *Controls* and *Indicators* include switches, knob, graphical and numerical displays. They represent and resemble elements found in physical systems. The LabVIEW® programs, as appearing through the *front panel,* are called *virtual instruments* (VI). In the *block diagram,* the user constructs the actual graphical source code of the VI. It consists of objects (represented by icons) wired together that send or receive data, perform specific functions, and control the flow of execution (Thanat Jitpraphai, 1997). Fig 4.2 shows an example of a simple VI, that computes a sum and the mean of four numbers. The front panel (a) displays four numeric controllers and a numeric indicator. The block diagram (b) shows the operations taking place to compute the mean and the sum.

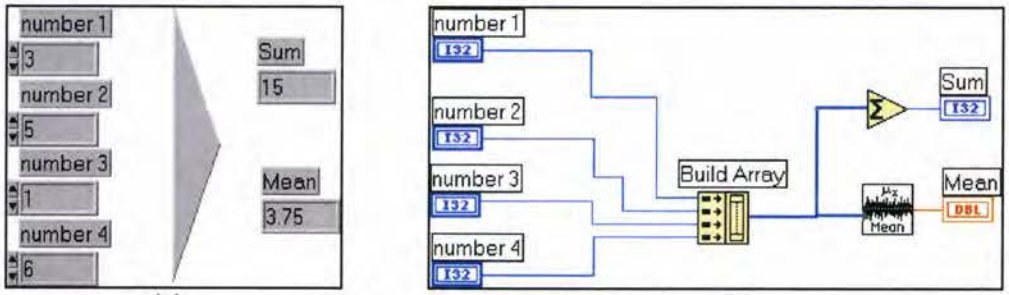

Figure 4.2 An example of a LabVIEW program:(a) Front panel (b) Block diagram (VI).

The power and the practical appeal of LabVIEW® rely on the extensive libraries of functions and subroutines, for example, application-specific libraries for data acquisition, data analysis, data presentation, and data storage. In the data acquisition domain, LabVIEW® can, for example, control a DAQ board or GPIB interfaced device (National Instrument, 1994).

4.2 Data Acquisition System for Vehicle Body Vibration Measurement

DAQ system designed for vehicle vibration measurements requires specific features like low frequency and DC measurement capacity (as explained in Section 2.3), easy transportability, overall small dimension, and easy setup capability. The DAQ employed in this research is a computer-based instrument. The DAQ control is implemented through a LabVIEW® program. The memory and the readout device are provided by a laptop computer (Toshiba 266Mhz Pentium® II running Windows 98®). The analog-to-digital converter (ADC) is located on a plug-in DAQ board (16 bits AI-16XE-50 from National Instrument PCIMIA format). The sampling frequency used is 1000Hz. The sensor is either a Kistler K-beam® 8390A2 accelerometer or a Litton G-2000 gyroscope (see Fig. 5.1 for illustration).

4.2.1 Signal Aliasing Consideration

The '*aliasing*' phenomenon can occur when converting an analog signal to a digital data. It occurs when the sampling frequency of the digitization process is too low with respect to the actual frequency of the signal being digitized. The reconstructed signal is then '*aliased*' and does not correspond anymore to the original analog signal. To prevent this phenomenon, a minimum sampling rate should be set at least twice the highest frequency component of the measured signal. The exact requirement is stated by the Nyquist criterion (Doebelin, 1990), and the corresponding frequency is called the Nyquist frequency.

The vibration phenomena considered in this study are of fairly low frequency, usually below 100 Hz. The DAQ board is running with a sampling rate chosen at 1000 Hz. According to the Nyquist criterion, this is large enough to prevent any '*aliasing*' effect.

4.2.2 Attenuation of Noise in Data Acquisition

The noise is caused by imperfections of elements in the data acquisition system: sensor, cable, plug, computer board. The signal drift can be considered as noise since it corrupts the output and causes distortion of the data recorded. This section introduces some simple techniques, both in hardware and software, allowing the reduction of the noise level in the output signal.

Generally, a subtraction of the average value of the acquired signal significantly reduces the noise by removing a DC component of the error introduced (Doebelin, 1990), as explained in Section 2.4. Cable shielding and grounding design within the instruments should also be taken into account. Moreover, a so-called tribo-electric noise is often induced into the accelerometer cable due to the mechanical

motion of the cable itself. It originates from local capacity and charge changes due to dynamic bending, compression and tension of the layers making up the cable. This problem is mitigated by using proper graphite accelerometer cables and taping or gluing the cable down to a surface as close to the sensor as possible. Moreover, all plugs should have a secured connection to ensure the stability and the rigidity of the connections (Brüel & Kjaer, 1982).

4.2.3 Data Acquisition Control Program

The data acquisition program used in this research, named"*Daqv2st.vi*", has been developed at Oregon State University (T. Jitpraphai, 1997). The program provides an interface between the user and the DAQ plug-in board employed for digitization of the signal. The user is able to command the board to acquire signals with the desired parameters (sampling frequency, full-scale range, scan length). The program allows the saving of data recorded for future use. The user can easily inspect the acquired signals, select suitable sampling parameters and re-acquire data.

4.3 Displacements Estimation from the Experimental Data

Once that the acceleration and/or the angular velocity signal is recorded and stored, the next step is to generate the respective displacements. First, adequate signal processing has to be carried out. Second, the parameter estimation is performed and yields an actual displacement estimate. All of those steps are chained and carried out by one program developed in LabVIEW®. A flowchart of the program is shown in Fig.4.3. It shows the program operations for the case of an acceleration record. If the record is coming from a gyroscope, the process is the same except the second integration and mean subtraction are not carried out. Details on every step are given in the following sections.

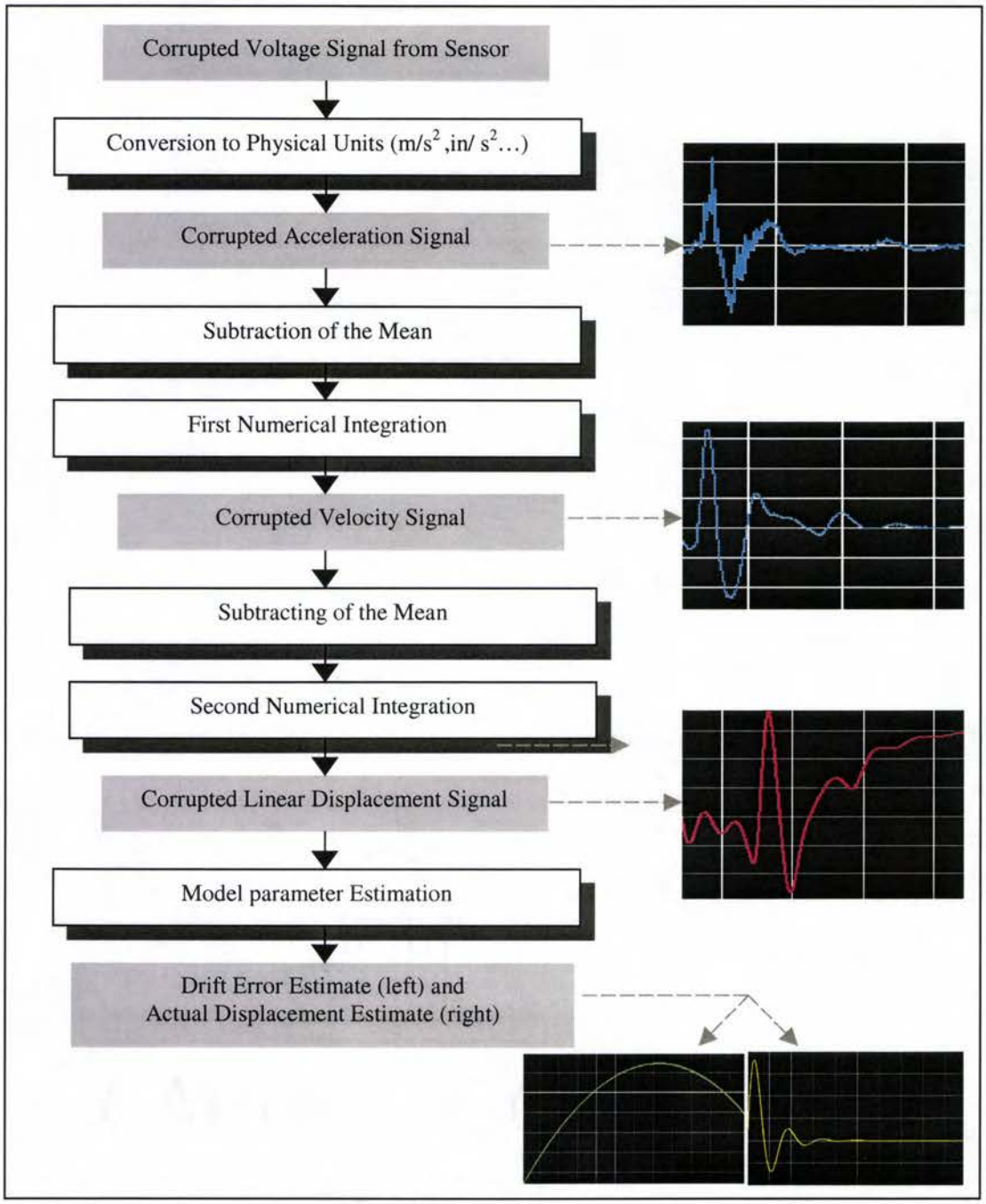

Figure 4.3 Flowchart of the signal processing and estimation procedure.

4.3.1 Conversion to Physical Units and Subtraction of the Mean

The analog signal captured by the sensor is a voltage signal. Therefore, it should be converted to represent the actual physical value of acceleration or angular velocity. This is done by multiplying the voltage signal by a adequate conversion factor as shown in Eq. 4.1.

$$a(t) = \frac{g}{S_v} U(t) \tag{4.1}$$

where

$a(t)$ - the acceleration measured (m/s^2, in/s^2 or ft/s^2),

U - the voltage signal (V),

g - the acceleration of the gravity (m/s^2, in/s^2 or ft/s^2),

S_v - the accelerometer sensitivity (V/g).

Thus if Eq. 4.1 is used with $g = 9.81\ m/s^2$, the obtained signal will be in m/s^2.

The subtraction of the mean is primarily required to remove the possible offset in the signal due to the gravity acting on the sensor (in the vertical direction only) as well as the DC component of the error as explained in Section 4.2.2. For the tests considered in this research (see Section 5.4), the actual displacements are physically starting at zero and decay as time goes on. Therefore, a second subtraction of mean, after the first numerical integration, is required to ensure that the displacement signal starts and finishes at zero.

4.3.2 Double Integration Procedure

After converting the signal to physical units and removing the average value of the signal, a numerical integration is performed (one integration for a gyroscope, two for an accelerometer). The integral, *Y[i]*, of an input time series signal, *X[i]*, is calculated using the following equation (LabVIEW® National Instrument, 1994):

$$y_i = \frac{1}{6}\sum_{j=0}^{i} (x_{j-1} + 4x_j + x_{j+1})\,\Delta t \quad , \quad i = 0, 1, 2, 3..., n-1 \tag{4.2}$$

where

y_i - the i^{th} element of the sequence *Y[i]*,

x_j - the j^{th} element of the sequence *X[i]*,

n - the number of points in sequence *Y[i]* or *X[i]*,

Δt - the sampling period (inverse of the sampling frequency).

x_{-1} and x_n are, respectively, the initial and final conditions and have to be specified. For the test performed in this research (see Section 5.4), the actual displacement, velocity and acceleration start and end at a zero level. Therefore the initial conditions for each numerical integration are:

$$x_{-1} = 0 \tag{4.3a}$$

$$x_n = 0 \tag{4.3b}$$

4.3.3 Displacements Estimation (the Levenberg-Marquardt method)

The tasks described in the previous section, once performed, yield corrupted displacements (linear or angular). Indeed the error caused by disturbances is still present and has been amplified at low frequency by the integration process. This

section describes the parameter estimation procedure algorithm used for estimation of the actual displacements.

A non-linear estimation procedure used in this research employs the Levenberg-Marquardt method. As introduced in Section 3.3, the algorithm begins with a trial solution (derived from the initial parameter values provided by the user in the program) and continuously improves that solution to minimize the chi-square function used as the merit function. Suppose that N data points (x_i, y_i) with $i=0,\ldots,(N-1)$ are to be fitted to a model $Y(\{\alpha_1,\ldots,\alpha_m\}, x)$. The chi-square merit function is defined as (Press ,1986):

$$\chi^2 = \sum_{i=0}^{N-1}\left[\frac{y_i - Y(\{\alpha_1,\ldots,\alpha_m\}, x_i)}{\sigma_i}\right]^2 \tag{4.4}$$

where

χ^2 - the chi square value,

σ_i - the standard deviation of the data point (x_i, y_i).

σ_i represent the standard deviation of the random measurement error on (x_i, y_i) distributed as a normal distribution. For the problem considered in this study, σ_i is assumed to be constant for all i and is set equal to1. In this research, $Y_{SBE}(t)$ is to be fitted by $Y_{out}(A, B, t)$ (using the same notation as in Section 3.2);

- (x_i, y_i) with $i=1,\ldots,N$ corresponds to $(t_i, Y_{SBE}(t_i))$, the discrete representation of $Y_{SBE}(t)$,
- $Y(\{\alpha_1,\ldots,\alpha_m\}, t)$ is the model function $Y_{out}(A, B, t)$,
- $\{\alpha_1,\ldots,\alpha_m\}$ corresponds to the set $\{a_0, a_1, a_2, a_3, a_4, a_5, b_0, b_1, b_2, b_3\}$ (see Eq. 3.12).

The time sequence is given by the original record from the data acquisition system, which is a discrete series of numbers starting at zero and spaced at the sampling period.

LabVIEW® 4.1 provides a built-in estimation procedure based on the Levenberg-Marquardt method. The effectiveness of this procedure depends upon the initial parameter values. Therefore, the initial parameters should be chosen carefully considering any available resources before using the function (National Instruments, 1994). Moreover this built-in function offers two ways of performing the Levenberg-Marquardt method. The derivatives of the model used with respect to each parameter, necessary to derive the best coefficients, can be either numerically computed, or their analytical expressions can be specified by the user. The accuracy of the fit is not affected by this choice. However, the use of analytical derivative expressions renders the procedure a little faster.

4.3.4 Displacement Estimate Display

Corrected displacements in this research, are the estimated displacements obtained from the estimation procedure. Therefore, the corrected displacements constitute a perfect impulse response since they are based on Eq 3.9.

CHAPTER 5

EXPERIMENTAL IMPLEMENTATION AND RESULTS

The programs developed in this research, especially the estimation program, are complex and, therefore, prone to conceptual and programming errors. It is necessary to test and validate these programs before further use. This chapter presents the data acquisition interface, the programs used, and different tests performed to verify the entire system. Specifically, a "bump test" is presented, and the results obtained are discussed. The implementation has been undertaken only with an accelerometer, but the package is also applicable to a gyroscope.

5.1 Experimental Set-up

The data acquisition system (DAQ) described in Section 4.2 has been setup in both a generic passenger car and a motor home. The sensor was located right above the rear axle, on the car body. A minimum length of cables has been used to avoid excessive tribo-electric noise (see Section 4.2.2). The start of the acquisition is initiated by human hand (no auto trigger with impulse).

The system allowed selection of the following parameters before acquisition.

- Sampling frequency: 0 – 40,000 Hz.
- Number of signals recorded.
- Number of data points 512 to 16,384 per channel.

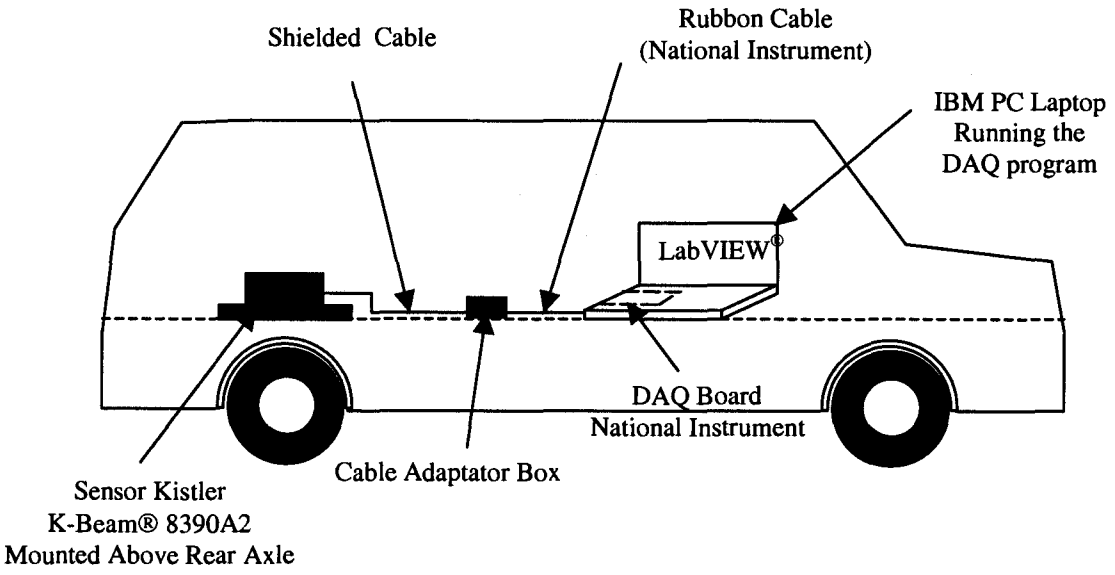

Figure 5.1 The on-board DAQ system used.

Every plug in the DAQ system has a screw retention device. To gain space and facilitate the set-up of the DAQ on board of the vehicle, the power supply for the sensor is the laptop itself. This has been rendered possible by the utilization of suitable cables and a adaptation device (home made cable adaptator box as shown on Fig. 5.1).

5.2 Data Acquisition Controller and Displacements Estimation Software

Those two programs constitute the software part of the package. The data acquisition program had been developed with LabVIEW® 3.1 (student edition) and the displacement estimation program with LabVIEW® 4.1. The data acquisition program is designed to run "on-board" inside the vehicle tested. The displacement estimation program is designed to run "post test" from the data acquired and saved during the test.

5.2.1 Data Acquisition Program

The data acquisition software *"Daqv2sy.vi"* will not be presented in great detail in this report. The program has been adapted for a three-axis accelerometer use. For "on board" utilization, the front panel provides large buttons and switches for easier access with the touch-pad of the laptop. The *virtual instrument* (VI) features shortcut keys for all major functions (like launch acquisition, setup, save data). A picture of the front panel of the VI is shown in Fig. 5.2.

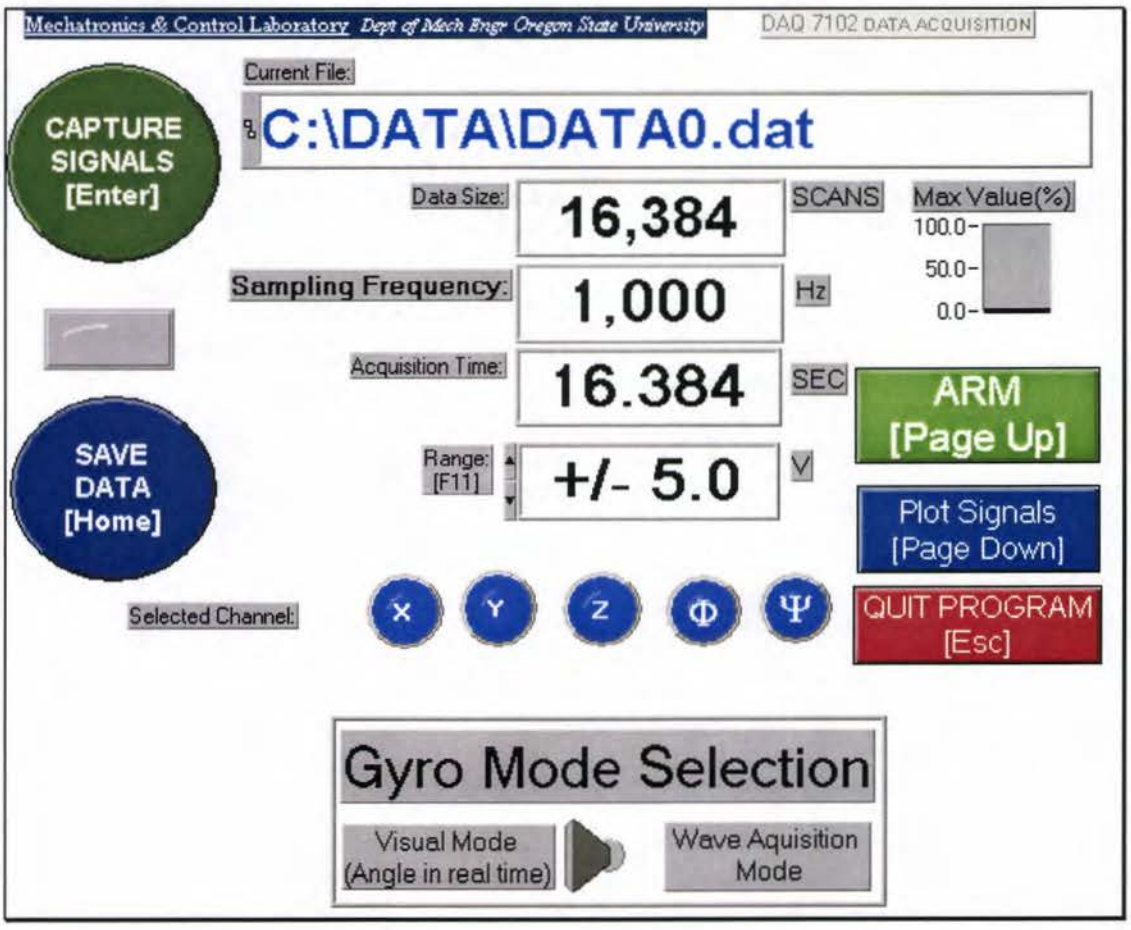

Figure 5.2 Front panel of the "on-board" DAQ control software.

5.2.2 Displacement Estimation Program

The core of the "*Displacement Estimation.vi*" program is composed of the sub-VI's *"Nonlinear Lev-Mar Fit.vi"* and "*Target Fnc & Deriv NonLin.vi*". The icon *"Nonlinear Lev-Mar Fit.vi"* is shown in Fig. 5.3.

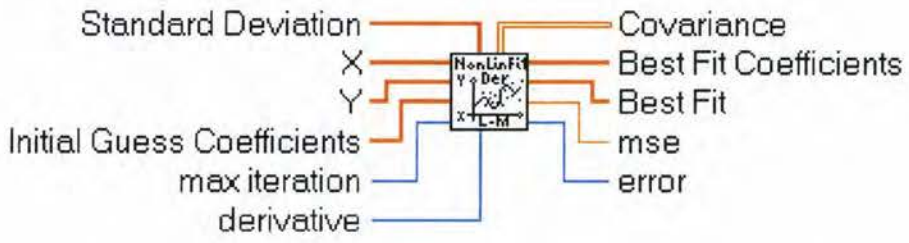

Figure 5.3 The "Non linear Lev-Mar.vi" LabVIEW® icon.

The *Y* input is the raw double integrated acceleration signal and the *X* input is the corresponding time series. The sub-VI will compute the estimated parameters which corresponds to the set $\{a_0, a_1, a_2, a_3, a_4, a_5, b_0, b_1, b_2, b_3\}$ as specified in Eq. 3.12 (*Best Fit Coefficients* output on Fig. 5.3). The *Best Fit* output is the model $Y_{out}(A, B, t)$ evaluated for the time series *X* and the estimated parameters.

"*Target Fnc & Deriv NonLin.vi*" is used to specify the target function ($Y_{out}(A, B, t)$). This is a built-in sub-VI included in LabVIEW® 4.1. It is called during the execution by the *"Nonlinear Lev-Mar Fit.vi"* sub-VI and not directly by the main program "*Displacement Estimation.vi*". Therefore, even if it is a crucial component of the estimation program, it does not actually appear in the main block diagram ("*Displacement Estimation.vi).* A part of its *block diagram* is shown in Fig. 5.4

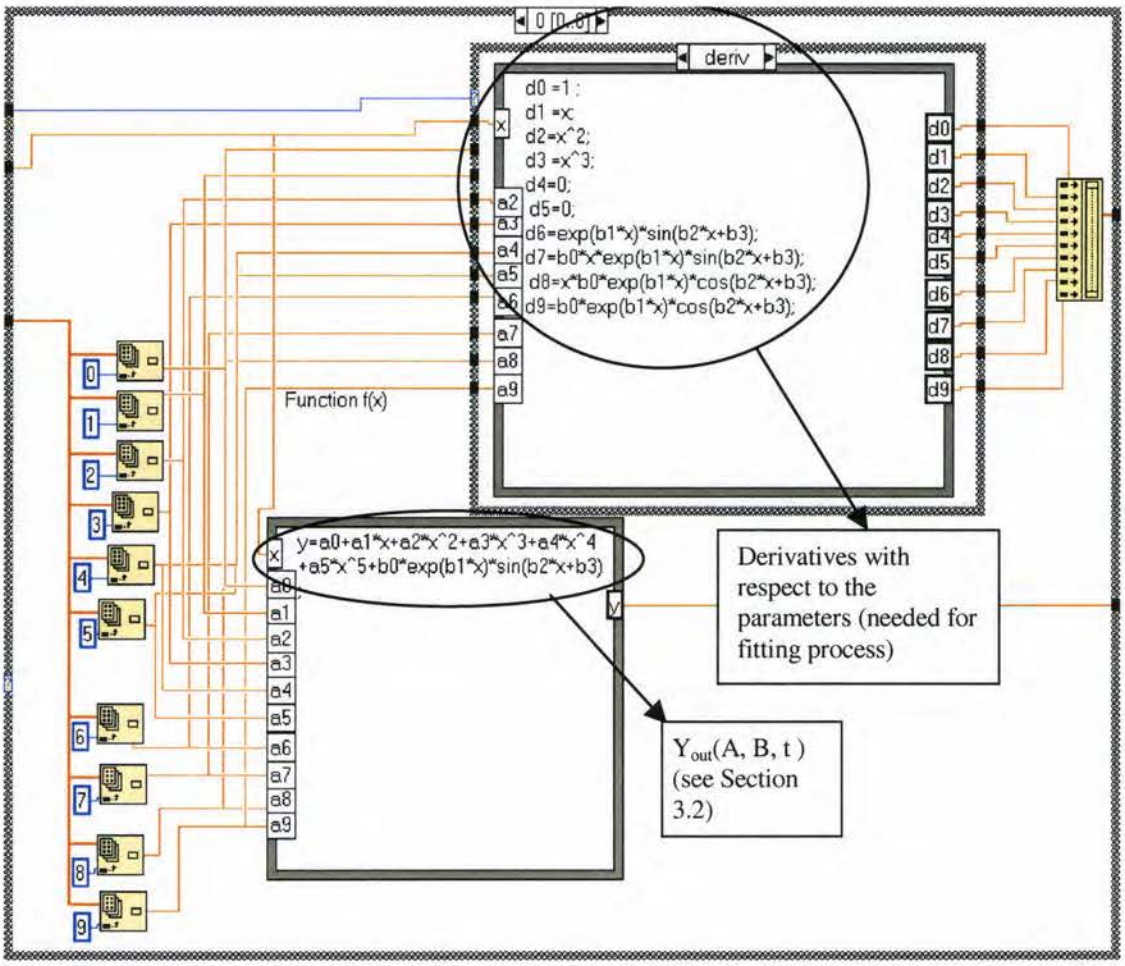

Figure 5.4 Partial block diagram of "*Target Fnc & Deriv NonLin.vi*" sub-VI.

"*integral_x(t).vi*" and "*read from spread sheet.vi*" are the two other essential sub-VI of the program. The first one performs a numerical integration as presented in Section 4.3.2, and the second one allows the loading of a data file. A summary of the "*Displacement Estimation.vi*" program in the form of a simplified block diagram uses the sub-VI's as appearing in the actual LabVIEW® code (Fig. 5.5). Fig. 5.6 shows the main front panel of the "*Displacement Estimation.vi*" program.

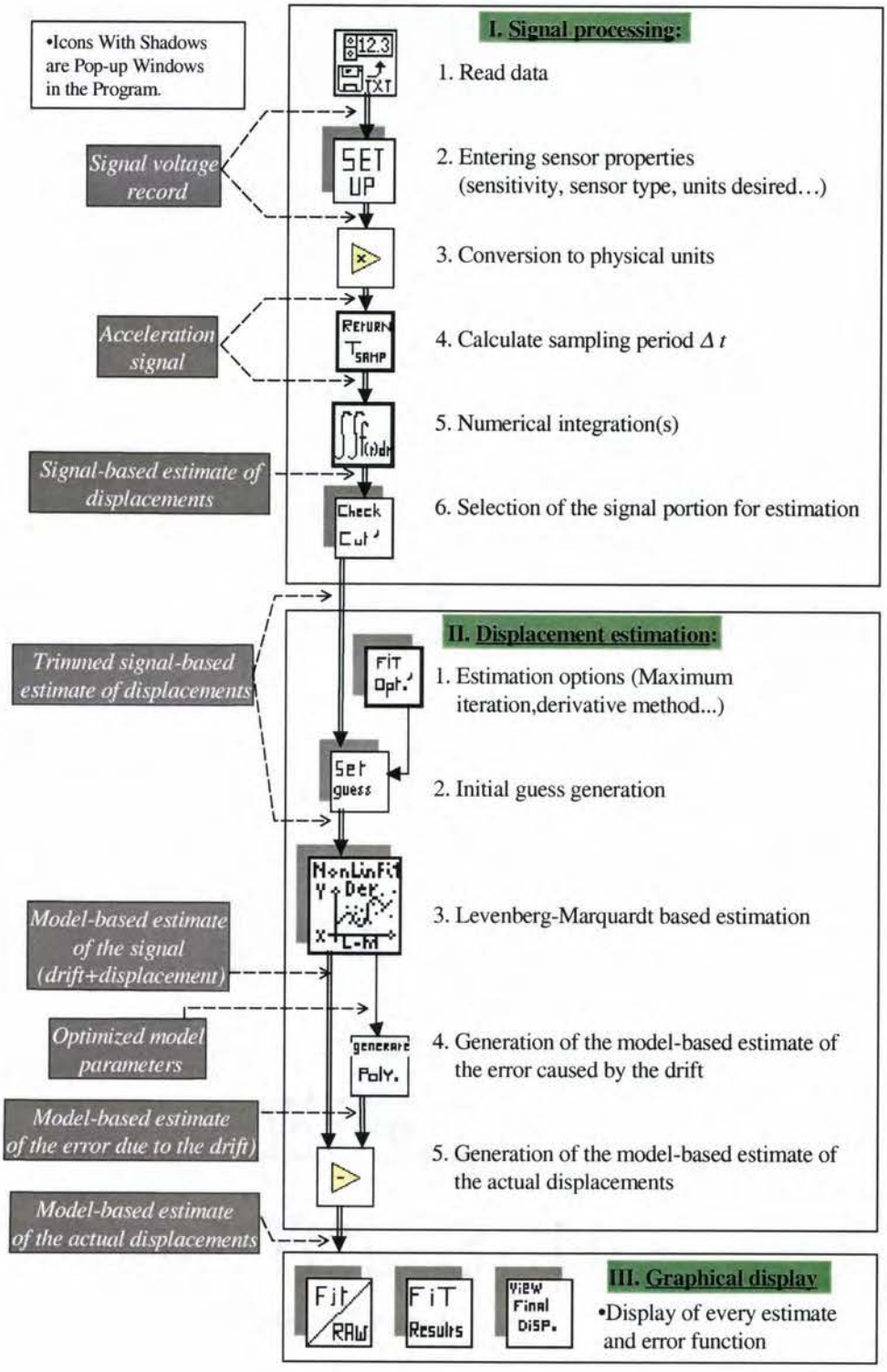

Figure 5.5 Simplified block-diagram of "*Displacement Estimation.vi*".

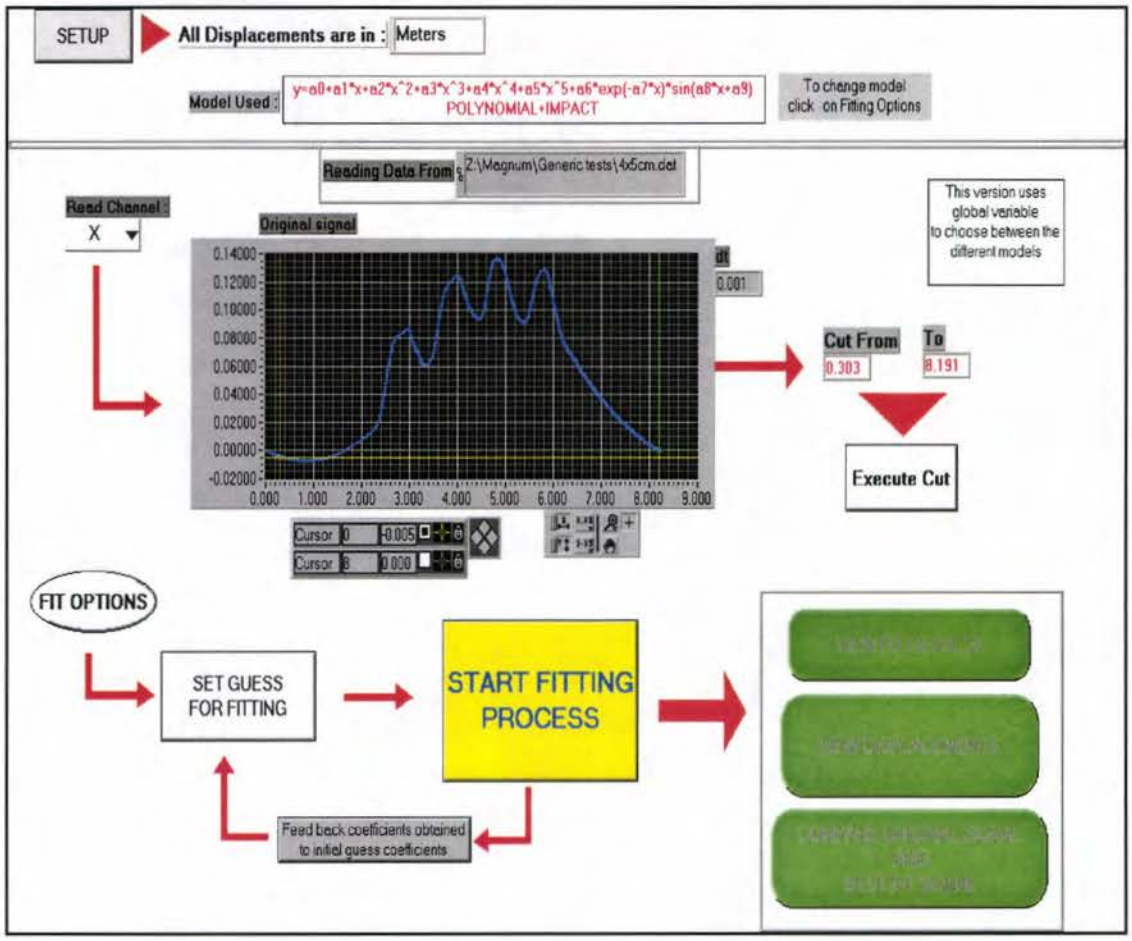

Figure 5.6 Front panel of the "*Displacement Estimation.vi*" instrument.

The program has been examined with different types of models for verification and testing purpose (polynomial model for the fit of undisturbed sensor output, Weibull function model for sensor after impact). However, for a general vehicle chassis impulse response data file, the best results are obtained with the model of Eq. 3.12. The model ($Y_{out}(A, B, t)$) can simply be chosen in the fit-options windows. The models and their respective equations are:

- Impulse response 1: Impulse response + Fifth order polynomial

$$Y_{out}(A,B,t) = a_0 + a_1 t + a_2 t^2 + a_3 t^3 + a_4 t^4 + a_5 t^5 + b_0 \exp(b_1 t)\sin(b_2 t + b_3) \tag{5.1a}$$

- Impulse response 2: Impulse response + Sum of exponential functions

$$Y_{out}(A,B,t) = a_0 \exp(a_1 t) + a_2 \exp(a_3 t) + b_0 \exp(b_1 t)\sin(b_2 t + b_3) \tag{5.1b}$$

- Impulse response 3: Impulse response + Weibull function

$$Y_{out}(A,B,t) = a_3 \frac{a_0}{a_1}\left(\frac{x}{a_1}\right)^{a_0-1} \exp\left[-\left(\frac{x}{a_1}\right)^{a_0}\right] + b_0 \exp(b_1 t)\sin(b_2 t + b_3) \tag{5.1c}$$

- Pure drift 1: Fifth order polynomial

$$Y_{out}(A,t) = a_0 + a_1 t + a_2 t^2 + a_3 t^3 + a_4 t^4 + a_5 t \tag{5.1d}$$

- Pure drift 2: Sum of exponential function

$$Y_{out}(A,t) = a_0 \exp(a_1 t) + a_2 \exp(a_3 t) \tag{5.1e}$$

- Pure drift 2: Weibull function

$$Y_{out}(A,t) = a_3 \frac{a_0}{a_1}\left(\frac{x}{a_1}\right)^{a_0-1} \exp\left[-\left(\frac{x}{a_1}\right)^{a_0}\right] \tag{5.1f}$$

- Pure Impulse response

$$Y_{out}(B,t) = b_0 \exp(b_1 t)\sin(b_2 t + b_3) \tag{5.1g}$$

5.3 Validation of the Displacement Estimation LabVIEW® Program

Two key aspects of the program have been verified: (1) the reliability of the estimation procedure and (2) the coherence of the estimated displacements. Two series

of tests have been conducted for that purpose. The first series tests the reliability of the parameter estimation algorithm. The second series aims to validate the polynomial model for the signal drift.

5.3.1 Testing the Reliability of the Parameter Estimation Procedure

To verify the efficiency of the separation of the drift error (modeled as a polynomial function) from the real displacements (modeled as an impulse response), the parameter estimation provided by LabVIEW®, i.e. the *"Non linear Lev-Mar.vi"* sub-VI, has to be tested.

5.3.1.1 Test Description

In that purpose, dummy experimental data files have been created using Eq. 3.12. For each file the time ranges from 0 to 16.384 s (equivalent to 16384 data at 1000 Hz). Arbitrary parameters have been chosen, as specified in Table C.1 (Appendix C), so that the signals created resemble to real experimental data. Comparing the arbitrarily chosen parameters and the estimated parameters (given by the estimation algorithm) allows the evaluation of the reliability of the procedure used in the program.

5.3.1.2 Results

Each file is processed five times (with "*Displacement Estimation.vi*") with different initial parameters. The error between the actual parameters (arbitrarily chosen) and estimated parameters is computed according to the Eq. 5.2.

$$Err = 100 \times \left| \frac{|p_{actual}| - |p_{estimated}|}{p_{actual}} \right| \tag{5.2}$$

where,

Err - error in percentage,

p_{actual} - actual value of the parameter,

$p_{estimated}$- estimated value of the parameter.

The complete and detailed results are given in Appendix C (Table C.2). It shows that the estimation algorithm is very accurate for parameters superior to 1E-2.

By demonstration, for the parameters defining the impulse response (b_0 to b_3 in Eq. 3.12), the average error is 0.023, which constitutes a ±2% accuracy. For very small parameters (inferior to 1E-3), the algorithm gives fairly inaccurate results with up to a ±200% error with respect to the original coefficient. However, this does not constitute a real problem since the small size of the coefficient does not influence the overall precision of the fit. Starting with bad initial parameters leads, in most cases, tovery inaccurate parameter estimations.

5.3.2 Testing the Performance of the Displacements Estimation

To validate the polynomial model for the signal drift, it is necessary to check the plausibility of the results given by the program. Experimental data files, where the displacements are precisely known, have been collected and used to test the program.

5.3.2.1 Test Description

To achieve highly accurate and precise displacements, a numerically controlled positioning system (XY table) has been used (Fig. 5.7). A LabVIEW® program, especially made for this series of tests, controls the table. The sensor used is a capacitive DC accelerometer (Kistler model 8302A10). It is mounted on the surface using wax. The data is recorded using the same data acquisition system as in Section 4.2. Another computer is necessary to run the positioning system controller program. The positioning system and the computer communicate through a serial port.

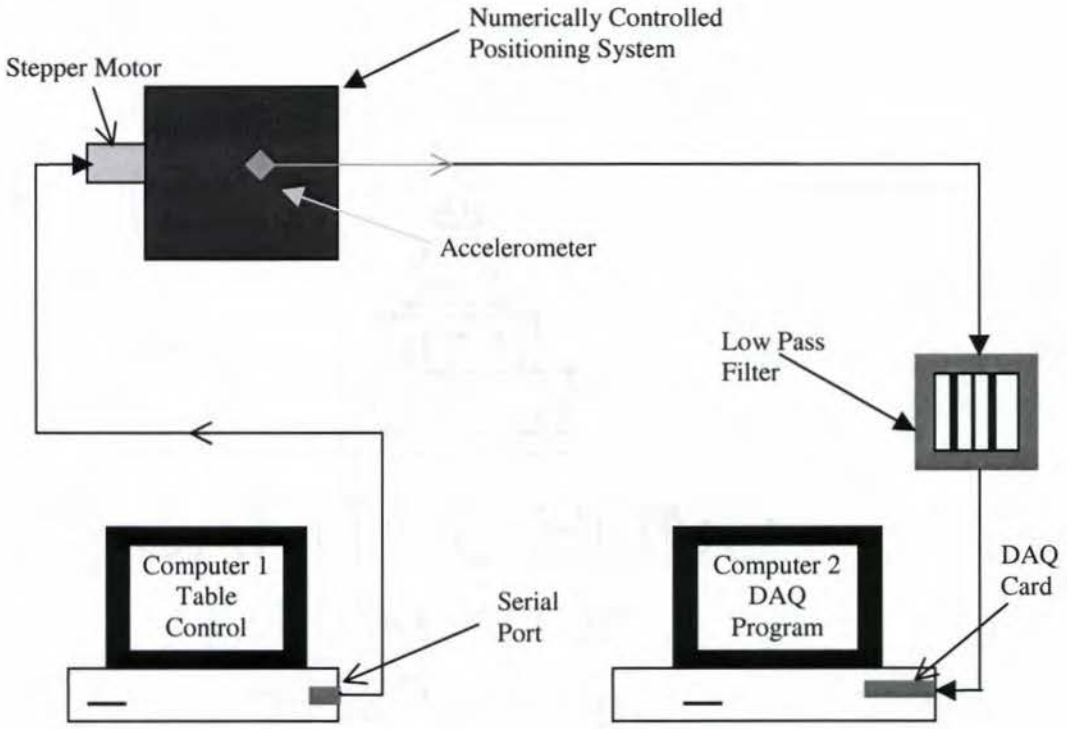

Figure 5.7 Positioning system test experimental setup.

The positioning system has been preliminarily calibrated. From the front panel of the table controller program, the user can choose between two modes of

displacement. For the first mode, the controller sends one single pulse train to the step motor, which triggers a displacement in one phase. For the second mode, the controller sends one pulse train to the step motor, pauses, and sends another pulse train, which triggers a displacement in two phases. A setup feature allows the adjustment of the length of each pulse train (cm) and the length of the pause (ms). The controller program's front panel is shown in Fig. 5.8

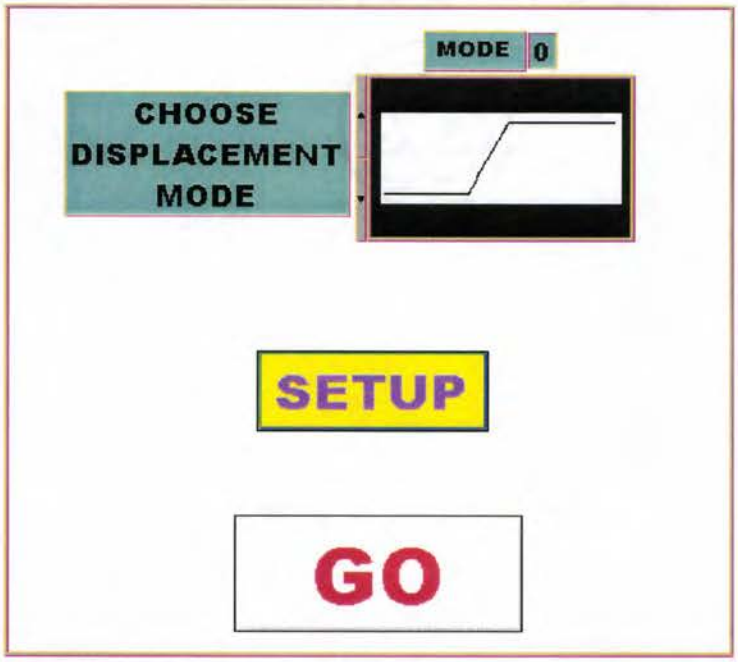

Figure 5.8 Front panel of the positioning system controller.

Several data files were recorded and processed. The processing has been done with an adapted version of *"Displacement Estimation.vi"*. The actual estimation is performed only on the stationary part of the signal (0 to t_1, t_2 to t_3, and t_4 to t_5 on Fig. 5.9). The actual displacements generated by the system are illustrated in Fig 5.9

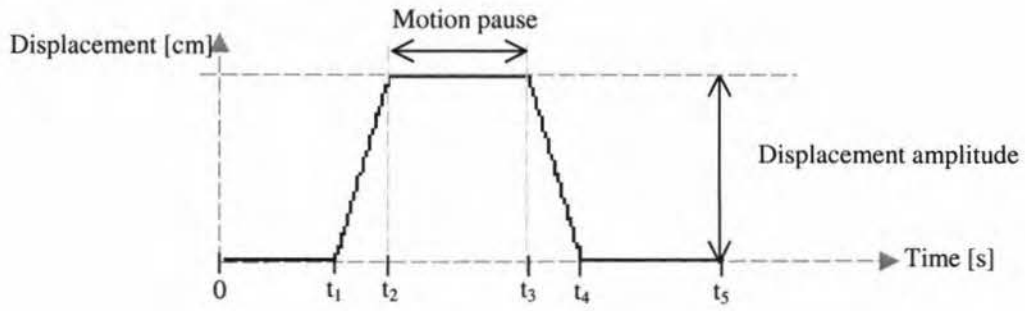

Figure 5.9 Example of anticipated actual displacements.

The model for the raw displacement, $Y_{out}(A,B,t)$, is the sum of a fifth order polynomial (drift) and discontinuous step function for the real displacement, as defined in Eq. 5.3.

$$Y_{out}(A,B,t) = \begin{cases} a_0 + a_1 t + a_2 t^2 + a_3 t^3 + a_4 t^4 + a_5 t^5 + 0 & for\ 0 < t < t_1 \\ a_0 + a_1 t + a_2 t^2 + a_3 t^3 + a_4 t^4 + a_5 t^5 + x_0 & for\ t_2 < t < t_3 \\ a_0 + a_1 t + a_2 t^2 + a_3 t^3 + a_4 t^4 + a_5 t^5 + 0 & for\ t_4 < t < t_5 \end{cases} \quad (5.3)$$

Therefore in this case, A is the set $\{ a_0, a_1, a_2, a_3, a_4, a_5 \}$ and B is the singleton $\{x_0\}$. After obtaining the estimates of the parameters for the drift model (A), the estimated drift error is recomputed for t ranging from 0 to t_5 and then subtracted from the original displacement signal. The x_0 value obtained from the estimation procedure represents the estimated actual displacement. The actual displacement value is already known from the values used in the positioning system controller program setup.

The specifications of the test are summarized in Table 5.1. The displacements generated are identical to those on Fig. 5.9.

File Number	0, 1 and 2	3, 4 and 5
Sampling Frequency [Hz]	1000	1000
Number of Data	8192	16384
Measured Peak-to-peak acceleration	4.8 m/s^2	4.8 m/s^2
Velocity of Motion	1.3 cm/s	1.3 cm/s
Actual Displacement Amplitude [cm] (For $t_3<t<t_4$)	3	5
Motion Pause Length [ms]	1000	1000

Table 5.1 Test specifications

Two pulse trains are sent: one moves the table in one direction and the second returns the table to its starting position after a pause. The precision on the displacement amplitude generated by the positioning system is approximately half a millimeter.

5.3.2.2 Results

The next series of figures compares the signal-based and model-based estimates of displacement for two tests.

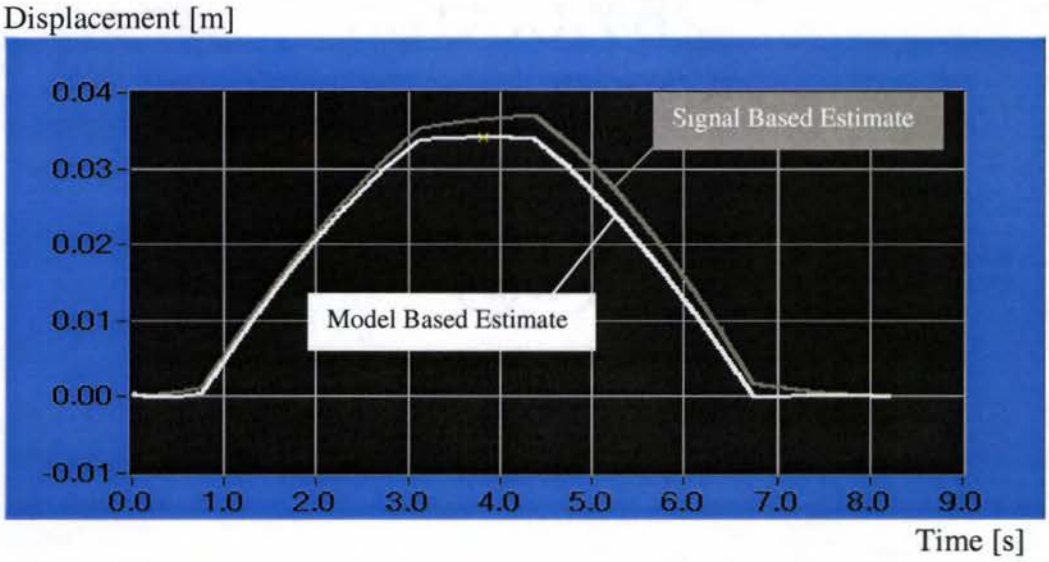

(a)

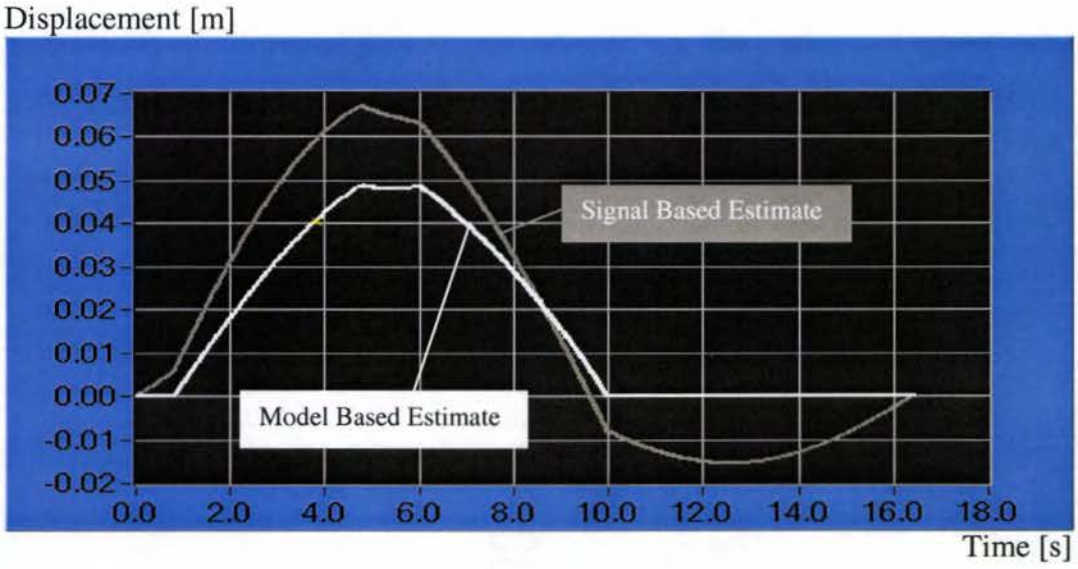

(b)

Figure 5.10 Estimates of displacements obtained for test 1 (a) and test 5 (b)

Table 5.2 compares the amplitude of the displacement for the signal-based estimate and the model-based estimate (X_0 in Eq. 5.3). The percentage error is computed according to Eq. 5.2.

Test #	Actual Value [cm]	Signal Based Value [cm]	%Error	Model Based Value [cm]	%Error
				Xo	
1	3	3.7	23.33	3.4	13.33
2	3	3.3	10.00	3.2	6.67
3	3	3.7	23.33	3.2	6.67
4	5	7.1	42.00	5.1	2.00
5	5	6.3	26.00	4.8	4.00
6	5	7.9	58.00	4.9	2.00
		Average	30.44		5.78

Table 5.2 Error percentage obtained on signal-based and model-based estimates of the displacement.

The average accuracy achieved by the estimation procedure decreases the error to less than 6%, constituting a significant improvement with respect to the 30% error obtained before the estimation procedure. This test shows that the method developed significantly improves the accuracy of the displacement measurement. However, the model-based estimate of displacements (Fig. 5.10) does not match actual anticipated displacements (Fig.9). Translations by the XY table are accomplished at a constant speed. On Fig. 5.10, the model-based estimate of displacement between (t_1 and t_2) and (t_3 and t_4) do not exhibit constant velocity. This shows that, even if the error has been significantly reduced by the estimation procedure, the actual displacement signal is not totally recovered. However, the amount of error remaining (<6%) shows that the displacement signal has been improved.

5.4 Bump Test Experiment

The bump test experiment constitutes the actual implementation of this research in terms of vehicle dynamics evaluation. The visualization of the chassis' response to a sudden impulse, like riding over a bump, and considering only the vertical displacements, yields information useful for the evaluation of the chassis dynamics.

5.4.1 Test Apparatus and Records Processing

The test was performed on a standard car (Saturn Station Wagon) and on a large recreational vehicle (Safari motor home, having a chassis manufactured by Magnum, Inc). The test performed on the car will be described in detail. The tests with the recreational vehicle have not been performed on campus, but by the manufacturing company itself. The only difference between the two series of tests is that the recreational vehicle is driven over a ditch, instead of a bump.

The car was driven over the obstacle at a low speed (5 Mph). The obstacle consists of two pieces of wood (section: height 4'' by width 8''), one for each wheel. The backseat was reclined so that the sensor could be mounted on the trunk's frame. Thus, the sensor is located right above the rear axle where the backseat normally rests. The acceleration was recorded using the data acquisition system described in Section 5.1. The test set-up is illustrated below:

Figure 5.11 Bump test set-up

The same DAQ system has been used (see Section 5.2.1). Each record was sampled at 1000 Hz and started manually just before the front wheels touch the obstacle. Five records have been taken. Each is composed of 8192 data points for each of the three channels, one channel being assigned to each direction (vertical, horizontal and lateral). Two records acquired with the recreational vehicle are available.

The records have been processed with the LabVIEW® program "*displacement_estimation.vi*" using Eq 3.12 as a model of the signal-based displacement, ($Y_{out}(A, B, t)$). The estimation procedure has to be performed on the impulse response of the system. This implies that the signal has to be trimmed so that it starts at the instant of impact on the rear wheels.

5.4.2 Results

First the results obtained with the car are presented (based on 5 different files). Second, the results obtained for motor home are presented (based on 2 different files).

5.4.2.1 With the Car

The following figures illustrate the results obtained for one of the data file collected. Each figure represents one step in the analysis procedure.

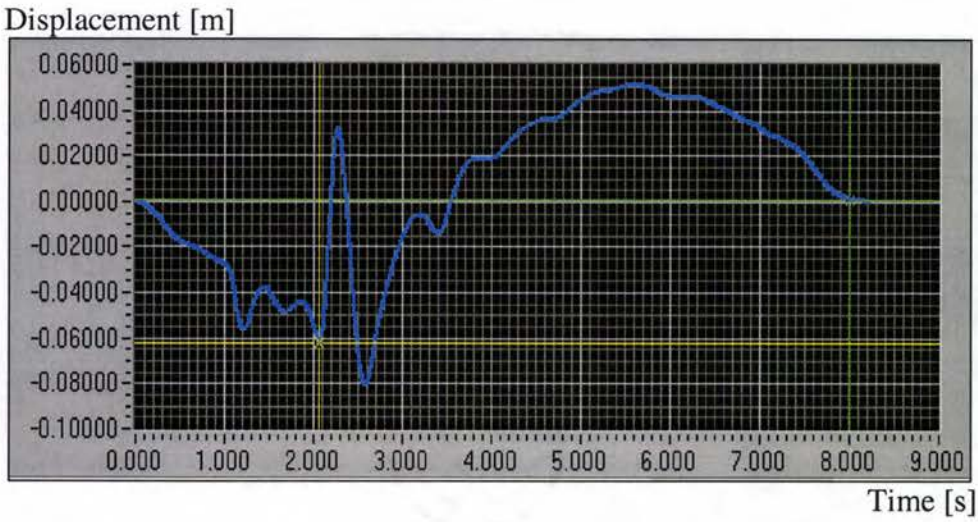

Figure 5.12 Displacement signal based estimate

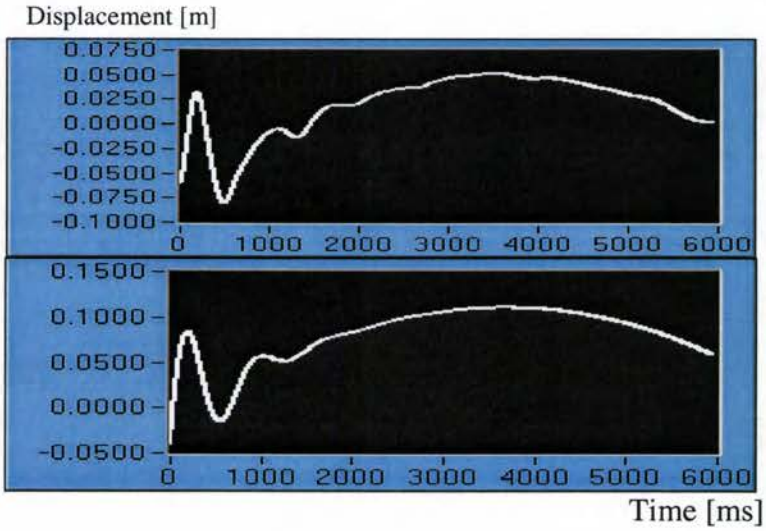

Figure 5.13 Signal after trim (top) compared to initial parameters signal (bottom).

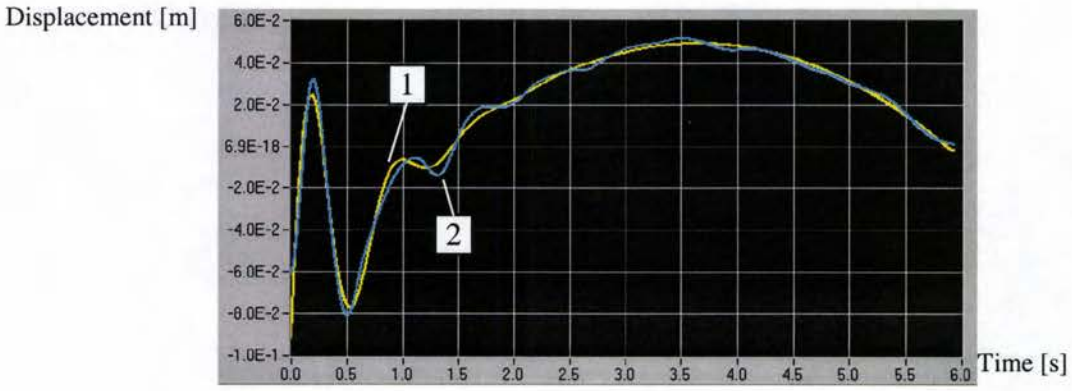

(a)

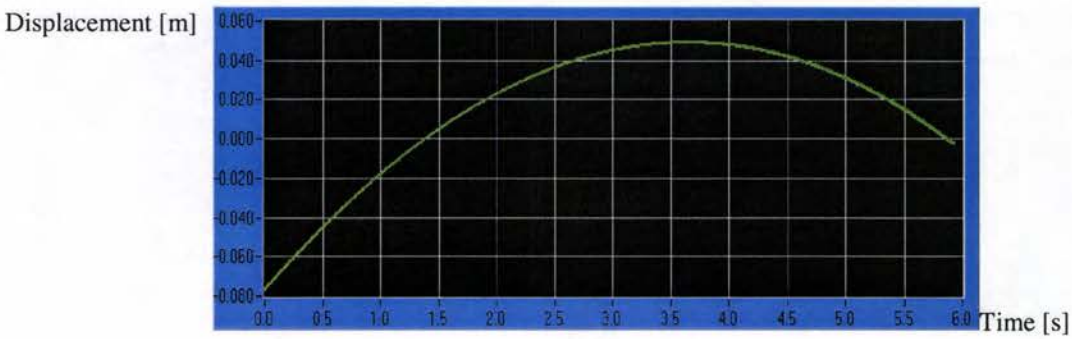

(b)

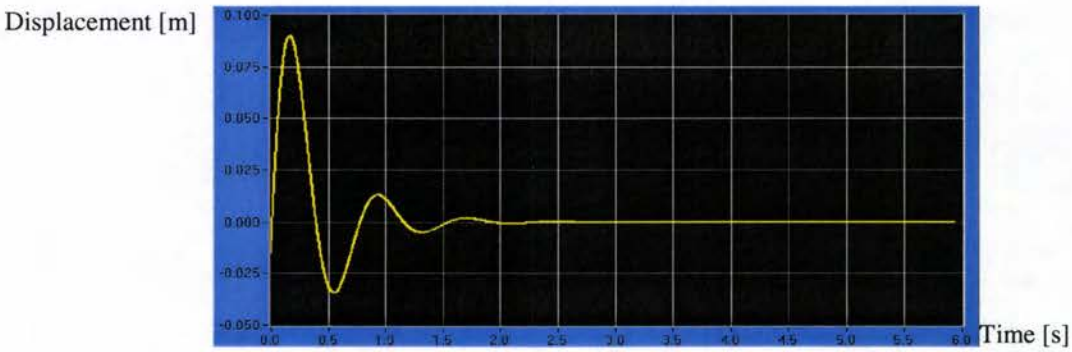

(c)

Figure 5.14 Model-based estimate of displacement signal (1) compared to the original signal (2) (a) and decomposition in estimated drift (b) and estimated actual displacements (c).

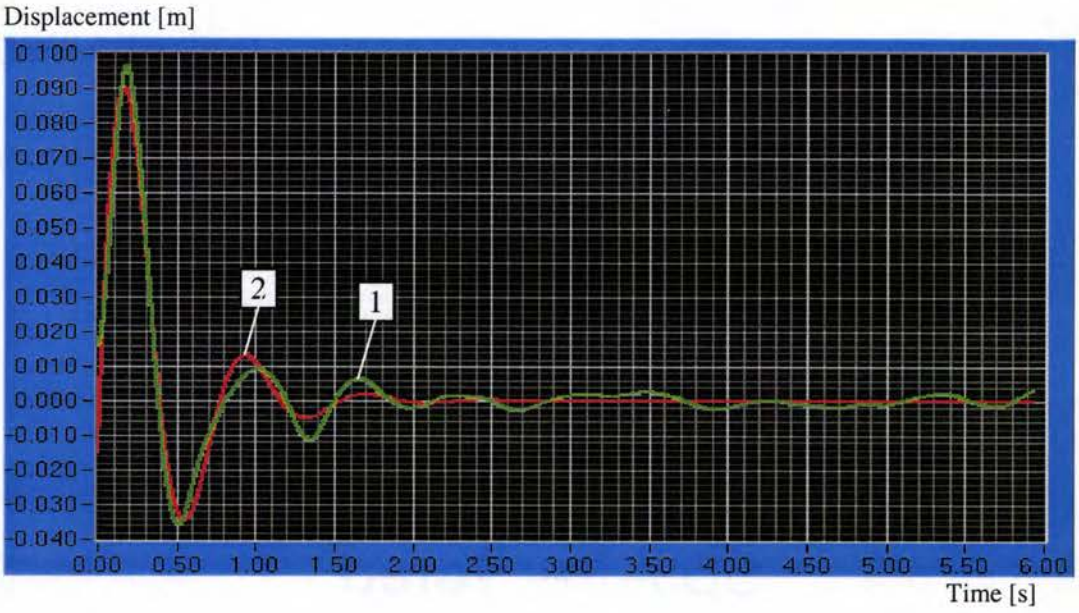

Figure 5.15 Error due to non modeled phenomena: comparison of the model-based estimate of displacement (1) and the raw signal minus the model-based estimate of the error caused by drift (2).

The Table 5.4 shows the estimated parameters (yielded by the Levenberg-Marquardt algorithm). For this test, according to the parameters estimated, the natural angular frequency and the damping ratio are:

$$\begin{aligned} \omega_n &= 8.39\, rad/s = 1.34\, Hz \\ \xi &= 0.281 \end{aligned} \tag{5.3}$$

a_0	-7.68E-02
a_1	6.79E-02
a_2	-8.85E-03
a_3	-8.44E-05
a_4	0.00E+00
a_5	0.00E+00
b_0	1.44E-01
b_1	2.52E+00
b_2	8.21E+00
b_3	-1.03E-01

Table 5.3 Estimated coefficients obtained for a "bump test" data file.

Table 5.4 shows the different values obtained for ω and ξ for the 5 data files recorded.

test	ω [*rad/s*]	ξ
#4	9.58	0.336
#5	9.44	0.287
#6	8.51	0.271
#7	8.3	0.263
#8	8.29	0.264
Average	8.824 = 1.4 Hz	0.2842

Table 5.4 Values for the natural frequency and damping ratio.

5.4.2.2 With the Motor-home

The investigations on the recreational vehicle have been conducted on two different files taken in similar conditions as with the car. The same program is used to process the files ("*displacement_estimation.vi*"). For one data file, the signal-based estimate of displacements, the model-based estimate of displacements and the decomposition into estimated error caused by drift and estimated actual displacement are presented.

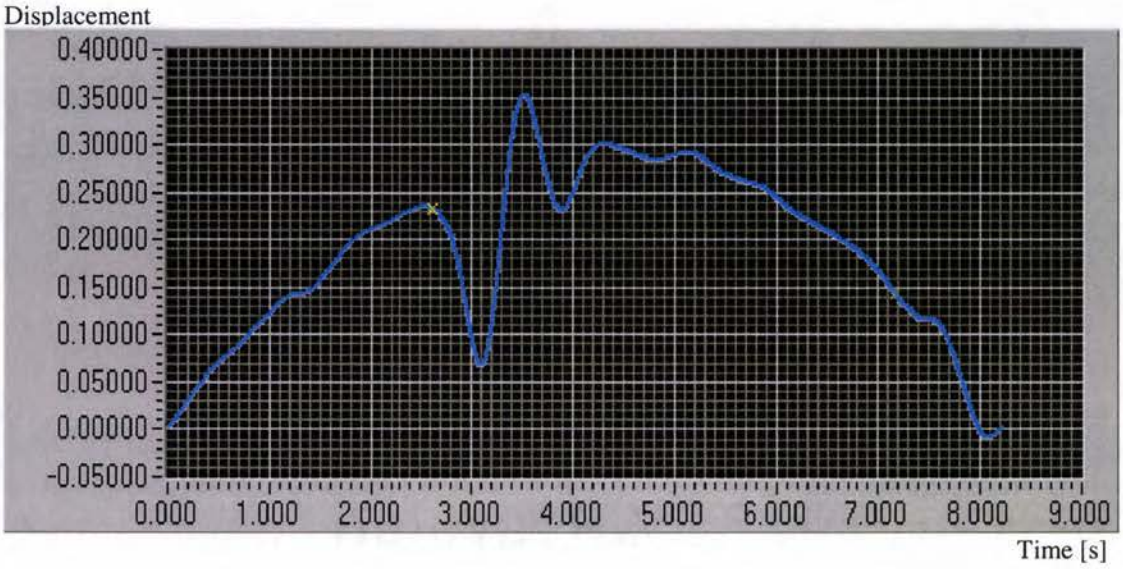

Figure 5.16 Signal-based estimate of displacements.

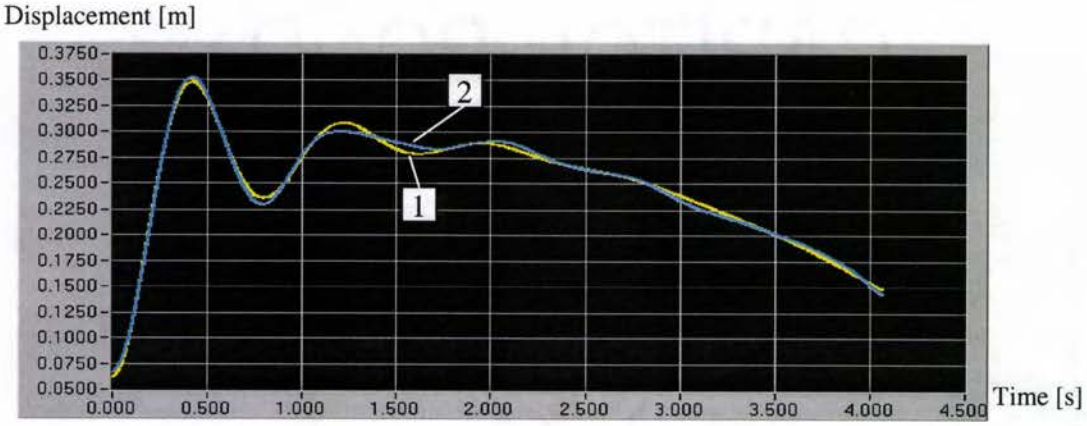

(a)

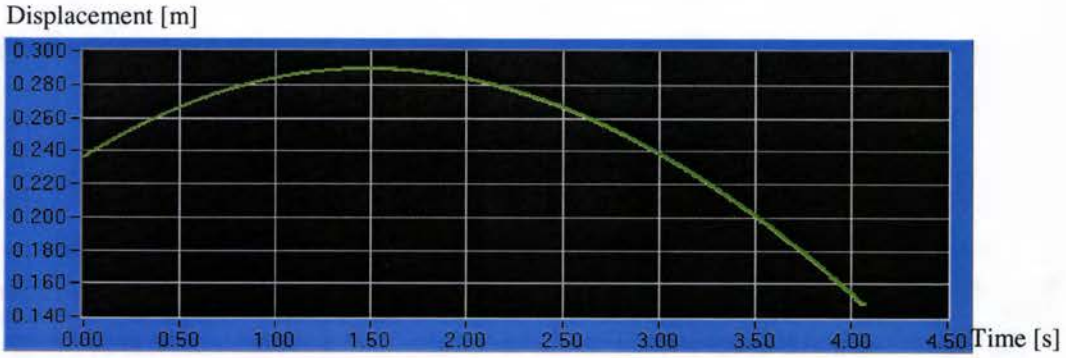

(b)

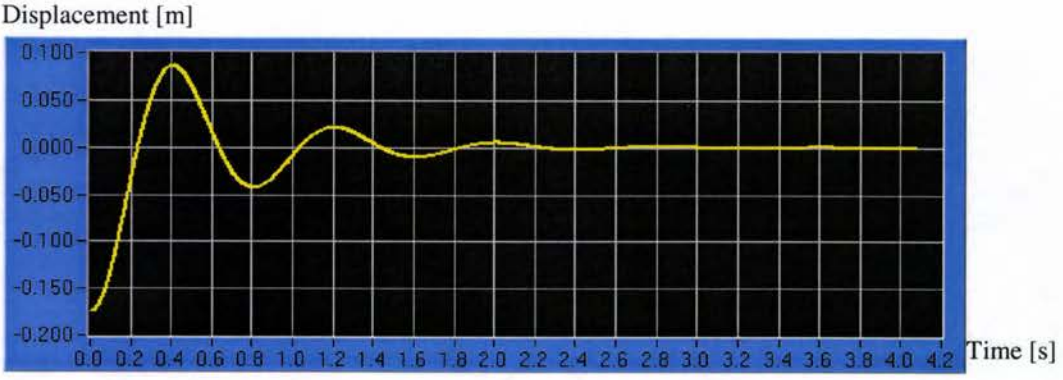

(c)

Figure 5.16 Model-based estimate of displacement signal (1) compared to the original signal (2) (a) and decomposition in estimated error caused by drift (b) and estimated actual displacements (c).

Table 5.5 shows the different values obtained for ω and ξ for the 2 data files recorded.

test	ω [*rad/s*]	ξ
#0	8.07	0.220
#1	8.83	0.244
Average	8.45 = 1.34 Hz	0.232

Table 5.5 Values obtained for the natural frequency and damping ratio.

5.4.3 Discussion of the Results Obtained

The estimation procedure proves to be insensitive to inaccurate estimates of initial parameters. By classical design of motor vehicles, the sprung mass (Fig. 2.5) is chosen to have its natural frequency just above 1Hz. (SAE, 1992). Therefore, the natural frequency and the damping ratio evaluated by the program yields realistic values. Moreover, The procedure yields reasonable values for the first oscillation's peak-to-peak amplitude of the model-based estimate of displacements (25 cm for the recreational vehicle and 10 cm for the car). This demonstrates that the combination of the bump test and the displacement estimation procedure render feasible the evaluation of physical characteristics of the system

CHAPTER 6

CONCLUSIONS AND RECOMMENDATIONS

6.1 Conclusions

A method to estimate displacement of a vehicle body using an accelerometer combined with a model based signal estimation procedure is proposed. The whole operation, from data acquisition to displacement estimation, has been implemented using computer programs written in the LabVIEW® programming environment.

As demonstrated herein, impact excitation of a sensor triggers a significant drift in the output signal. This drift is attributed to an internal heat release. This thermal phenomenon renders traditional signal drift attenuation techniques unusable. The underlined concepts involved in the actual displacement estimation can be summarized as the use of mathematical models for the; (1) anticipated vehicle displacement and (2) signal drift. The empirical model used for the drift (fifth order polynomial) is validated by tests performed on a numerically controlled positioning system (XY table). The average error in the displacement value obtained from the signal-based estimate (30.5%) is reduced, by applying the model-based estimation, to 5.8%. The estimation method applied on vertical displacements of a vehicle riding over a bump yields very acceptable values (peak-to-peak value of 10 cm for a car and 25 cm for a large recreational vehicle). Moreover, realistic values for the natural frequency and damping ratio of the suspension system have been obtained (f_n = 1.4 Hz and ξ = 0.284 for the car, f_n = 1.34 Hz and ξ = 0.232 for the large recreational vehicle). Using accelerometers to measure vehicle chassis displacements appears to be feasible.

The simple models used allow a significant reduction of the computational time needed by the estimation algorithm. On the other hand, they do not model every

phenomenon occurring in the sensor and acquisition processes, resulting in limited reliability and accuracy of the estimation procedure. The difference function between the estimated signal and the original signal, even though of a small magnitude, does not exhibit a random nature. It demonstrates limitations in the output signal model used. As a result, the actual displacements are not totally recovered from the corrupted signal. Therefore the model needs improvement to obtain more accurate results. Moreover the method proposed herein require the instant of impact in the raw displacement signal to be precisely identified. This is difficult with field testing of vehicles. Moreover, a bad identification of the impact instant can notably affect the parameter estimation results.

6.2 Recommendations and Possible Applications

The model based displacement estimation can be improved by employing the following development options.

- Considering the axle and the chassis as two independent masses (quarter car model) would increase the fidelity of the model, which aids the identification of the chassis response. Besides, non-linearity of shock absorbers should be included in the suspension modeling.

- Inclusion of time shift as an additional estimated parameter. Precise identification of the instant of impact in the raw displacement signal would not be required anymore.

- The internal heat released in the sensor after an impact, as highlighted in this thesis, causes a drift that can be modeled as a Weibull function. A combination of polynomial and Weibull function should be, therefore , a better descriptor of the total signal drift.

- The signal drift is not the only source of distortion of the output signal. Other phenomena, for example tribo-electric noise, should be investigated, ultimately for inclusion in the sensor output model development, which would expand the capabilities of the whole model.

- The Levenberg-Marquardt method is efficient and easy to implement. However, as it can only detect local minimums for unconstrained problem, its applicability is limited. Robust estimation procedures are needed for reliable application of the proposed displacement measurement technique.

- The use of a high quality servo accelerometer should be investigated for further improvement of the accuracy of the proposed model-based estimation of displacements.

- Good results obtained in the tests performed with a numerically controlled positioning system indicate that the proposed method has potential applications in short term precision displacement measurement for machine tools. It is especially efficient with simple displacement signals (step, ramp displacement). The feasibility and expected accuracy of the method in this application should be further investigated.

BIBLIOGRAPHY

Barak, P. Magic Numbers in Design of Suspension for Passengers Cars. GMI Engineering & Management Institute, SAE Paper #911921, 1988.

Bjorn, Knudsen and Sprunger. Design and Development of Gyroscope Testing Equipment for Vehicle Dynamics Testing (Senior Project). Oregon State University, 1999.

Bruel & Kjaer. Measuring Vibration. Available from Bruel & Kjaer, 1982.

Bruel & Kjaer. Vibration Testing. Available from Bruel & Kjaer, 1983.

Corolla, D.A. Chen, D.C. Whitehead, J.P. & Alstead, C.J. Vehicle Handling Assessment Using a Combined Subjective-Objective Approach. The Motor Industry Research (MIRA) Web site, 1998.

Doebelin, E. O. Measurement System: Application and Design. McGraw-Hill, Inc., 1990.

Doscher, J. Accelerometer Design and Applications. Analog Devices, Inc., 1998.

Durham Instruments. Accelerometer Products. Available from Durham Instruments, 1998.

Dycor Industrial Research. Ltd. Piezoresistive Accelerometers. Available from Dycor Industrial Research Ltd., 1997.

Gillespie, T. D. Everything You Always Wanted to Know about the IRI. The University of Michigan Transportation Research Institute, 1992.

Gillespie, T. D. Heavy Truck Ride. Society of Automotive Engineers, Inc., 1985.

Heitzman, E. J., Heitzman, E. F. Topsy, the Heitz Chassis Lab Measurement System. Available from Heitz chassis Lab, Inc web site. 1995.

IDIADA vehicle dynamics department. Vehicle Dynamics. Available from www.idiada.es, 1998.

ISO 2631. Evaluation of human exposure to whole-body vibration. International Organization for Standardization, 1997.

Jitpraphai, T.. Model Based Visualization of Vibrations in Mechanical Systems. Oregon State University, 1997.

Kistler Corporation. Technical Glossary. Available from Kistler Instrument Corporation, 1998.

Kistler Corporation. K-Beam Capacitive Accelerometers: Operating Instructions. Available from Kistler Instrument Corporation, 1997.

Kitchin, C. and Brokaw, P. Compensating for the 0 g Offset Drift of the ADXL50 Accelerometer (AN-380). Available from Analog Devices, 1997.

Kitchin, C. Make Wide Temperature Range, ultra Low Drift Accelerometer Using Low Cost Crystal Oven. (AN-385). Available from Analog Devices, 1997.

LaPierre, C. Personal Navigation System for the Visually Impaired. Carleton University, 1998.

Lawrence, A. Modern Inertial technology. Springer-Verlag, 1992.

Lemaire, Christophe and Sulouff, Bob. Surface Micromachined Sensors for Vehicle Navigation Systems. Analog Devices, Inc., 1995.

Litton Systems, Inc. G2000 Gyroscope: Users Guide. Available from Litton Systems, Inc., 1997.

Livesay, E. Design, Creation, and Proper Use of a Drag Device for the Determination of Drag factor, 1998.

Lotus Engineering. Vehicle Dynamics. Lotus Engineering Web page, 1999.

Martin, G.J. IEEE Spectrum., 1986.

National Instruments. LabVIEW Analysis VI Reference Manual. National Instruments, 1994.

National Instruments. LabVIEW for Windows User Manual. National Instruments, 1994.

Nwagboso, C. O. Automotive sensory systems. Chapman & Hall, 1993.

Phun, F. How to make your car handle. HP books, 1981.

Olkin, I., Gleser, L., Dernam, C. Probability Models and Applications. Macmillan Publishing Co., Inc., 1985.

Press, Flannery, Teukolsky and Vetterling. Numerical Recipes. Cambridge University Press, 1986.

Putnam, W., Knapp, R. B. Input/Data Acquisition System Design for Human Computer Interfacing. Stanford University, 1996.

Schaller, C. Introduction à la mesure de vibrations avec capteur piézoéléctrique et amplificateur de charge. Ecole d'Ingénieurs du Canton de Neuchâtel, 1997.

Smith, J. D. Vibration Measurement and Analysis. Butterworths, 1989.

Society of Automotive Engineers. Truck Systems Design Handbook. Warrendale, PA, 1992.

Space Telescope Science Institute Aspec. Online User Guide. STScI Web Page, 1997.

Verplaetse, C. Inertial proprioceptive devices: Self-motion-sensing toys and tools. MIT Media Lab, 1993.

Verplaetse, C. Can a Pen Remember What It Has Written Using Inertial Sensors?. Physics and Media, 1995.

Wong, J.Y. Theory of Ground Vehicles. John Wiley & Sons, Inc, 1996.

Zeid, A. Introduction to Vehicle System Dynamics. Wayne State University,1989.

APPENDICES

Appendix A
Issued That Must Be Addressed In Ride Quality

What follows are the areas that must be dealt for the interpretation of accelerometer data in terms of ride quality evaluation.

A.1 Mounting accelerometers

One of the first areas, which will need to be addressed, is the mounting location of the accelerometers. The location of accelerometers used to measure ride quality is extremely important. Accelerometers are required at several different locations. As a general rule, vibration transmitted to the body should be measured between the body and the transmitting surface. These locations are between the person and the seat bottom, the seat back, the floor, and the steering wheel. The reason so many accelerometers are needed is that no single interface determines whether a ride is good or bad. ISO paper number 10326-1 gives a commonly used design for seat vibration measurements (ISO, 1997). Along with placing the accelerometers at the transmitting surface they also need to be aligned with the relevant principle axes, which are shown in Fig. 1.

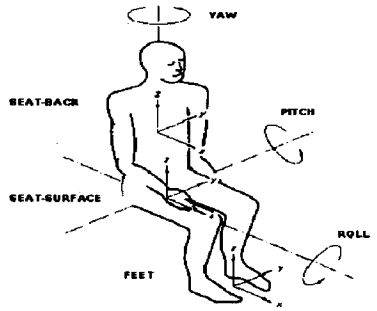

Figure A.1 Primary Axes in seated position (ISO 2631, 1997).

If the person is seated on an incline seat, the axis of the body is considered preferential and therefore the z-axis does not have to be vertical. However, the angle between the z-axis and the direction of gravity should be noted. ISO paper 2631-1 also notes that, when it is not possible to measure vibrations at the point of contact, accelerometers can be placed on a rigid section of the vehicle at the center of rotation or center of gravity (1997). However, this method requires additional calculations and knowledge of the vehicles dynamic characteristics in order to evaluate the response of the driver or passenger. Another alternative to measuring the response at the back is to relocate the accelerometer to the seat structure directly behind the contact point. The problem associated with this method is that the transmissibility of the seat must be taken into consideration.

In past experiments, accelerometers were used to measure the level of vibration associated with the vertical, lateral, and fore-aft directions. Since there are set limits to the level of vibration, which is comfortable to the average human, a rating of comfort based on vibration is possible to attain. A vehicle's ride quality can then be found by comparing results to human comfort curves. However, the comfort curves (Figs. 5-6) which exist are only broad indicators of what is considered by most people to be comfortable or not. Since no two people are going to have identical feelings on what is comfortable and what is not, interpretation of the data collected would require an enormous amount of testing and setting of benchmarks.

A.2 Evaluation of the results

The information collected is going to be used as a standard to be compared against. In the future, each model of motor coach for Magnum will be taken out and tested for its handling performance. This data will then be stored until someone has a complaint about his or her vehicle's handling. At this time, the customer's vehicle can be tested under the same conditions and compared to the original test. If the data turns out to be the same as the standard, then the problem is with the person's perception of

the handling. If the data turns out to be different, then the vehicle needs to be inspected to determine the cause of the problem.

Since every person's perception of a "good" or "bad" ride differs from the next person, a final set of guidelines for determining ride quality would be almost impossible to make. This is perhaps the reason that throughout our research we have found no mention of gyroscopes being used to evaluate ride quality. The correlation of human feelings to linear accelerations and rotational movements is an enormous task and will require much testing.

Individual factors that can effect perception of ride quality are age, gender, size, fitness, experience, expectation, arousal and motivation, body posture, financial involvement, and activities (driver or passenger). Perception of ride quality is also different due to "Power Absorption". Power absorption is defined by Wong as the rate at which vibrational energy is absorbed by the human body (1993). With every person having a different body composition, his or her power absorption is also going to be different. This leads to each person having a different perception of how the ride feels to them.

Due to the subjectivity of ride quality and power absorption, engineers have been trying for years to collect data and set benchmarks that would differentiate between a "good" and "bad" ride. To do this, comfort curves were created that show a person's level of comfort based on the frequency and magnitude of vibration.

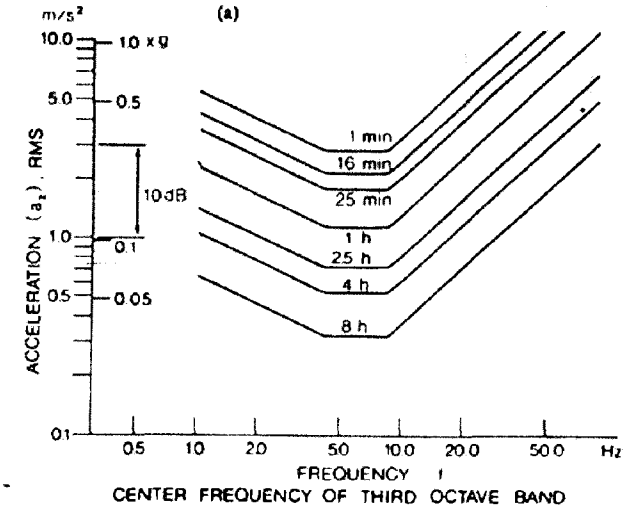

(a)

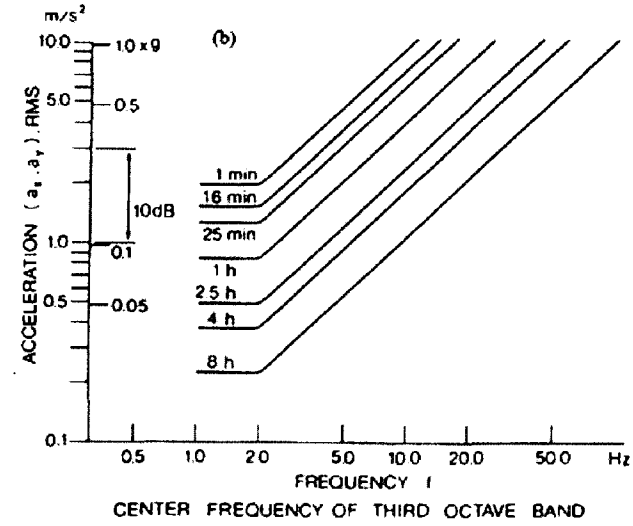

(b)

Figure A.2 Limits of whole-body vibration for fatigue or decreased proficiency in (a) vertical direction and (b) transverse direction, recommended by ISO 2631 (ISO, 1997)

The problem with these curves is that most of the data collected for their creation was gathered using only one testing frequency at a time. This is different from real

driving conditions where vibrations occur randomly. So, while these curves give us a good idea of what vibrations to avoid, they are not an exact measure of what is a "good" or "bad" ride.

A.3 Current methods of determining ride quality

Today, there are four different ways of testing for the ride quality of motor vehicles. They are as follows (Wong, 1993).

1. *Subjective Ride Measurements.* The traditional technique for comparing vehicle ride quality in the automotive industry in the past is to compare vehicles driven over a given road section with a trained ride jury. With a large enough jury and a well-designed evaluation scheme, this method could provide a meaningful comparison of the ride quality, however, ride cannot be quantitatively determined by this type of subjective evaluation.

2. *Shake Table Tests.* In an attempt to quantitatively study human response to vibration, a large number of shake table experiments have been performed over the years. Most of this research pertains to human response to sinusoidal excitation. It is intended to identify zones of comfort (or discomfort) for humans in terms of vibration amplitude, velocity, or acceleration in a given direction (such as foot-to-head, side-to-side, or back-to-chest) over a specific frequency range.

3. *Ride Simulator Tests.* In these tests, ride simulators are used to replicate the vibration of the vehicle traveling over different road surfaces. In some facilities, an actual vehicle body is mounted on hydraulic actuators, which reproduce vehicle motions in pitch, roll, and bounce (see Fig. 2.20). Using the simulator, it is possible to establish a human subjective tolerance limit in terms of vibration parameters.

4. *Ride Measurements in Vehicles.* Shake table tests and ride simulators tests described above are conducted under laboratory conditions. They do not necessarily provide the same vibration environments to which the passenger is subject while on the road. Therefore, on-the-road ride measurements, particularly for passenger cars, have been performed. This test method attempts to correlate the response of test subjects in qualitative terms, such as "unpleasant" or "intolerable," with vibration parameters measured at the location where the test subject is situated under actual driving conditions.

Appendix B

Drift Tests on Accelerometer Kistler K-Beam® (model 8302A10 S1)

B.1 Test Setup

The tests have been conducted on a Kistler K-Beam® (model 8302A10 S1). This accelerometer is similar to the one described in section 2.3.3.1, but with only one operating axis instead of three. The following DAQ setup has been designed to perform the tests.

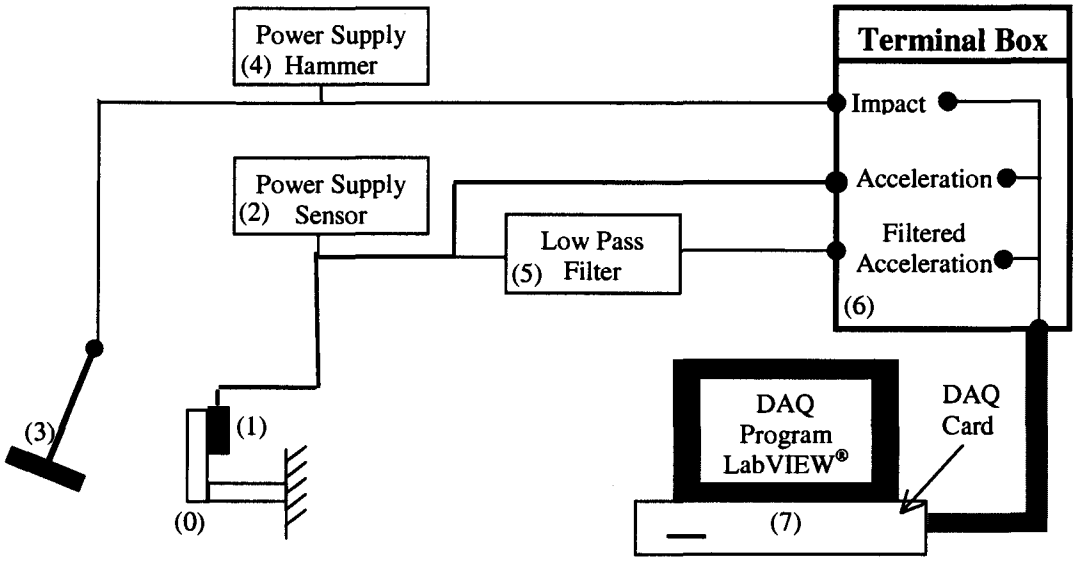

Figure B.1 Drift tests experimental setup.

It includes: (0) a steel "C"-shaped fixture, (1) the accelerometer, (2) and its power supply, (3) an impact hammer (Load cell type 208b03 from PCB®)and (4) its power supply, (5) an analog low pass filter (Precision® 88B cutoff frequency on 100Hz), (6) a terminal box (from National Instruments®), and (7) a computer equipped

with a DAQ card (AT-MIO 16 E2 from National Instruments®) and running a DAQ program designed with LabVIEW®. The sensor was glued on a steel clamp with soft wax so that it measures the acceleration along the horizontal axis. With this setup, the program is able to record at the same time; the sensor output, the sensor output filtered and the impact signal.

B.2 Test on a undisturbed Accelerometer (no External Excitation)

Signals coming from a undisturbed accelerometer were recorded (both with and without filter). Since there is no displacement the signal recorded is theoretically a flat zero line. Therefore any fluctuations around the zero level can be attributed to the signal drift and noise corrupting the signal. 13 records where taken while the undisturbed sensor.

B.2.1 Tests Specifications:

13 similar tests have been made. All of them have been performed at a 1000 Hz sampling rate with ±0.1 V full-scale sensitivity, which is the smallest available for the A/D card used converted respect to the accelerometer sensitivity allow the acquisition of data within a ±0.2 g or ±1.862 $m.s^{-2}$ range. The specifications of these tests are recalled in Table 3.1.

Sampling Frequency	1000 Hz
Full-scale Range (on DAQ card)	±0.1 V
Max Acceleration Measurable	0.2g
Filter Cutoff Frequency	100 Hz
Number of Data	16384
Records Length	16.384 s
Number of Records Acquired	13

Table B.1 Tests specification for undisturbed sensor

B.2.2 Complete Results

Fig. B.1 shows an example of the result obtained for the polynomial fit. A LabVIEW program specially designed as been used.

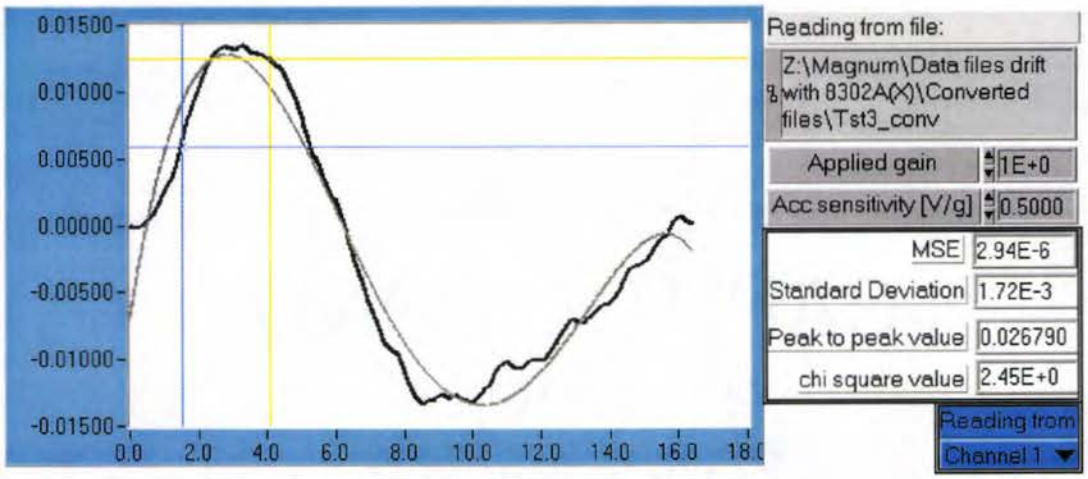

Figure B.2 Polynomial fit (gray) on the double integrated output of an undisturbed accelerometer (black).

On Fig B.2, the signal begins and ends at the zero level. This is a consequence of the integration process. The boundary conditions applied here are a null displacement at the beginning and the end of the sample, which corresponds to the physical reality. This forces the double integrated signal to go to zero at each end.

Two features has been examined for each double integrated data file; firstly its peak to peak value is computed and secondly its polynomial shape is investigated by a fit to a 5^{th} order polynomial. Results for each data file (fit and peak to peak value).The average value of the peak to peak value over the 13 records is 1.9 cm. The interval of confidence for 95 percent level is ±1.2 cm . In other word, we can be 95 percent confident that (for a record of 16 second long), the peak to peak value of the error resulting for the signal drift lie in the in the interval 1.9 ± 1.4 cm.

The Table B.2 shows the mean square error (MSE), standard deviation of the double integrated output of the sensor and the fitted polynomial as well as the peak to peak (still for the double integrated output of the sensor).

Data file:		MSE	Sd deviation	Peak to Peak
		[m]	[m]	[m]
Tst1 no filter		3.20E-06	1.79E-03	0.04880
Tst1 w/ filter		9.54E-07	9.77E-04	0.04653
Tst2 no filter		2.37E-06	1.54E-03	0.06421
Tst2 w/ filter		1.51E-07	3.89E-04	0.01275
Tst3 no filter		2.94E-06	1.72E-03	0.02679
Tst3 w/ filter		8.69E-07	9.32E-04	0.01806
Tst4 no filter		1.73E-05	4.16E-03	0.06252
Tst4 w/ filter		3.05E-06	1.75E-03	0.01263
Tst5 no filter		8.35E-06	2.89E-03	0.03959
Tst5 w/ filter		2.03E-06	1.42E-03	0.02500
Tst6 no filter		1.20E-07	3.46E-04	0.00420
Tst8 no filter		6.76E-08	2.60E-04	0.00650
Tst9 no filter		4.73E-07	6.88E-04	0.00790
Tst10 no filter		6.79E-08	2.61E-04	0.00098
Tst11 no filter		1.22E-07	3.50E-04	0.00681
Tst12 no filter		2.55E-08	1.60E-04	0.01669
Tst15 no filter		7.19E-07	8.48E-04	0.02425
Tst15 w/ filter		2.66E-07	5.16E-04	0.00644
Tst16 no filter		4.58E-07	6.77E-04	0.02088
Tst16 w/ filter		5.93E-07	7.70E-04	0.02066
Averages on:	With filer	1.13E-06	9.65E-04	0.02030
	No filter	2.78E-06	1.21E-03	0.02539
	All	2.21E-06	1.12E-03	0.02361

For all data file [m]	
Std deviation of peak to peak values	95 % confidence on peak to peak values
0.0191	0.0141

For data file with filter [m]	
Std deviation on peak to peak values	95% confidence on peak to peak values
0.0131	0.0097

Table B.2 Complete result report for undisturbed sensor.

The fit of the double integrated output of a undisturbed sensor by a 5^{th} order polynomial turns out to be give good results. Therefore a polynomial function is appropriate to model the drift error as a function of time.

B.3 Test on an Excited Accelerometer Subjected to no Net Displacement

This second section relates to the tests performed on an excited sensor (See Section 3..2.2)

B.3.1 Tests Specifications:

10 similar tests have been made. The A/D card has been setup at a 1000 Hz sampling rate with ±0.5 V full-scale sensitivity for the filtered output and ±5 V for the non filtered output. The specifications of the test are given in Table B.3

Sampling Frequency	1000 Hz
Full-scale Range (on A/D card)	±5 V and ±0.5V
Max Acceleration Measurable	10 g and 1 g
Number of Data	16384
Records Length	16.384 s
Number of Records Acquired	11

Table B.3 Tests specification for an excited sensor

B.3.2 Complete Results

For each data file the amplitude of the drift given by the Weibull function fitted as described is Section 3.1.3 is reported along with the amplitude of the corresponding impact.

File #	Impulse Amplitude [V]	Drift Amplitude [m/s2]
17	0.7	0.57
18	0.789	0.82
19	0.964	2.08
20	0.691	1.0235
21	1.309	3.19
22	1.03	1.42
23	2.163	3.45
24	1.3	2.47
25	1.63	3.07
26	1.462	2.09
27	1.07	1.22

Table B.4 Complete result report

The following figure shows a graph of the amplitude of the impact given by the hammer versus the drift amplitude given by the Weibull estimation process. The pattern given by the different experimental values (points on Fig. B.3) can be described as a line, which indicates that the impact and the drift amplitude are directly proportional.

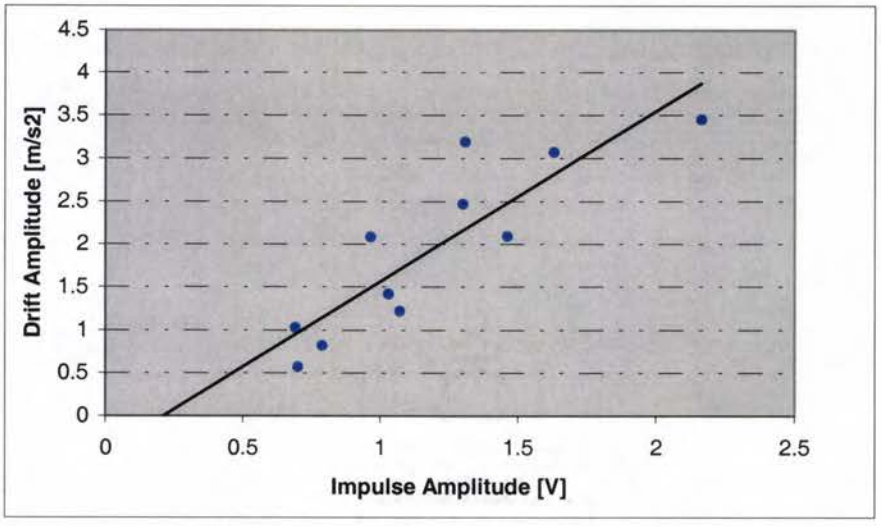

Figure B.3 Impulse Amplitude vs. Drift Amplitude

Appendix C

Details on the Validation Tests Conducted on the LabVIEW® Estimation program

C.1 Complementary Results on the Test of Section 5.3.1

Table C.1 shows the arbitrary coefficients chosen for the four dummy files created. The time variable t is ranging from 0 to 16.384 s.

File Name	Equation Used
File Imp+poly_1	$1+0.5t-0.05t^2-(1E-5)t^3-(1E-5)t^4+(1E-5)t^5+5\exp(0.5t)\sin(5t+1)$
File Imp+poly_2	$2+1t-0.01t^2-(4.2E-3)t^3-(4E-6)t^4+(6E-6)t^5+10\exp(1.48t)\sin(6.9t+1.5)$
File Imp+poly_3	$4+0.8t-0.03t^2-(2.5E-4)t^3-(3.5E-5)t^4-(1E-6)t^5+6.5\exp(1t)\sin(2.9t+0)$
File Imp+poly_4	$0-0.8t+0.08t^2-(3E-4)t^3-(1E-4)t^4-(5E-6)t^5+10\exp(0.956t)\sin(4.541t-0.5)$

Table C.1 Tests reference files coefficients

Each file is passed through the parameter estimation program 5 times, each time the starting trial solution (specified by the user) is different.

A comparison of the values estimated and the real values for each file are shown in Table C.2. Each error value (computed according to Eq. 5.2) has to multiply by 100 to get a valid percentage.

File Imp+poly_1							
Coeff	**Ref**		**Try 1**	**Try 2**	**Try 3**	**Try 4**	**Try 5**
a0	1		1.01E+00	1.01E+00	1.01E+00	1.01E+00	1.03E+00
a1	0.5		4.89E-01	4.90E-01	4.90E-01	4.92E-01	4.69E-01
a2	-5.00E-02		-4.72E-02	-4.75E-02	-4.75E-02	-4.80E-02	-4.26E-02
a3	-2.00E-04		-2.40E-04	-2.04E-04	-2.04E-04	-1.59E-04	-2.53E-04
a4	-5.00E-06		-3.80E-06	-5.00E-06	-5.00E-06	-6.30E-06	-5.10E-06
a5	1.00E-05		6.00E-08	0.00E+00	6.38E-08	6.19E-08	5.30E-07
b0	5		4.99E+00	5.00E+00	5.00E+00	5.00E+00	4.99E+00
b1	0.5		4.99E-01	5.00E-01	5.00E-01	5.00E-01	4.98E-01
b2	5		5.00E+00	5.00E+00	5.00E+00	5.00E+00	5.00E+00
b3	1		1.00E+00	1.00E+00	1.00E+00	1.00E+00	1.00E+00
		Error on b0	0.0100	0.0087	0.0088	0.0071	0.0288
		Error on b1	0.0219	0.0191	0.0192	0.0155	0.0613
		Error on b2	0.0568	0.0492	0.0492	0.0395	0.1490
		Error on b3	0.2024	0.0200	0.0191	0.2039	0.2646
		Error on b4	0.2400	0.0000	0.0000	0.2600	0.0200
		Error on b5	0.9940	1.0000	0.9936	0.9938	0.9470
		Error on c0	0.0010	0.0009	0.0009	0.0007	0.0029
		Error on c1	0.0011	0.0010	0.0010	0.0008	0.0031
		Error on c2	0.0001	0.0001	0.0001	0.0001	0.0002
		Error on c3	0.0010	0.0009	0.0009	0.0007	0.0029
		Average	0.1528	0.1100	0.1093	0.1522	0.1480
		Average on c0 to c3	**0.0010**				

(a)

File Imp+poly_2							
Coeff	**Ref**		**Try 1**	**Try 2**	**Try 3**	**Try 4**	**Try 5**
a0	2		1.73E+00	1.73E+00	1.73E+00	1.74E+00	1.74E+00
a1	1		1.27E+00	1.27E+00	1.27E+00	1.26E+00	1.26E+00
a2	-1.00E-02		-7.30E-02	-7.30E-02	-7.30E-02	-7.13E-02	-7.13E-02
a3	-4.20E-03		2.03E-04	2.03E-04	2.03E-04	9.55E-05	9.55E-05
a4	-4.10E-06		-6.10E-06	-6.10E-06	-6.10E-06	-7.00E-06	-7.00E-06
a5	6.00E-06		3.19E-07	3.19E-07	3.19E-07	4.99E-07	4.99E-07
b0	10		1.01E+01	1.01E+01	1.01E+01	1.01E+01	1.01E+01
b1	1.48		1.51E+00	1.51E+00	1.51E+00	1.50E+00	1.50E+00
b2	6.9		6.95E+00	6.95E+00	6.95E+00	6.95E+00	6.95E+00
b3	1.5		1.46E+00	1.46E+00	1.46E+00	1.46E+00	1.46E+00
		Error on b0	0.1333	0.1333	0.1333	0.1297	0.1297
		Error on b1	0.2694	0.2694	0.2694	0.2622	0.2622
		Error on b2	6.3004	6.3004	6.3004	6.1347	6.1347
		Error on b3	0.9516	0.9516	0.9516	0.9773	0.9773
		Error on b4	0.4878	0.4878	0.4878	0.7073	0.7073
		Error on b5	0.9469	0.9469	0.9469	0.9168	0.9168
		Error on c0	0.0100	0.0100	0.0100	0.0097	0.0097
		Error on c1	0.0173	0.0173	0.0173	0.0168	0.0168
		Error on c2	0.0072	0.0072	0.0072	0.0070	0.0070
		Error on c3	0.0254	0.0254	0.0254	0.0248	0.0248
		Average	0.9149	0.9149	0.9149	0.9186	0.9186
		Average on c0 to c3	**0.0148**				

(b)

File Imp+poly_3							
Coeff	**Ref**		**Try 1**	**Try 2**	**Try 3**	**Try 4**	**Try 5**
a0	4		4.54E+00	4.16E+00	4.16E+00	4.16E+00	4.13E+00
a1	0.8		3.51E-01	6.69E-01	6.69E-01	6.69E-01	6.90E-01
a2	-3.00E-02		6.70E-02	-9.54E-04	-9.54E-04	-9.54E-04	-5.55E-03
a3	-2.50E-04		-6.94E-03	-2.42E-03	-2.42E-03	-2.42E-03	-2.11E-03
a4	-3.50E-05		-4.00E-06	-5.70E-06	-5.70E-06	-5.70E-06	-5.80E-06
a5	-1.00E-06		6.00E-06	4.33E-07	4.33E-07	4.33E-07	6.00E-08
b0	6.5		5.68E+00	6.25E+00	6.25E+00	6.25E+00	-6.29E+00
b1	1		9.13E-01	9.73E-01	9.73E-01	9.73E-01	9.78E-01
b2	2.9		2.98E+00	2.92E+00	2.92E+00	2.92E+00	2.92E+00
b3	0		-5.27E-02	-1.44E-02	-1.44E-02	-1.44E-02	3.13E+00
		Error on b0	0.1362	0.0399	0.0399	0.0399	0.0333
		Error on b1	0.5607	0.1642	0.1642	0.1642	0.1371
		Error on b2	1.2338	0.9682	0.9682	0.9682	0.8150
		Error on b3	26.7652	8.6649	8.6649	8.6649	7.4470
		Error on b4	0.8857	0.8371	0.8371	0.8371	0.8343
		Error on b5	5.0000	0.5667	0.5667	0.5667	0.9400
		Error on c0	0.1266	0.0390	0.0390	0.0390	0.0325
		Error on c1	0.0866	0.0266	0.0266	0.0266	0.0221
		Error on c2	0.0270	0.0080	0.0080	0.0080	0.0067
		Error on c3					
		Average	3.8691	1.2572	1.2572	1.2572	1.1409
		Average on c0 to c3		**0.0348**			

(c)

File Imp+poly_4							
Coeff	**Ref**		**Try 1**	**Try 2**	**Try 3**	**Try 4**	**Try 5**
a0	0		0.00E+00	0.00E+00	0.00E+00	0.00E+00	0.00E+00
a1	-0.8		-1.18E+00	-1.32E+00	-1.37E+00	-2.39E+00	-1.09E+00
a2	8.00E-02		1.71E-01	1.99E-01	2.11E-01	4.43E-01	1.48E-01
a3	3.00E-04		-6.75E-03	-7.62E-03	-8.71E-03	-2.44E-02	-4.81E-03
a4	-1.00E-04		-5.80E-06	-1.33E-04	-1.00E-04	-1.49E-04	-4.80E-05
a5	-5.00E-04		6.00E-08	6.69E-06	6.69E-06	2.92E-05	-6.27E-07
b0	10		9.63E+00	9.49E+00	-9.45E+00	8.67E+00	9.72E+00
b1	0.956		9.44E-01	9.34E-01	9.32E-01	8.86E-01	9.50E-01
b2	4.541		4.58E+00	-4.60E+00	4.60E+00	4.70E+00	4.57E+00
b3	-0.5		-5.36E-01	-5.58E-01	-5.23E-01	-4.86E-01	-5.27E-01
		Error on b0	0	0	0	0	0
		Error on b1	0.4763	0.6552	0.7127	1.9835	0.3598
		Error on b2	1.1374	1.4850	1.6334	4.5398	0.8493
		Error on b3	21.5116	24.3852	28.0227	80.2583	15.0443
		Error on b4	0.9420	0.3265	0.0000	0.4898	0.5200
		Error on b5	0.9999	0.9866	0.9866	0.9416	0.9987
		Error on c0	0.0368	0.0515	0.0552	0.1330	0.0284
		Error on c1	0.0123	0.0226	0.0252	0.0732	0.0065
		Error on c2	0.0085	0.0120	0.0130	0.0360	0.0065
		Error on c3	0.0724	0.1160	0.0465	0.0273	0.0548
		Average	2.5197	2.8041	3.1495	8.8482	1.7868
		Average on c0 to c3	**0.0419**				

(d)

Table C.2 Values obtained by the parameter estimation procedure and corresponding error for data file Imp+poly_1 (a) , File Imp+poly_2 (b) , File Imp+poly_3 (c) and File Imp+poly_4 (d).

C.2 Complementary Result on the Positioning System Test

Fig C.1 shows for each file processed the corrected displacement (raw displacement minus the estimated drift). On every graph the Y-axis in m/s^2 and the X-axis is in second.

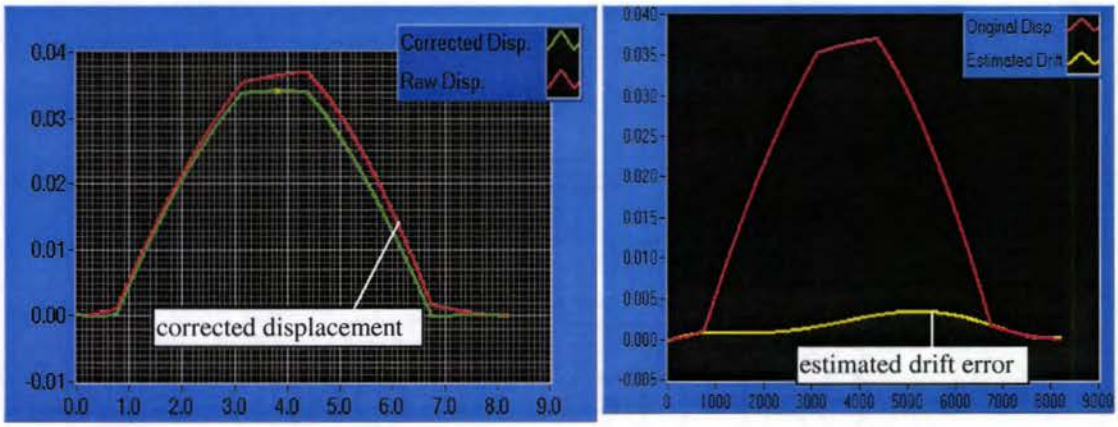

(a)

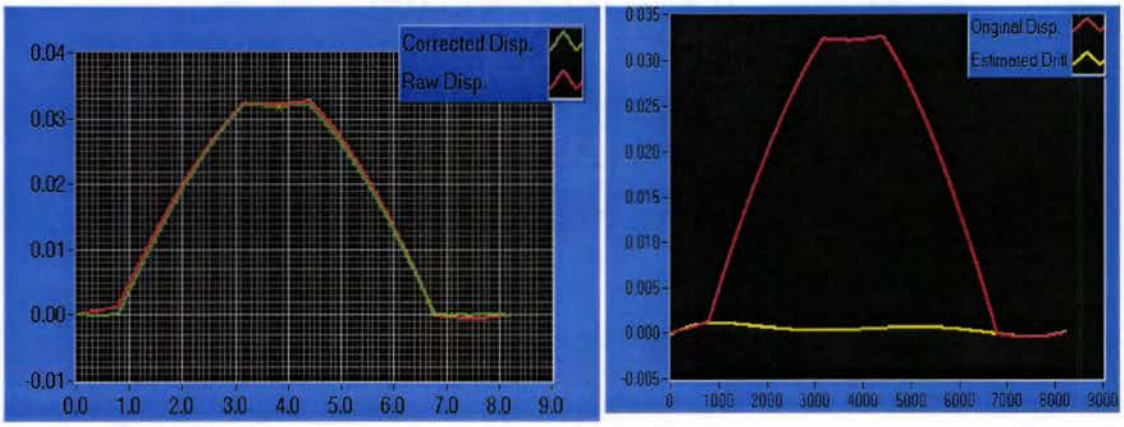

(b)

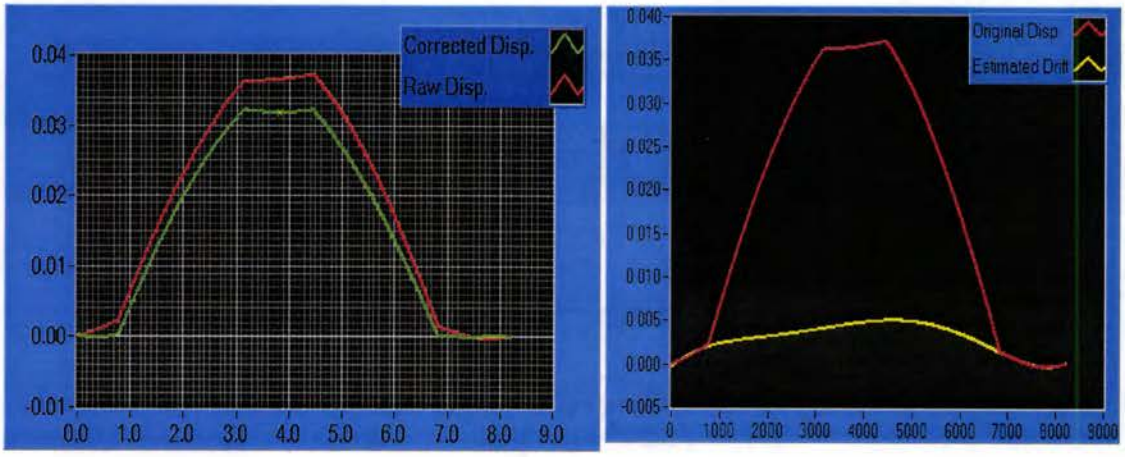
Corrected Disp.
Raw Disp.
Original Disp
Estimated Drift

(c)

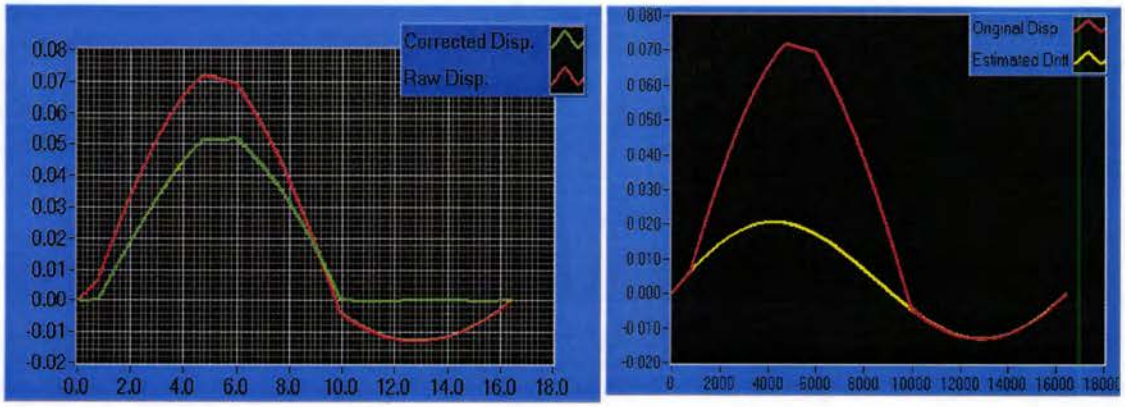
Corrected Disp.
Raw Disp.
Original Disp
Estimated Drift

(d)

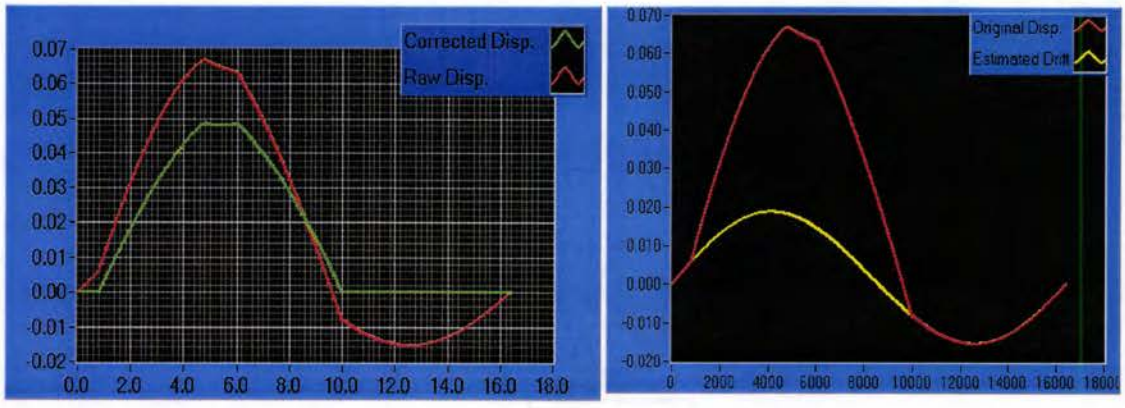
Corrected Disp.
Raw Disp.
Original Disp
Estimated Drift

(e)

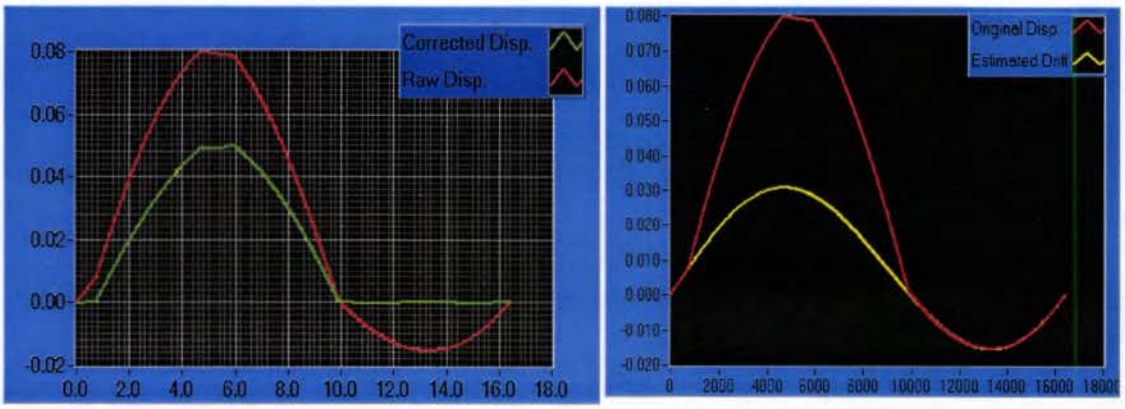

(f)

Figure C.1 XY Table test result for file 0 to 5 (a) to (f): corrected displacement and estimated drift error in comparison with the original displacement.